UNIVERSITY OF NAIROBI

FACULTY OF ENGINEERING

DEPARTMENT OF ELECTRICAL AND INFORMATION ENGINEERING

A Region-Based Histogram and Fusion Technique for Enhancing Backlit Images for Cell Phone Applications

By

Shaffa Korvawu Kokro Jr.

BSc. (Electrical Engineering) University of Liberia

F56/35720/2019

A thesis submitted in partial fulfilment of the degree of Master of Science in Electrical and Electronic Engineering in the Department of Electrical and Information Engineering in the University of Nairobi

July 2023

DECLARATION

This thesis is my original work and has not been presented for a degree in any other university.

Name of student: Shaffa Korvawu Kokro Jr.

Registration number: F56/35720/2019

Signature: ....Date: ...28th July 2023...............................

APPROVAL

This thesis was submitted with our approval as University supervisors.

SUPERVISORS:

Prof. Elijah Mwangi:

Signature…………………………...………Date.31st July 2023

Prof. George Kamucha:

Signature………………………...………Date……29th July 2023

DEDICATION

This thesis is dedicated to my Dad for always believing in me and supporting me in my pursuit of higher education. Love you, Dad!

ACKNOWLEDGEMENT

TABLE OF CONTENTS

ABBREVIATIONS AND ACRONYMS

1-D	One-dimensional
2-D	Two-dimensional
ABC	Adaptive Brightness Control
AE	Auto-exposure
BHE	Bi-Histogram Equalization
CCD	Charge-coupled devices
CCTV	Closed-circuit television
CDF	Cumulative Distribution Function
CFA	Colour Filter Array
CMOS	Complementary Metal-Oxide Semiconductors
CMY	Cyan, Magenta, Yellow
CMYK	Cyan, Magenta, Yellow, Black
DWT	Discrete Wavelet Transform
DWT-F	Discrete Wavelet Transform Fusion
EM	Electromagnetic
GUI	Graphical User Interface
HDR	High Dynamic Range
HE	Histogram Equalization
HS	Histogram Specification
HVS	Human Visual System
HSV	Hue, Saturation, Value
IEEE	Institute of Electrical and Electronics Engineers

IQA   Image Quality Assessment

ISO   International Organization for Standardization

ITU   International Telecommunication Union

ITU-R   Radio communication sector of the ITU

LIME   Low-Light Image Enhancement via Illumination Map

                   Estimation

NIQE   Natural Image Quality Evaluator

PSNR   Peak Signal-to-Noise Ratio

RBHF   Region-based Histogram Fusion

RBHS   Region-based Histogram Specification

RGB   Red, Green, Blue

SSIM   Structural Similarity Index

LIST OF FIGURES

xiii

LIST OF TABLES

ABSTRACT

Many cell phone cameras perform poorly in backlighting situations due to low dynamic range, which then leads to the creation of low-quality pictures known as backlit images. Conventional image enhancement algorithms are not well suited to improve the quality of backlit images. Over-saturation or a loss of contrast are typical outcomes when these methods are applied. In this thesis, a novel image enhancement algorithm is presented for improving the visual perception of a single backlit image. The algorithm uses a region-based histogram specification scheme in combination with the discrete wavelet transform image fusion to correct exposure disparities between foreground and background scenes. Computer simulations in MATLAB R2018a and on a dataset of 162 backlit images revealed that the proposed algorithm significantly improves the backlit image's visual perception without distorting colours or adding artefacts. The Peak Signal-to-Noise Ratio, Structural Similarity Index Measure, and Naturalness Image Quality Evaluator metrics objectively validated these results. The algorithm produced PSNR values ranging from 19 dB to 30 dB for images with low backlit degradation while retaining more than (60-70) % structural similarity to the inputs. Lower PSNR and SSIM values were consistent with severely degraded images. These findings agreed with the outcomes of the subjective evaluations. However, multiple iterations of the proposed algorithm increased the PSNR quality by up to 12 dB after the first three iterations. By comparison, the proposed algorithm significantly outperformed existing image enhancement techniques such as Histogram Equalization, Multiscale Retinex, and Low-light Image Enhancement via Illumination Map Estimation.

CHAPTER 1

INTRODUCTION

1.1. Background

Backlit images are low-quality digital pictures produced due to backlighting, a poor lighting condition that causes significant degradation in image quality. As shown in Figure 1.1, foreground areas (F-region) in a backlit image are frequently under-exposed, whereas background sectors (B-region) are either well-lit or over-exposed. Traditional image enhancement algorithms are rendered ineffective by this type of illumination. Therefore, research in this domain focuses on alternative methods that improve backlit images while preserving their details and colours [1].

(a)   (b)

Figure 1.1. Examples of backlit images (a) Backlit portrait (b) Backlit cityscape [2]

1.2. Assessment of backlighting

Backlighting is a poor illumination setting that occurs when an excessive reflection of light is incident to an image-capturing device or when the dominant light source in a picture scene lies behind the main object(s) [1]. As seen in

Figure 1.1, it creates low contrast in an image's foreground and impairs its overall quality.

Many digital cameras cannot perform well in backlighting due to their low dynamic range. An image sensor capable of detecting extremely low and high luminance simultaneously would be required to capture high-quality pictures in such a situation. A device of this type would have a dynamic range compared to the human visual system (HVS). Nonetheless, professional photographers have used digital cameras' low dynamic range to convey mystery, drama, emotion, and mood. This is known as silhouette photography, and it has grown in popularity over the last decade [3]. Figure 1.2 depicts a silhouette image.

Figure 1.2. Example of silhouette photography [3]

1.3. Problem Statement

Backlighting is a commonly encountered problem for cell phone users. It usually results in low-quality images known as backlit images. Conventional image enhancement methods such as the well-known histogram equalization algorithm [4] or Retinex-based algorithms [5]-[7] cannot achieve the desired

enhanced effects of backlit images. Oversaturation and loss of contrast are typical outcomes when these methods are applied.

Various research investigations have been conducted in recent years to address these challenges. The majority of these efforts have not however focused on the use of backlit image enhancement algorithms in cell phone applications. As a result, despite recent developments in smartphone technology, there is no commercially accepted technique for improving backlit pictures on cell phones.

Alternative methods such as Auto-exposure (AE) [8] and High Dynamic Range (HDR) imaging [9] are being used by smartphone manufacturers to handle backlighting and other types of poor illumination situations. However, these methods have significant drawbacks that outweigh their benefits in poor lighting situations. For instance, under backlighting, AE cannot reveal items in the foreground while simultaneously exposing details in the background. As a result, a well-exposed foreground will cause a loss of information in the background scene and vice-versa. Likewise, HDR, developed primarily to handle low-light situations, is susceptible to motion blur since it relies on fusing two or more sequential images with varying exposures [9]. Furthermore, it cannot enhance low-quality photographs after they have been acquired. Therefore, this research investigation sought to develop a more optimal technique for enhancing backlit images, particularly on cell phones.

1.4. Objectives

1.4.1. Main objective

This work aimed to develop a new image enhancement algorithm that can be employed in cell phone applications to improve the visual quality of backlit images.

1.4.2. Specific objectives

The specific objectives were:

(i) To investigate the use of histogram-based contrast-stretching techniques for backlit image enhancement, taking into consideration their applicability to cell phones.

(ii) To develop an optimized backlit image enhancement algorithm with low-computational cost using a novel region-based histogram specification (RBHS) scheme in combination with the discrete wavelet transform (DWT) image fusion approach.

(iii) To evaluate the performance of the work on standard backlit images captured in various backlit situations by commercially available cell phones, based on existing image quality assessment (IQA) techniques.

1.5. Justification for the study

Smartphones have become the standard design for cell phones and other mobile devices, and they currently represent the fastest-growing market segment in the telecommunications industry [10]. According to *Statista*, global smartphone sales increased from 680 million in 2012 to about 1.54 billion in 2019, as shown in Figure 1.3 [11]. This significant increase is often due to the

many capabilities offered within the device compared to regular mobile devices. Among these capabilities, the camera remains one of the most important. It is a principal factor influencing consumer choice of one mobile device over another.

As the smartphone industry expands, consumers will continue to expect and demand high-quality cameras on their cell phones. Manufacturers, on the other hand, cannot achieve the optimal performance of cell phone cameras in backlit situations due to the hardware constraints of smartphone camera sensors and a lack of adequate software to compensate for such hardware limitations. As a result, this research investigated a more effective and less expensive software-based approach to handle backlighting and improve the quality of backlit images on cell phones.
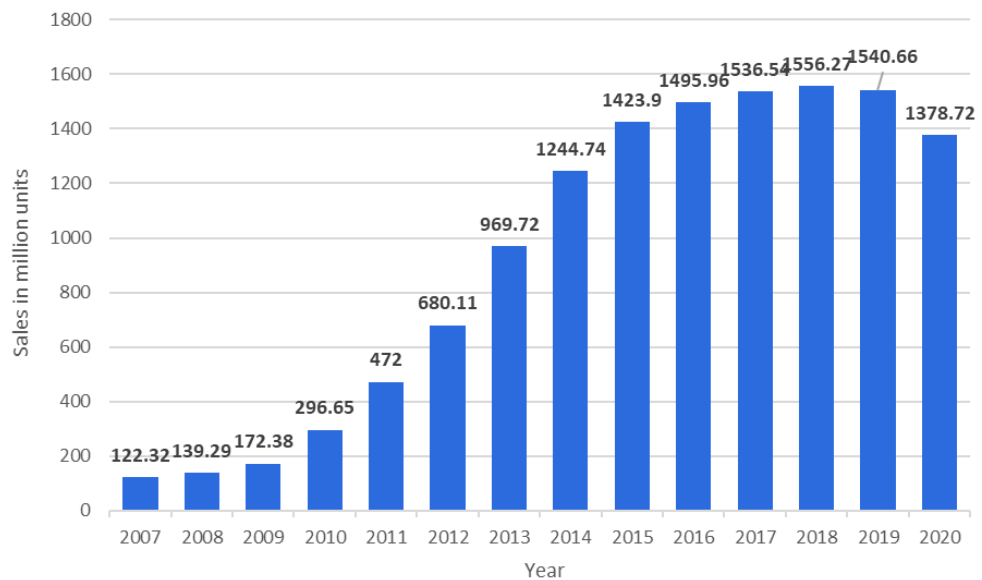
Figure 1.3. Global smartphone sales [11]

1.6. Beneficiaries of the research findings

The results of this research investigation are beneficial to:

(i) Cell phone manufacturers: the results of this research investigation could provide smartphone companies with a practical software approach for handling backlight illumination. Small cell phone companies with limited resources to invest in high-quality camera hardware can leverage the research findings to improve the quality of their mobile camera system.

(ii) Smartphone users: since many smartphone users are not professional photographers, they are unaware of the ideal lighting conditions for taking photos. As a result, the research outcome could allow them to capture high-quality pictures even in poor lighting situations.

(iii) The computer vision community: the proposed technique in this research investigation is useful as a pre-processing task in object detection and image recognition scenarios.

(iv) Manufacturers and end-users of small-scale computer displays with similar hardware limitations to cell phones.

(v) Manufacturers and end-users of surveillance apparatus such as CCTV cameras, bodycams, and spyware: Governments, private or public institutions could leverage the results of this research investigation to improve the picture quality of these devices.

(vi) Technology companies that develop third-party mobile or desktop photo-editing applications: The results of this research investigation could be used as a tool in existing photo-editing software.

1.7. Scope of work

This research focused on the following areas:

(i) The use of global contrast stretching with image fusion for backlit image enhancement

Over the years, researchers have proposed several techniques for improving backlit images. They include but are not limited to global and local contrast stretching, image fusion, and learning-based modelling. This research focused on the integration of histogram-based contrast stretching with the discrete wavelet transform image fusion to improve the under- and over-exposed regions of a single backlit image. The discrete wavelet transform image fusion was selected because of its minimum colour distortion property.

(ii) The selection of a single mobile environment

Although there are numerous mobile platforms available, the scope of this research was limited to cell phones that run the Google Android operating system. Google Android smartphones are widely available, ranging from budget-friendly options to high-end flagship devices. This makes Android a suitable choice for conducting cost-effective research. The platform's popularity also ensures a large user base, maximizing the potential impact of the research findings. Within the dataset, degraded backlit images captured with the Samsung Galaxy A7 were included, for which adequate enhancement solutions have been proposed.

(iii) Exposure correction in degraded backlit images

Backlit images captured by commercial cell phones degrade due to different exposure settings for foreground and background illumination. Therefore, the focus of this research was limited to correcting exposure disparities after acquisition to improve image quality. Other types of degradation, such as those caused by digital noise or lens aberrations, were not addressed.

1.8. Organization of the thesis

The rest of the thesis is organized as follows: chapter two covers topics related to the development of the proposed method. Chapter three contains the materials and methods of the proposed framework, following a section on the type of measures used to evaluate its performance. Experimental results are presented with their analysis in chapter four, while the conclusion and recommendations are provided in chapter five. The Appendix contains additional information, including the MATLAB source code and the research prototype.

1.9. Note on publications and patent application

As part of the research, significant contributions were made towards knowledge dissemination through the submission of papers and a patent. This section provides details on the submitted papers and the patent application associated with the research findings.

(i) A paper titled "A Region-based Histogram and Fusion Technique for Single Backlit Image Enhancement" was submitted to the Elsevier journal. This paper presented a novel approach for enhancing backlit

images using the proposed region-based histogram and fusion approach.

(ii) Another paper titled "A Low-Light Image Enhancement Technique Based on Histogram Matching and Fusion" was submitted to the Institute of Electrical and Electronics Engineers (IEEE) Imaging Systems and Techniques conference, scheduled for October 17-19, 2023, in Copenhagen, Denmark. This paper focused on addressing the challenges of low-quality photos captured in low-light situations. The paper presented a novel technique to enhance such images via histogram matching and image fusion.

(iii) In addition to the submitted papers, a patent application was filed through the University of Nairobi Intellectual Property Management Office to the Kenya Industrial Property Institute. The application disclosed the research methods with an aim to protect the intellectual property associated with the research findings.

CHAPTER 2

LITERATURE REVIEW

This chapter provides the theoretical basis of important image processing concepts as well as related works. The discussion begins with an overview of fundamental concepts in digital image processing, such as wavelet theory, wavelet transforms, and image fusion, before a review of related works in backlit image enhancement. At the end of the chapter, the knowledge gaps in the existing enhancement procedures are identified.

2.1. Digital image acquisition

A digital image is a discrete and finite two-dimensional (2-D) representation of a physical or abstract phenomenon that has been recorded, processed, and stored electronically. Mathematically, it is defined as a 2-D function *F(x,y)*, where *x* and *y* are spatial coordinates, and the amplitude of *F* at any pair of coordinates *(x,y)* is the intensity or grey level of the image at that point. The range of intensity levels $[0, L - 1]$, where $L = 2^n$, is determined by the bit-depth (n) of the image. For an 8-bit image, grey levels range from 0 to 255, with 0 representing a black pixel and 255, a white pixel. Similarly, a binary or 1-bit image will have levels ranging from 0 (black) to 1 (white) [12].

Digital image acquisition, also known as digital imaging, is the process of creating a digital image from an energy source [12]. Electromagnetic (EM) waves are often used as the primary energy source for generating digital images. For example, ionizing radiation from gamma rays is used in nuclear medicine and astronomy. X-rays are frequently used in medical diagnostics and industrial

inspection of products, while ultraviolet light has seen applications in lithography and microscopy [12].

Gamma-rays, X-rays, and Ultraviolet light are a few sources of the EM spectrum. Other sources include visible light, infrared, microwave, and radio waves. Visible light is the most common energy source used for multimedia, security, and entertainment. Infrared has also been employed in security and surveillance [12].

Electromagnetic waves are not the only sources of energy used in digital imaging. Other sources include sound waves and electron beams. Electron beams are used in electron microscopy, and sound waves are used in sonar imaging and ultrasound applications [12]. Regardless of the nature of the energy source, the fundamental components in a digital imaging system, as depicted in Figure 2.1, include an imaging sensor, a processing and storage unit, and an output device, usually a computer display. This, however, does not apply to synthetic images generated by a computer.
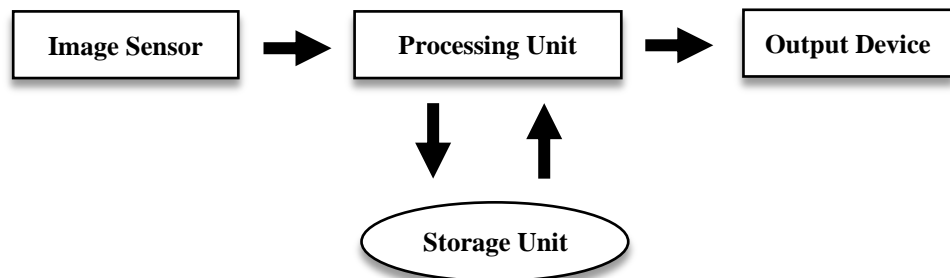
Figure 2.1. The basic structure of a digital imaging system

2.2. Digital image sensors

The first task of a digital imaging system is to convert the energy emitted by a source into electrical signals. A digital image sensor handles this task. Charge-coupled devices (CCD) and complementary metal-oxide semiconductors (CMOS) are the two main types of digital image sensors. They both use arrays of light-sensitive elements (photosites) that convert photons into electrons. Over time, the charge collected at each site within the sensing plane is converted to a voltage which is processed and then assigned a pixel value [13],[14].

Several distinctions can be made between the CCD and CMOS sensors. First, the charge-to-voltage conversion in a CCD sensor is performed externally from the sensing plane. As for the CMOS sensors, each picture element contains its charge-to-voltage and amplifier circuits that yield faster readout times [15]. Other differences include energy efficiency, cost, and noise. A CMOS sensor has a lower fabrication cost and higher energy efficiency than CCD, but they frequently yield more image noise [16]. However, cost and energy efficiency make CMOS more popular in cell phone cameras [17].

2.3. Colour image processing

A colour image can be defined as a record of the chromatic light reflected by objects in a picture scene. Every pixel in a colour image is defined by the intensities of three colour components, red, green, and blue [12]. Generically, a digital camera would require three unique sensors to record data for each component. However, to reduce cost, many camera systems utilize the Bayer colour filter array (CFA) to generate colour images with a single imaging sensor, as illustrated in Figure 2.2. The Bayer CFA allows one of the three

colour components to be recorded at each pixel location. Then by interpolation, a demosaicking algorithm generates values for the remaining components [18][19].
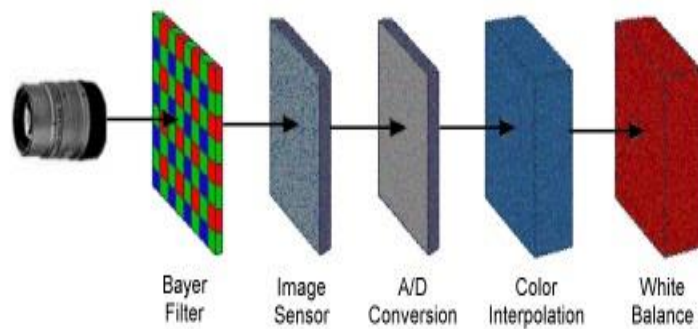
Figure 2.2. Imaging sensor with Bayer CFA [18]

2.4. Colour models

A colour model or colour space is a mathematical system used to describe how colours are represented [12]. Several colour models have been developed for recording, displaying, printing, and processing digital images. The RGB (red, green, blue) model is widely used for recording and displaying digital images on a computer screen. Digital printers use the CMY (cyan, magenta, yellow) and CMYK (cyan, magenta, yellow, black) models for colour printing. For image processing, some algorithms utilize the HSV (hue, saturation, value) model, which is synonymous with how humans perceive colours [12],[20]. The most attractive feature of the HSV model is that it separates the luminance information from the image colour profile, thus facilitating the development of a variety of grey-scale enhancement applications [12].

2.5. Colour space conversion

Digital images can be processed using a variety of colour models. The process of converting an image from one colour model to another is known as colour space conversion. Numerical computation software such as the Matrix Laboratory (MATLAB) [21] by MathWorks provides various tools to convert from one colour model to another. Table 2.1 lists some MATLAB transformations between RGB and different colour models [22].

Table 2.1. Colour space conversion in MATLAB

Description	Function	Description	Function
RGB to HSV	rgb2hsv	HSV to RGB	hsv2rgb
RGB to L*a*b	rgb2lab	L*a*b to RGB	lab2rgb
RGB to YCbCr	rgb2ycbcr	YCbCr to RGB	ycbcr2rgb
RGB to YIQ	rgb2ntsc	YIQ to RGB	ntsc2rgb

2.6. Dynamic range and exposure

Various factors influence the quality of an image captured with a digital camera. These factors can be attributed to internal and external effects. Internal effects include software and hardware limitations such as lens quality, colour accuracy, type of compression used in storing the image, noise, and dynamic range of the imaging sensor. External effects include ambient lighting as well as the skill of the photographer [23]. This section focuses on the dynamic range effect since it directly contributes to the formation of backlit images.

2.6.1. Dynamic range in digital imaging

Dynamic range is defined as the ratio of light to dark in a photographic image [24]. It is determined by the "*stops of light*" that a digital camera sensor can

14

capture. The term "*stops of light*", also known as *f-stops* or exposure value (EV), refers to how many increments between pure black and white an image sensor can detect [24],[25]. The average camera sensor can detect up to 8 *f-stops* while a high-end sensor like the Sony A7R IV captures up to 15 *f-stops* [26]. By comparison, the human visual system (HVS) detects approximately 20 *f-stops* [27]. These values are illustrated in Figure 2.3.

Dynamic Range by Comparison

The Human Visual System

High-end camera sensor

Average camera sensor

1 2 3 4 5 6 7 8 9 10 11 12 13 14 15 16 17 18 19 20

Picture scene referenced in f-stops (EV)
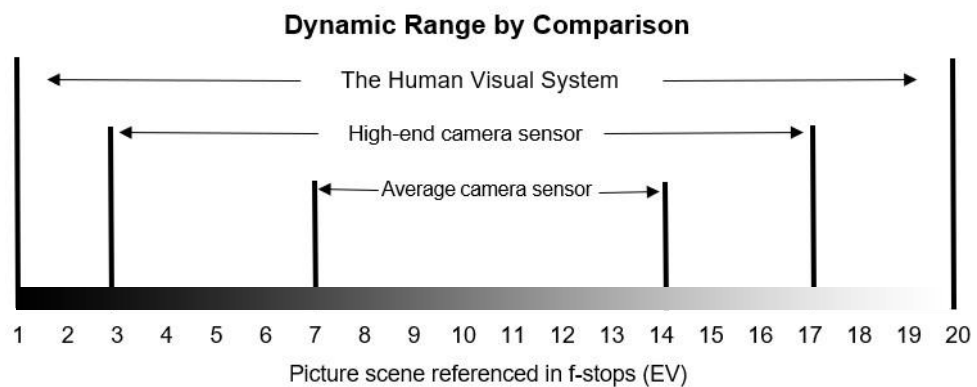
Figure 2.3. Dynamic range of various imaging sensors

2.6.2. Exposure in digital images

The exposure of an image describes how light or dark the image appears when captured by a camera [28]. A digital picture can be classified as under-exposed, over-exposed, or well-exposed. Under-exposed pictures tend to be darker than they appear when photographed because they do not capture all the light present in the scene, whereas over-exposed images include too much light and thus look bright and overexposed. Images that are well-exposed capture enough light to reveal the entire picture scene [28].

Figure 2.4 depicts the three kinds of exposure. Figure 2.4(a) shows an underexposed image with low visibility in both the foreground and background

scenes. The same photo is displayed in Figure 2.4(b) but with better clarity. Finally, in Figure 2.4(c), the image is overexposed, as evident by the loss of details in the sky.

Figure 2.4. Exposure level in a digital picture (a) Under-exposed (b) Well-exposed (c) Over-exposed [29]

Two interesting phenomena can be observed in Figure 2.4. The first is the transition from dark to light exposure levels. Digital cameras include a software feature that allows users to change the camera exposure settings to accommodate different ambient lighting situations within the limited dynamic range of the image sensor [30]. Usually, this is achieved by the adjustment of three parameters: ISO (International Standards Organization), lens aperture, and shutter speed. The ISO is a dial that increases or decreases the camera's light sensitivity. Aperture determines how wide or narrow the camera lens is set, while shutter speed controls how long the shutter is open [28],[30]. Together, these three parameters influence the overall image exposure level.

2.6.3. Impact of low dynamic range

The second phenomenon observed in Figure 2.4 reveals the impact dynamic range has on image quality. The dynamic range limit of an image sensor depends on the number of photons each photosite can capture [24]. Photosites become saturated when exposed to too much light. At such point, they cannot detect light variations in the picture scene which leads to blown-out highlights as seen in Figure 2.4(c). In other words, the highlights are limited to the maximum intensity value which is white. This effect is known as highlight clipping. Shadow clipping is another effect which occurs when shadows are limited to the minimum grey level, black, due to the significantly low amount of light. Both highlight and shadow clippings are attributes of low dynamic range problems in digital imaging.

2.6.4. Auto-exposure in smartphones

Auto-exposure (AE) is a feature that automatically adjusts the camera's exposure settings based on the ambient lighting situation [8]. This feature is embedded in almost all native camera applications to improve picture quality in poor lighting situations. Many smartphone users find it useful because adjusting exposure parameters manually can be a challenge to those who are not professional photographers. The major drawback to auto-exposure, however, is it cannot reveal objects in the foreground of a backlit scene while simultaneously exposing the background. As a result, a well-exposed foreground will result in a loss of details in the background scenes and vice-versa.

2.6.5. High dynamic range in smartphones

Modern smartphone technology uses high dynamic range (HDR) imaging techniques to extend the dynamic range of images captured in poorly illuminated scenes. A smartphone camera with HDR automatically captures two or more successive images with different exposure settings and fuses them to produce a significantly higher-quality image [9]. Figure 2.5 gives an example of the HDR mode activated on a Google android phone. As seen in the figure, HDR improves the visual perception of the image by increasing its range of grey levels.

Figure 2.5. High Dynamic Range imaging on a smartphone [31]

The first drawback to HDR is its susceptibility to motion blur. While high dynamic range imaging performs best for stationary scenes, in active scenes, fast-moving objects frequently appear blurry since their positions are changing with each successive image [32]. This is illustrated in Figure 2.6. Another drawback is that HDR cannot enhance low-quality pictures after they have been

acquired. This is because HDR relies on the fusion of two or more sequential images with varying exposures [9],[32].

Figure 2.6. Motion blur effects of HDR [33]

2.7. Digital image enhancement

The primary objective of digital image enhancement is to process an image signal so that viewers can assess the information it contains with greater clarity. This process is considered subjective because it depends on the specific information the user intends to extract. The information, however, must be present in the image and not obscured by noise [12].

Many well-known approaches for digital image enhancement are fundamentally based on contrast stretching, histogram modification, edge sharpening, interpolation, thresholding, false colouring, or denoising. In this section, the focus is placed on the theory of contrast stretching, image thresholding, and histogram processing in relevance to their applications in backlit image enhancement research.

2.7.1. Contrast stretching

Contrast is defined as the difference in luminance or colour that distinguishes one object from another [34]. An image is said to have a low contrast when its features are not distinguishable. Contrast stretching algorithms enhance low-contrast images by re-distributing pixels to span a wider range of grey levels based on a transformation function T given by equation (2.1) [12].

$$g(x, y) = T[f(x, y)] \qquad (2.1)$$

where $f(x,y)$ is an input image and $g(x,y)$ is the output image. The enhancement effects on the output image depend on the type of transformation function.

Linear and nonlinear contrast-stretching are the two most well-known techniques. A linear contrast stretching is performed when T is a linear function. Otherwise, the procedure is nonlinear. In linear contrast-stretching, the grey levels of $f(x,y)$ are uniformly distributed to span the full dynamic range, while in non-linear contrast-stretching, the grey levels are re-distributed depending on the type of nonlinear function, T [12],[35].

Some applications of linear contrast-stretching include correcting the settings of lens aperture during image acquisition [36], improving low contrast images, and high dynamic range (HDR) [9]. Piecewise linear is a variation of the linear approach. It is used to increase contrast only in some parts of the image [1]. This has applications in leukaemia detection [37]. Nonlinear contrast stretching has been used in the study of micro-calcifications in breast tissue [38]

and backlit image enhancement research, including Trongtirakul *et al.* [1] and Ueda *et al.* [39].

2.7.2. Image thresholding

Thresholding is a basic approach in image segmentation, and it is widely used as a pre-processing step in some backlit image enhancement algorithms [1],[40]. Simple global thresholding is performed by setting a grey level *T* as the threshold value. Pixel intensities above the set value are converted to white (binary 1), and those below are converted to black (binary 0) as given in equation (2.2) [12].

$$g(x,y) = \begin{cases} 1 \text{ if } f(x,y) \geq T \\ 0 \text{ } otherwise \end{cases} \tag{2.2}$$

where *f(x,y)* is an input image, *g(x,y)* is the output image, and *T* is a threshold value. The result is a binary image with the foreground as white and the background as black.

Threshold-based segmentation depends entirely on the threshold value. As a result, a poor threshold can lead to undesirable outcomes. Otsu's [41] method is popular for obtaining optimal thresholds. It involves iterating through all the possible states and calculating a measure of spread for the pixel levels on each side of the threshold representing the foreground and background. The optimal threshold is determined where the sum of foreground and background escalates at its minimum [41].

2.7.3. Histogram processing

A histogram is a powerful tool for displaying the grey-level distribution in an image. Mathematically, it is a discrete function $h(r_k)$ that returns the relative frequency with which each grey level occurs.

$$h(r_k) = n_k \qquad (2.3)$$

where r_k is the kth grey level and n_k is the number of pixels having the grey level r_k. Equation (2.4) defines a normalized histogram $p(r_k)$ which estimates the probability of occurrence for grey level r_k. The value of $p(r_k)$ is obtained by dividing n_k by the total number of pixels in the image, n.

$$p(r_k) = \frac{n_k}{n} \qquad (2.4)$$

Histograms are simple to compute using a computer, and they do not require significant hardware resources. For this reason, histogram-based techniques have become popular in real-time image enhancement applications [12]. The procedure to construct an image histogram is summarized below:

Step (i): Input image with grey level $[0, L-1]$

Step (ii): Initialize all bins $h(r_k)$ to zero, for $0 \leq k \leq L\text{-}1$

Step (iii): For every grey level r_k, count the number of pixels having the respective grey level and assign the value to n_k.

Step (iv): Set $h(r_k) = n_k$ and move to next bin $h(r_{k+1})$ for $0 \leq k \leq L\text{-}1$

The above procedure describes the process of obtaining the histogram for a grey-scale image. To display the pixel distribution of multichannel images such

as colour images, the histogram of each colour channel needs to be constructed independently.

2.7.4. Histogram specification

Histogram specification (HS) is a global contrast stretching technique used to modify the pixel intensities of an input image to match a target histogram [12],[39]. The target histogram is often derived from a mathematical model or a typical image [12]. The primary objective of HS is to obtain a transformation function that establishes a relationship between the input and the desired output.

Let $I(x, y)$ be a greyscale input with a normalized histogram $p_I(r_i)$ and $p_D(z_j)$ be a normalized target histogram. The cumulative distribution functions (CDFs) for $p_I(r_i)$ and $p_D(z_j)$ are obtained using equations (2.5) and (2.6), respectively.

$$T(r_k) = \sum_{i=0}^{k} p_I(r_i) \; ; \; k \in \{0, L-1\}/(L-1) \tag{2.5}$$

$$G(z_k) = \sum_{j=0}^{k} p_D(z_j) \; ; \; k \in \{0, L-1\}/(L-1) \tag{2.6}$$

Furthermore, letting $U(\cdot)$ be a transformation function such that $U(r_k) = z_k$, the grey level r_k can be mapped to the target value z_k to satisfy the condition $T(r_k) = G(z_k)$. The histogram-specified image is then obtained by applying $U(\cdot)$ to every pixel in $I(x, y)$ [12].

2.8. Wavelet transform theory

Wavelets are signals that oscillate for a finite duration. Wavelet bases, unlike Fourier bases, can sparsely represent signals with transient characteristics since

they are limited in both time and frequency. This property, among others, has

made wavelets useful in applications such as data compression, image fusion,

and analysis of signals with transient properties [12],[42],[43].

2.8.1. Wavelet families

A wavelet family is characterized by its "mother wavelet" $\psi(x)$. A "daughter

wavelet" $\psi_{a,b}(x)$ can be obtained by the scaling and shifting of the mother

wavelet, as given in equation (2.7) [44].

$$\psi_{a,b}(x) = \frac{1}{\sqrt{a}}\psi\left(\frac{x-b}{a}\right); \; a,b, \in \mathbb{R} \tag{2.7}$$

where a is a scaling or dilation factor, $a \neq 0$, and b is a translation factor.

To ensure that the wavelet transform of $\psi(x)$ is stably invertible, the mother

wavelet must satisfy the condition of having normalized energy and zero mean

[45]. Some wavelets from the Haar, Daubechies, Symlets, and Coiflets families

are displayed in Figure 2.7. The x-axis shows the temporal variation units and

the y-axis is the normalized amplitude. The index number, for example, *db4*,

refers to the number of wavelet coefficients. A particular family is selected

based on the kind of application.
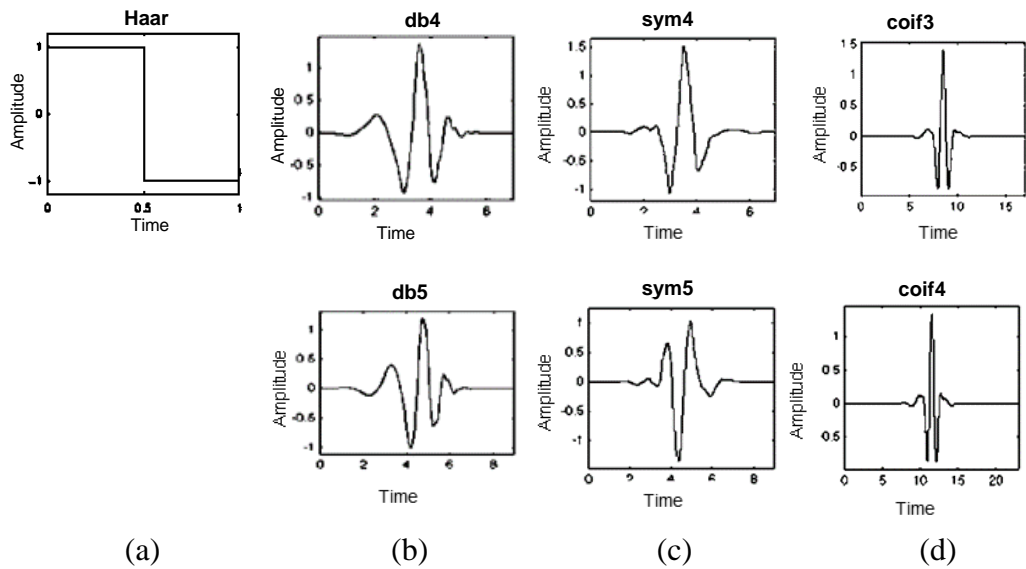
Figure 2.7. Examples of wavelet families (a) Haar (b) Daubechies (c) Symlets (d) Coiflets [46]

2.8.2. Scaling functions

Scaling functions are another group of wavelets which is considered the "father wavelet" in a family of wavelets. They are used to compute the wavelet transform of a signal. If the mother wavelet $\psi(x)$ is regarded as a high pass filter, then the scaling function $\varphi(x)$ must be a low pass filter that covers the low-frequency components of the signal [43]. For such conditions, $\varphi(x)$ must have a mean of one. i.e.

$$\int_{-\infty}^{\infty} \varphi(x)\, dx = 1 \tag{2.8}$$

2.9. Discrete wavelet transforms

Wavelet transforms, particularly the discrete wavelet transform (DWT), are widely used in the multiresolution analysis of signals. This section presents a theory on discrete wavelet transforms (DWT). The presentation starts with an

introduction to the 1-D DWT and then the 2-D DWT used in the proposed algorithm.

2.9.1. One-dimensional DWT

The 1-D discrete wavelet transform decomposes a signal *f(x)* with length *M*, into two types of wavelet coefficients known as approximation and detail coefficients. As the name suggests, the approximation coefficients, denoted $W_\varphi(m_0, k)$, contain an approximate representation of the input, and it is obtained by a scaling function as shown in equation (2.9) [12],[44].

$$W_\varphi(m_0, k) = \frac{1}{\sqrt{M}} \sum_{k=0}^{M-1} f(x)\varphi_{m_0,k}(x) \tag{2.9}$$

where $\varphi_{m_0,k}(x)$ is the scaled and translated version of the scaling function $\varphi(x)$. The detail coefficients $W_\psi(m, k)$, given by equation (2.10), contain salient features that have been extracted from the input [12],[44].

$$W_\psi(m, k) = \frac{1}{\sqrt{M}} \sum_{k=0}^{M-1} f(x)\psi_{m,k}(x) \tag{2.10}$$

where $\psi_{m,k}(x)$ is the scaled and translated version of the wavelet $\psi(x)$. Given equations (2.9) and (2.10), an input signal can thus be represented as a linear combination of the wavelets and scaling function [12]. Also, the signal can be reconstructed by computing the inverse DWT of the approximation and detail coefficients, as given in equation (2.11).

$$f(x) = \frac{1}{\sqrt{M}} \sum_{k=0}^{M-1} W_\varphi(m_0, k)\, \varphi_{m_0,k}(x)$$

$$+ \frac{1}{\sqrt{M}} \sum_{m=0}^{M-1} \sum_{k=0}^{L-1} W_\psi(m, k, n)\, \psi_{m,k}(x)$$

$$(2.11)$$

where m_0 is an arbitrary starting scale, $W_\varphi(m_0, k)$ is the approximation coefficient, and $W_\psi(m, k, n)$ is a detail coefficient. The 1-D DWT can only be applied to 1-D signals. Therefore, to analyse two-dimensional signals such as digital images, the 2-D DWT is required.

2.9.2. Two-dimensional DWT

Similar to the 1-D DWT, the 2-D DWT decomposes a signal *f(x,y)* into sets of wavelet coefficients given by equations (2.12) and (2.13).

$$W_\varphi(j_0, m, n) = \frac{1}{\sqrt{MN}} \sum_{x=0}^{M-1} \sum_{y=0}^{N-1} f(x, y)\varphi_{j_0,m,n}(x, y)$$

$$(2.12)$$

$$W_\psi^{\,i}(j, m, n) = \frac{1}{\sqrt{MN}} \sum_{x=0}^{M-1} \sum_{y=0}^{N-1} f(x, y)\psi^i_{\,j,m,n}(x, y)$$

$$(2.13)$$

where $\varphi_{j_0,m,n}(x, y)$ is the scaled and translated version of the 2-D scaling function $\varphi(x, y)$; $\psi^i_{\,j,m,n}(x, y)$ for $i \in \{H, V, D\}$ are the scaled and translated versions of the 2-D wavelets $\psi^H(x, y)$, $\psi^V(x, y)$, and $\psi^D(x, y)$, which measure the signal variations in the horizontal, vertical, and diagonal directions respectively; while $W_\varphi(j_0, m, n)$ and $W_\psi^{\,i}(j, m, n)$ are the respective approximation and detail coefficients. As shown in equations (2.14) to (2.17), the 2-D scaling and wavelet functions are derived from the product of two 1-D basis functions [12],[44].

$$\varphi(x, y) = \varphi(x)\varphi(y) \tag{2.14}$$

$$\psi^{H}(x, y) = \psi(x)\varphi(y) \tag{2.15}$$

$$\psi^{V}(x, y) = \varphi(x)\psi(y) \tag{2.16}$$

$$\psi^{D}(x, y) = \psi(x)\psi(y) \tag{2.17}$$

Finally, the signal $f(x,y)$ can be reconstructed by calculating the inverse DWT as given in equation (2.18) [12],[44].

$$f(x, y) = \frac{1}{\sqrt{MN}} \sum_{m=0}^{M-1} \sum_{n=0}^{N-1} W_{\varphi}(j_0, m, n)\varphi_{j_0, m, n}(x, y)$$

$$+ \frac{1}{\sqrt{MN}} \sum_{i=H,V,D} \sum_{j=j_0}^{J-1} \sum_{m=0}^{M-1} \sum_{n=0}^{N-1} W_{\psi}^{i}(j, m, n)\psi^{i}_{j, m, n}(x, y) \tag{2.18}$$

2.10. Image fusion

The fundamental idea of image fusion is to combine features from two or more sources to form a composite image [47],[48]. The most basic image fusion techniques are maximum selection, minimum selection, and averaging. In the maximum and minimum selection methods, pixel intensity values are compared at each spatial position [48]. The highest or lowest value (in the case of minimum selection) is selected as the resulting pixel in the composite image. As for the averaging approach, the mean is calculated and used as the resultant pixel [48]. Following these basic techniques, advanced methods based on the multiresolution analysis of signals were investigated. Some of these methods included the Laplacian pyramid and DWT-based image fusion.

2.10.1. Laplacian pyramid-based image fusion

Image pyramids are data structures used for processing digital pictures at various spatial scales [48]. Two of the most widely used pyramids are the Gaussian and Laplacian [47],[48]. In many image processing applications, the low memory requirement of the Laplacian pyramid is more beneficial than the Gaussian.

A block diagram of the Laplacian pyramid-based image fusion is given in Figure 2.8. The first step in the procedure is to obtain the pyramid decomposition for images *A* and *B*. Next, a selection or averaging method is applied at each corresponding pyramid level. The fused image is generated by calculating the inverse pyramid transform of the fused pyramid.
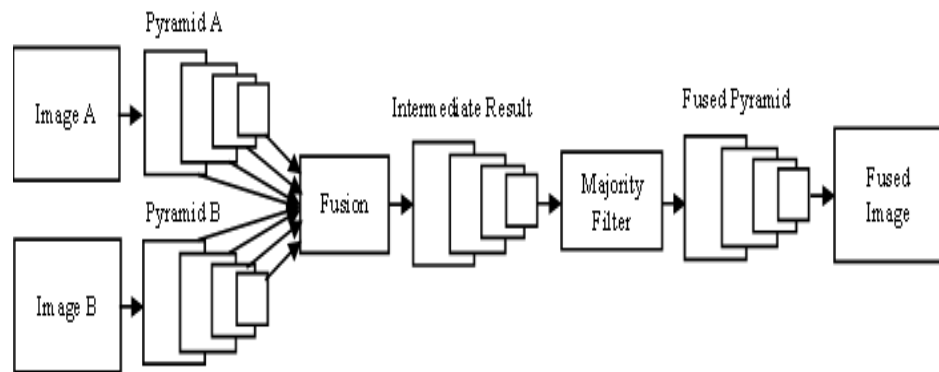
Figure 2.8. Laplacian pyramid-based image fusion [48]

2.10.2. Discrete wavelet transform-based image fusion

The DWT-based image fusion takes a similar approach to the Laplacian. However, instead of pyramid decomposition, the DWT fusion is based on wavelet decomposition [43]. Figure 2.9 shows a block diagram of a single-level DWT-fusion. The procedure begins with a wavelet decomposition of each input signal into four sub-bands, namely, low-low (LL), high-low (HL), low-high

(LH), and high-high (HH). The LL sub-band is calculated using equation (2.12) and it holds an approximate representation for each input. The HL, LH, and HH sub-bands are calculated using equation (2.13). These sub-bands contain salient features such as lines or edges. The composite image is finally obtained by computing the inverse DWT of the fused coefficients using equation (2.18).
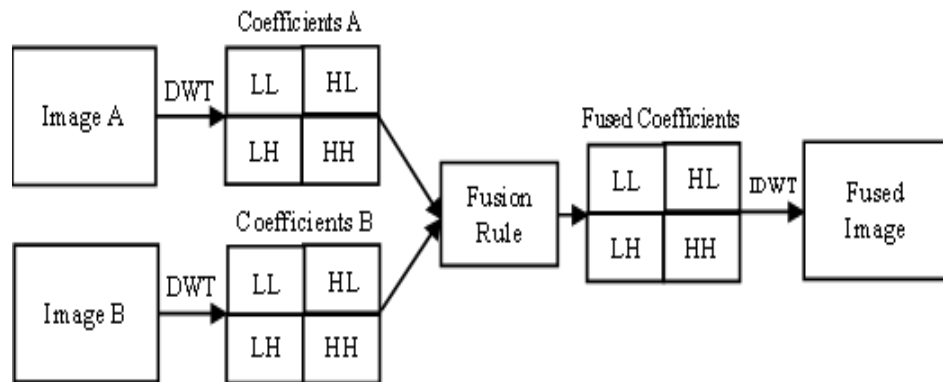
Figure 2.9. Single-level 2-D DWT image fusion [43]

2.11. Related works

Over the years, researchers have proposed several techniques for backlit image enhancement. They include contrast stretching, image fusion, and learning-based approaches. This section examines some of the contrast-stretching and image fusion techniques relevant to the development of the proposed method.

2.11.1. Contrast stretching approach

Trongtirakul et al. [1] proposed a single backlit image enhancement algorithm that employs a full-piecewise non-linear stretching function that improves the brightness discriminately in local regions of the backlit image [1]. The procedure begins with the decomposition of the input image luminance

component into under-exposed, over-exposed, and common regions via a set of thresholds. As given in equation (2.19), the threshold T separates backlit and common regions by calculating the relative local bright average of all intensities yielding the highest correlation of dark and bright components [1].

$$T = arg\ max_t \left(-\mu_t^{-d} log \left(\frac{\mu_t^{-d}}{\mu_t^{-b}} \right) \right) \tag{2.19}$$

where,

$$\mu_t^{-d} = \frac{\mu_t^d - min\{_t^d\}}{max\ \{_t^d\} - min\{_t^d\}} \quad \text{and}$$

$$\mu_t^{-b} = \frac{\mu_t^b - min\{_t^b\}}{max\ \{_t^b\} - min\{_t^b\}} \tag{2.20}$$

The parameters d, b, and t represent a dark component, a bright component, and the intensity level of an original backlit image, respectively. μ_t^{-d} and μ_t^{-b} are the normalized average brightness of the dark and the bright components. Next, pixels within the dark, bright, and common regions are stretched to occupy a wider range of grey levels using a set of non-linear functions given by equations (2.21) to (2.23) [1].

$$S_{i,j} = \begin{cases} f^d(I_{i,j}), & 0 < I_{i,j} \le x_t \\ I_{i,j}, & x_t < I_{i,j} \le x_o \\ f^d(I_{i,j}), & x_o < I_{i,j} \le x_{L-1} \end{cases} \tag{2.21}$$

$$f^d(I_{i,j}) = \left(S_{max}^d - S_{min}^d \right) \left(\frac{I_{i,j} - I_{min}^d}{I_{max}^d - I_{min}^d} \right)^{\gamma_\alpha} + I_{min}^d \tag{2.22}$$

$$f^b(I_{i,j}) = \left(S_{max}^b - S_{min}^b \right) \left(\frac{I_{i,j} - I_{min}^b}{I_{max}^b - I_{min}^b} \right)^{\gamma_\beta} + I_{min}^b \tag{2.23}$$

where $I_{i,j}$ represents a backlit luminance at any i^{th} and j^{th} pixel placement. x_t and x_o define the backlit and common regions, respectively, while x_L is the

31

maximum grey level. I^d_{min}, I^b_{min}, I^d_{max}, and I^b_{max}, represent the minimum and maximum luminance of under-exposed regions and exposed regions. The functions S^d_{min}, S^b_{min}, S^d_{max}, and S^b_{max}, are the new minimum and maximum intensities of under-exposed regions and exposed regions, respectively. The coefficients γ_α and γ_β are used for contrast correction $(0 < \gamma_\alpha < \gamma_\beta < 1.0)$[1].

A logarithmic function was used to calculate the brightness level of the Bi-Histogram Equalization (BHE) mapping function T_t using equation (2.24) [1].

$$F_t = \rho T_t + (1 - \rho)\log(T_t); \qquad for \ \ 0 \leq \rho \leq 1 \qquad (2.24)$$

Equation (2.24) is a logarithmic weighted luminance function, where ρ is a weighting parameter. Finally, to achieve the final enhanced image, Trongtirakul et al. [1] defined a minimal weighting fusion metric that combines two image features into the same image. This was achieved by equation (2.25) [1].

$$[Y_{EN}]_{i,j,k} = [\sigma_{min}]_{i,j,k}[Y_{LBHE}]_{i,j,k} + [1 - \sigma_{min}]_{i,j,k}[Y_{LHE}]_{i,j,k} \qquad (2.25)$$

where (Y_{LBHE}) represents the logarithmic image, which is characterized by having uniform brightness in both backlit and common regions and (Y_{LHE}) represents the local enhanced image, which improves the details in backlit sectors as well as the overall contrast. The function $[\sigma_{min}]_{i,j,k}$ specifies a normalized minimal luminance metric that considers the lowest intensity of the original backlit image [1].

The approach by Trongtirakul et al. [1] has several limitations. First, well-lit areas in the background appear to be over-enhanced in the final image. Next is the use of thresholding to distinguish between foreground and common regions.

This is a drawback because thresholding methods are sensitive to unintended and uncontrolled changes in the light field. They require that the intensities of objects in the foreground are distinguishable from those in the background [49],[50].

Other contrast stretching techniques include Yelmanov et al. [51] and Toh et al. [37]. Yelmanov et al. [51] employed an adaptive non-linear contrast stretching approach using a piecewise non-linear transformation function to enhance images in an automatic mode. Toh et al. [37] focused on the use of High Dynamic Range (HDR) rendering and contrast stretching techniques to enhance images captured during the diagnosis of acute leukaemia. Although the application scenarios of these approaches are different, the stretching functions proposed in these works can be used to enhance backlit images. However, in terms of visual quality, they do not produce superior results compared to Trongtirakul et al. [1].

2.11.2. Histogram specification approach

Ueda et al. [39] proposed a "straightforward" histogram specification-based technique to enhance backlit images. In this approach, foreground-background segmentation is first performed using a linear discriminant analysis (LDA) threshold [41], which is then used to obtain the triangular target histogram shown in Figure 2.10(a). The goal was to convert the intensity of the backlit image via histogram specification. However, the conversion between the foreground and background scenes was observed to be unbalanced. Therefore, they employed two modified target histograms, Target 1 and Target 2, as shown in Figures 2.10(b) and 2.10(c). Target 1 was obtained by equalizing the ratio of

background and foreground regions with the area ratio of the input image, while
Target 2 was obtained by making the foreground region the same shape as the
input image histogram [39].
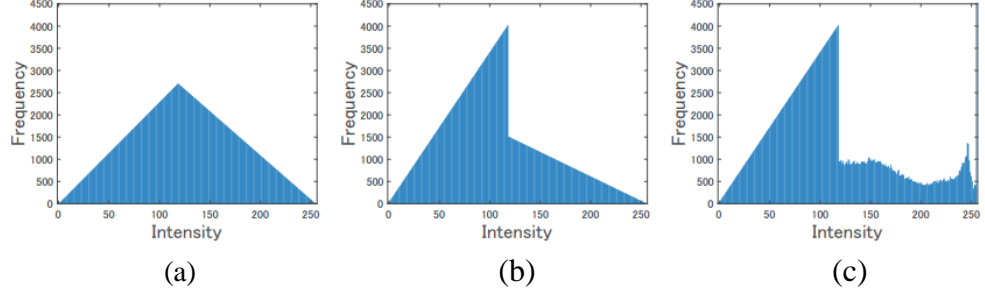
Figure 2.10. Target histograms proposed by Ueda et al. [39]. (a) Basic shape
(b) Target 1 (c) Target 2 [39]

The intensity conversion is given by equation (2.26). The result is an
intensity image I_{ij} obtained from an input colour image $x_{ij} = (x_{ij}^R, x_{ij}^G, x_{ij}^B)$ [36].

$$I_{ij} = \frac{(x_{ij}^R + x_{ij}^G + x_{ij}^B)}{3} \tag{2.26}$$

Next, the histogram specification of the intensity image with respect to the
target histogram was computed using equation 2.27.

$$I_{ij}^{HS} = \inf\{z | H(I_{ij}) \leq H^{tar}(z)\}, \tag{2.27}$$

where H and H^{tar} represent the normalized cumulative histogram of an input
image and the target histogram, respectively. Alpha blending, given by equation
(2.28), was used to compensate for intermediate low-contrast values [39].

$$\alpha = min\left\{1, \left|\frac{M_{ij}-\bar{I}}{\bar{I}}\right|\right\}, \tag{2.28}$$

where M_{ij} represents a Gaussian-filtered version of I_{ij}, having a radius of r
and $\bar{I}$ is a mean of I_{ij}. Following the alpha blending, a desirable conversion
coefficient was obtained by equation (2.29) [39].

$$I'_{ij} = \alpha I_{ij}^{HS} + (1 - \alpha)I_{ij}, \tag{2.29}$$

The intensity conversion is achieved by equation (2.30).

$$x'_{ij} = \frac{I'_{ij}}{I_{ij}} x_{ij} \tag{2.30}$$

To produce an enhanced backlit image with hue and saturation preserved, the algorithm searches for a point on a constant-hue plane in an RGB colour space with an intensity of I'_{ij} and saturation of x''_{ij}. The saturation d_{ij}, given by equation (2.31), was used to compute the saturation of x_{ij} [39].

$$d_{ij} = \sqrt{\frac{\left(x^R_{ij} - x^G_{ij}\right)^2 + \left(x^G_{ij} - x^B_{ij}\right)^2 + \left(x^B_{ij} - x^R_{ij}\right)^2}{3}} \tag{2.31}$$

The method proposed by Ueda et al. [39] has several limitations. The use of thresholding for segmentation is one of the drawbacks. Thresholding techniques have proven effective in a variety of applications; but, as described in [49], they do not account for spatial interactions between pixels and are vulnerable to unintended and uncontrolled changes in the light field in general. Furthermore, the target histograms used by [39] produce washed-out and unnatural hues. To minimize noise and prevent colour artefacts in the enhanced image, more processing is required. Lastly, the method increases details in both the foreground and the background without distinction. As a result, the well-exposed regions of the image are further exaggerated.

2.11.3. Image fusion approach

Over the years, fusion-based image enhancement technologies have received a lot of attention. The basic idea of image fusion is to combine features from

two or more images to form a composite image [52]. Wang et al. [47] proposed a fusion-based method for single backlit image enhancement using a multi-scale fusion approach. In this work, they combined three derived input images, each with a different weighted map, to form a single final image. Pre-processing was done on the input backlit image to derive three unique input images. This included converting the image from RGB to HSV colour space and improving luminance and contrast using a logarithm function and a gamma correction function [47]. The three input images and their weight maps were then fused using a multi-scale fusion approach proposed by Burt et al. [53].

Buades et al. [54] proposed a fusion-based method using global tone mappings and image fusion. In this approach, the tone mapping functions given in equations (2.32) and (2.33) were first applied to each colour channel of the input image.

$$G(\gamma)(I) = 255\left(\frac{I}{255}\right)^{\gamma}, \qquad \gamma \in \{0.4, 0.6, 0.8, 1, 2, 3\} \tag{2.32}$$

$$L(\alpha)(I) = \frac{255\log(\alpha I + 1)}{\log(255\alpha + 1)}, \qquad \alpha \in \{0.1, 0.2, 0.3, 0.\} \tag{2.33}$$

where I is the original RGB image and $G(\gamma)$ and $L(\alpha)$ are the gamma and the logarithmic tone mapping functions used to increase or decrease the overall luminance in the image depending on the value of γ and α, respectively [53]. Next, the images obtained by equations (2.31) and (2.32) were then combined using a variation of Merten's algorithm [54]. The fused image was sharpened to improve contrast. Finally, a chrominance correction procedure which attempts

to recover the original colours of the input image is used to create the final image [54].

Another approach was proposed by Li et al. [55]. In their work, they employ a pair of complementary gamma functions to enhance contrast in the under- and over-exposed sectors of the backlit image as follows:

$$y_1 = 1 - (1 - x)^\gamma \tag{2.34}$$

$$y_2 = (1 - (1 - x)^{1/\gamma})^\gamma \tag{2.35}$$

where x is the normalized input intensity image in the HSV colour space, and y_1 and y_2 are the normalized output images. The attributes of y_1 and y_2 are dependent on the coefficient γ. Using naive blending, the enhanced image y was derived as follows [55].

$$y = c_1 y_1 + c_2 y_2 \tag{2.36}$$

where y_1 and y_2 are the images obtained from equations (2.34) and (2.35), respectively. The parameters c_1 and c_2 are the weighting factors which are obtained by equation (2.37) [55].

$$c_i = \frac{\overline{V}_i}{\sum_i \overline{V}_i}, \qquad for\ i \in \{1,2\} \tag{2.37}$$

where $\overline{V}_i$ is the mean value of the image y_i. A fusion process is used to combine the output of equation (2.36) with a sharpened copy of the original input intensity image. The final enhanced colour image is produced by converting the fused HSV image to RGB.

Each method discussed in this section can improve contrast in the under- and over-exposed regions of the backlit image. The major drawback to these

approaches, however, is the high dependency on the choice of input and weight maps. This acts as a constraint, such that if the incorrect inputs and weight maps are used, the algorithm will not achieve the desired result [47]. Another drawback particular to the method proposed by Buades et al. [54] is the use of a chrominance correction algorithm to restore the original colour profile of the input. A better approach would be to extract and process only the luminance component of the input image, as demonstrated by Wang et al. [47] and Li et al. [55].

2.11.4. Learning-based approach

In recent years, supervised learning algorithms have seen some applications in backlit image enhancement. Li et al. [56] proposed a spatially adaptive learning-based algorithm to enhance a single backlit image using optimal tone mappings and image fusion. In this approach, a soft binary classifier based on two support vector machines (SVMs) is used to segment backlit and front-lit regions. Next, two unique tone mapping functions are employed to improve details in the backlit and front-lit areas of the image. The mapping functions are generated by maximizing contrast gain with bounded aberrations in tone and chromaticity. Finally, the results obtained by the two mapping functions are fused to form the final enhanced image [56].

The primary drawback with learning-based methods, in general, lies within their computational complexities. As a result, they cannot be implemented directly on cell phones. Another drawback particular to the method proposed by Li et al. [56] is the accuracy of the binary classifier in separating the front-lit and backlit regions of images with shadows and dark-coloured surfaces. In such

cases, the output of the classifier is frequently ambiguous [56]. The method proposed in this thesis takes a better approach that avoids image segmentation to improve the enhancement quality and reduce the algorithm's computational complexity.

2.12. Knowledge gaps

This research investigation exploits several gaps in the related works to develop a flexible, fast, and robust algorithm that achieves an enhancement quality comparable to state-of-the-art techniques but at a significantly lower cost of computation.

The first gap identified is based on exposure correction. Exposure correction has not been centric on the development of contrast stretching and image fusion-based techniques. In the related works on contrast stretching, no attempts have been made to balance the overall exposure in the output image after enhancements are done locally in the foreground scenes. Additionally, the image fusion-based approaches have not considered the variations in luminance from one backlit input to another since the same set of transformation functions proposed in each related work is consistently applied to all inputs regardless of the type of backlit degradation. These constraints have been enforced in this research investigation in such a way that the mapping functions generated by the proposed algorithm automatically adapt to the luminance profile of the backlit input image.

The second gap is as follows: Histogram-based approaches are known to be less computationally expensive compared to the pixel-wise contrast-stretching and image fusion algorithms, but they frequently result in over-saturation,

colour distortion, and washed-out hues when directly applied to backlit images. These effects however have not been addressed in previous methods. Moreover, a generalized framework for obtaining optimal target functions and handling low brightness problems in Histogram matching scenarios for backlit image enhancement has not been thoroughly investigated.

CHAPTER 3

METHODOLOGY

This chapter is divided into three sections. Section 3.1 presents the materials used in the research investigation. The materials include hardware and software resources and the dataset used for testing the performance of the proposed method. The methodology of the proposed enhancement algorithm is presented in section 3.2, and the image quality metrics used to validate its performance are discussed in section 3.3.

3.1. Materials

The section describes the hardware and software materials used in the research investigation.

3.1.1. Hardware

The hardware resources include:

(i) Dell XPS 15-9500 laptop [57]: The laptop has 32GB of RAM, a 2.60GHz Intel Core i7 processor, and a 1TB Solid State Drive (SSD) loaded with Microsoft Windows 10, 64-bit operating system. The hardware served as a processing and data storage unit.

(ii) Samsung Galaxy A7 smartphone [58], released 2018: The Galaxy A7 has 4GB RAM, a 24-megapixel rear camera equipped with the Sony IMX576 CMOS sensor, and operates on the Google Android 8.0 (Oreo) operating system. The device was used to collect backlit image samples for testing. Although this model has been discontinued, the Galaxy A7 acts as a baseline for current smartphone performance.

(iii)   Dell DA20 USB type-C to type-A v3.0 adapter: The Dell DA20 USB adapter [57] was used to transfer image data from the Samsung Galaxy A7 smartphone to the Dell XPS 15-9500 laptop because it uses only USB type-C ports.

3.1.2. Software

The proposed enhancement algorithm in this thesis was developed and tested using MATLAB R2018a software. MATLAB is a programming platform used worldwide by scientists and engineers for designing and analysing systems [21]. MATLAB R2018a was selected because it is readily available and offers various in-built toolboxes for image processing, image fusion, and wavelet analysis.

3.1.3. Data sources

The dataset for this thesis is comprised of 162 low-quality images with an 8-bit resolution. The Samsung Galaxy A7 was used to record 44 backlit samples in the dataset. Twenty-four (24) samples were selected from the widely used Li's database [2], which comprises over 38 standard backlit photos that have been used in similar research. In addition, 88 samples were taken from the Exclusively Dark (ExDark) database [59], which contains 7,363 images captured in various poor lighting situations. The remaining six (6) were obtained from internet sources [60]-[62].

The images were classified into four categories based on their backlit degradation. The categories were: low backlit sector, high backlit sector, low background highlight, and high background highlight, as shown in Figure 3.1.

The low backlit sector category contained 36 backlit images characterized by a well-lit background and soft shadows in the foreground. Conversely, the high backlit sector featured 29 images with a well-lit background and hard shadows in the foreground. The low background highlight category included 73 images with significantly lower background radiance, whereas the high background highlight category comprised 24 images with high background radiance. Images in the high backlit sector category are prone to shadow clipping. Similarly, highlight clipping is common in images with a high background highlight.
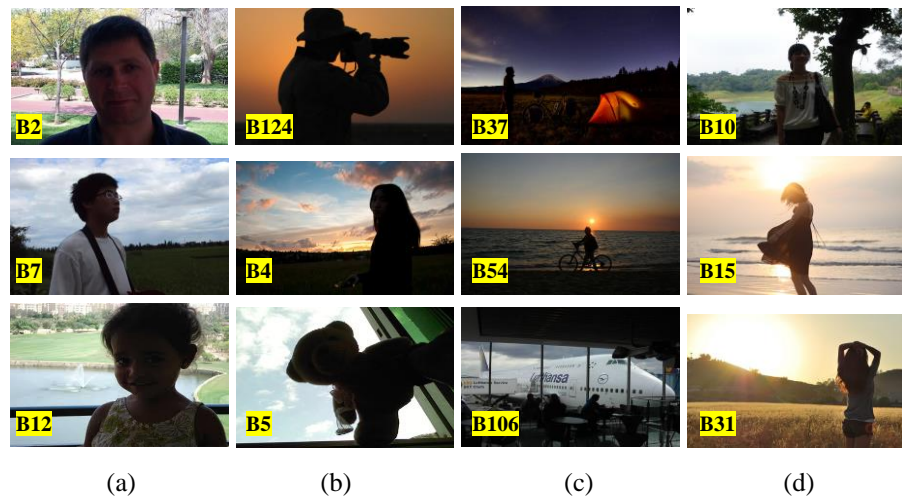
Figure 3.1. Classification of backlit images (a) low backlit sector, (b) high backlit sector, (c) low background highlight, and (d) high background highlight.

3.2. Methods

This section presents the proposed algorithm. Subsection 3.2.1 deliberates on the enhancement procedures. Section 3.2.2 discusses the optimization of the DWT fusion, and 3.2.3 introduces an iterative procedure that further improves the enhancement quality of the proposed algorithm.

3.2.1. The proposed method

The proposed method integrates a region-based histogram specification (RBHS) scheme with the discrete wavelet transform (DWT) image fusion to improve the visual quality of a single backlit image. Figure 3.2 and Figure 3.3 describes the proposed procedure. Figure 3.2 gives a summary of the overall procedure while Figure 3.3 is the architecture of the system relating each process to the input and output. The two descriptions provide useful insight into the enhancement algorithm. The key steps are:

Step (i):   Pre-processing the input image

Step (ii):   Generation of target histograms

Step (iii): Enhancement of F- and B- regions

Step (iv):   Adaptive brightness control

Step (v):   Fusion of input masks with the backlit input image.

These steps are further illustrated in the block diagram of Figure 3.2 and more details are provided in Figure 3.3.

```
┌─────────────────────────────────────────────────────────────────┐
│                      Input Backlit Image                         │
└─────────────────────────────────────────────────────────────────┘
                              │
                              ▼
┌─────────────────────────────────────────────────────────────────┐
│            Convert RGB to HSV and Decouple V-Channel             │
└─────────────────────────────────────────────────────────────────┘
                              │
                              ▼
┌─────────────────────────────────────────────────────────────────┐
│                 Create Input Mask M₁ and M₂                      │
└─────────────────────────────────────────────────────────────────┘
                              │
                              ▼
┌─────────────────────────────────────────────────────────────────┐
│          Generate Target Histograms Tar₁(z) and Tar₂(z)          │
└─────────────────────────────────────────────────────────────────┘
                              │
                              ▼
┌─────────────────────────────────────────────────────────────────┐
│   Enhance F- and B- regions using Region-based Histogram Spec.   │
└─────────────────────────────────────────────────────────────────┘
                              │
                              ▼
┌─────────────────────────────────────────────────────────────────┐
│          Apply Adaptive Brightness Control on M₁ and M₂          │
└─────────────────────────────────────────────────────────────────┘
                              │
                              ▼
┌─────────────────────────────────────────────────────────────────┐
│             Recouple HSV' Channels in M₁ and M₂                  │
└─────────────────────────────────────────────────────────────────┘
                              │
                              ▼
┌─────────────────────────────────────────────────────────────────┐
│                       Convert HSV' to RGB                        │
└─────────────────────────────────────────────────────────────────┘
                              │
                              ▼
┌─────────────────────────────────────────────────────────────────┐
│        Fuse F- and B- Masks with Backlit Input via DWT Fusion    │
└─────────────────────────────────────────────────────────────────┘
                              │
                              ▼
┌─────────────────────────────────────────────────────────────────┐
│                      Enhanced Image Output                       │
└─────────────────────────────────────────────────────────────────┘
```

Figure 3.2. A block diagram illustrating the proposed method
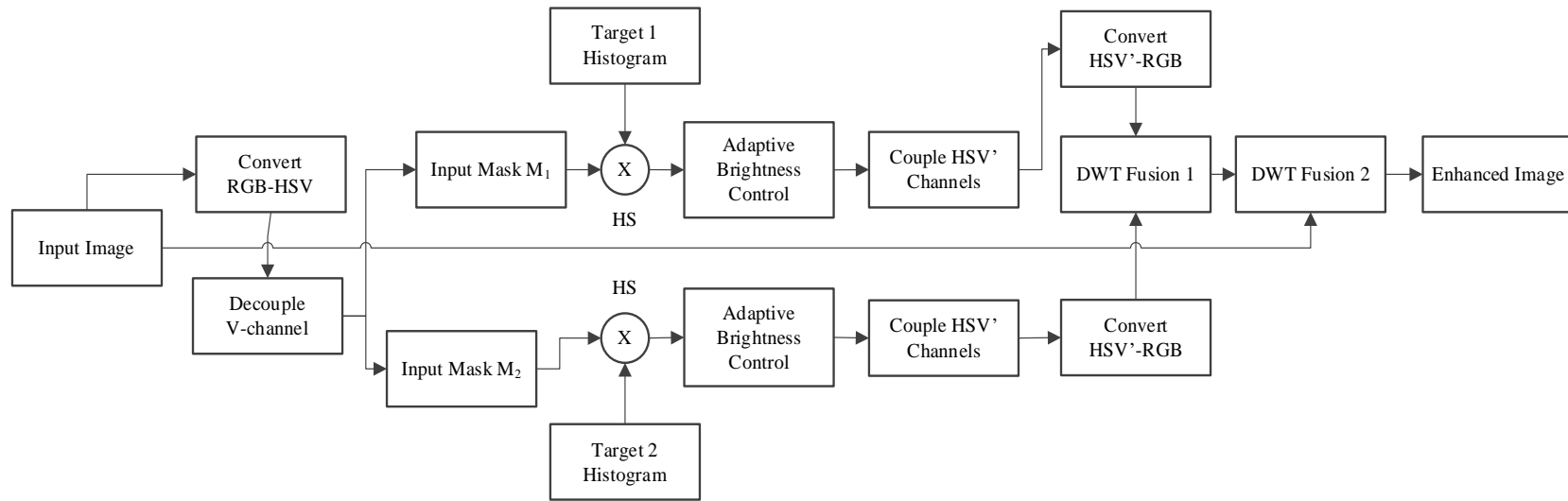
Figure 3.3. System Architecture of the proposed method

(a) Pre-processing of input image

Colour space conversion and input masking are the two major tasks realized in the pre-processing step. First, the RGB to HSV transformation [63] is performed on the backlit input image, denoted $I = (x^R, x^G, x^B)$. The transformation yields the resultant image $I' = (x^H, x^S, x^V)$, which represents the hue, saturation, and value properties of the backlit input. Two input masks M_1 and M_2, are then created using identical copies of the value or intensity image I'_v. Histogram specification will be performed discriminately on M_1 and M_2 to improve contrast in the under-exposed and over-exposed regions of I'_v.

(b) Generation of target histograms

The proposed algorithm enhances the F- and B- regions of a single backlit image using two unique target histograms, Target 1 and Target 2. The shapes of these histograms affect the output quality of the proposed algorithm. Therefore, generating the appropriate contours is a crucial step. In this thesis, a simple but intuitive approach is adopted to obtain the target histograms in Figure 3.4 from typical images. Target 1 in Figure 3.4(a) is obtained from a well-lit, high-contrast image, with no peaks in the dark and light tones of its histogram and Target 2 in Figure 3.4(b), from a relatively low-light photo with peaks in the dark tones but none in the lightest tones. Such selection for Target 1 is expected to enhance details in the under-exposed F-region at the expense of lowering contrast in well-lit areas, while Target 2 is expected to reduce high radiance in the over-exposed sectors of the B-region at the cost of exaggerating under-exposure in the F-region.
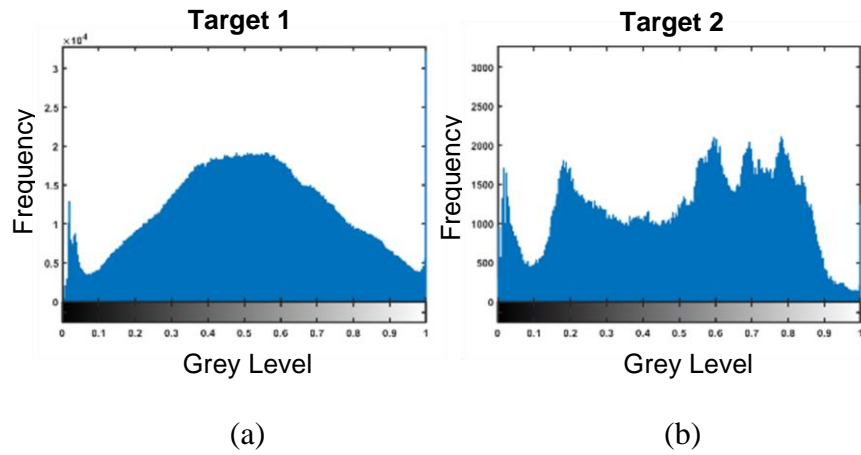
Figure 3.4. Target Histograms (a) Target 1 (b) Target 2

(c) Enhancement of F- and B- regions

The enhancement of the foreground and background regions is achieved by applying the region-based histogram specification (RBHS) scheme illustrated in Figure 3.5.
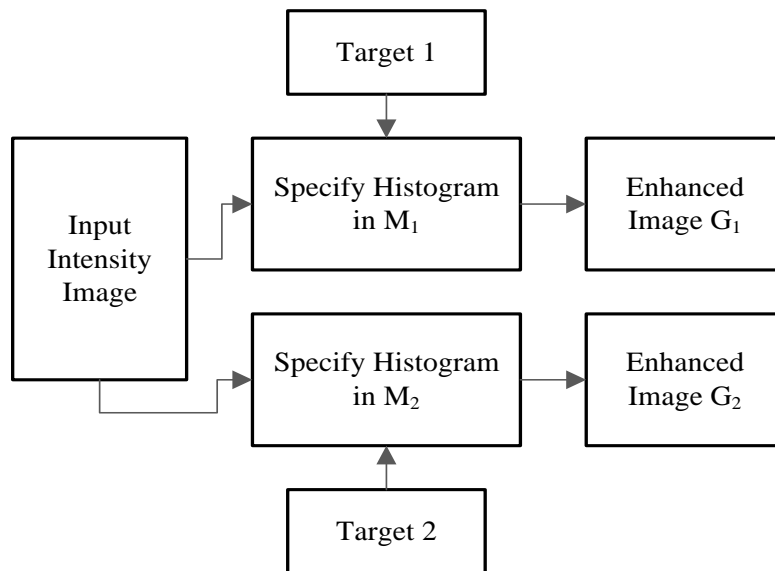
Figure 3.5. Region-based Histogram Specification Scheme

In Figure 3.5, the grey levels of the backlit input intensity image are mapped to that of the target histograms in Figure 3.4 using equation (3.1).

$$G_k(x, y) = HS\{I'_v(x, y), Tar_k(z)\} \qquad (3.1)$$

where $G_k(x, y)$ is the histogram-specified image of the input mask M_k, obtained by the target $Tar_k(z)$, for $k \in \{1,2\}$. The mappings are based on generalization. This means, the grey-level distribution in $G_k(x, y)$ only approximates the shape of the target $Tar_k(z)$. This flexibility, however, permits the proposed method to be employed in other types of poor illumination situations, such as low lighting.

Figure 3.6 displays the outcome of applying equation (3.1) on a sample backlit image. Figure 3.6(a) is the input intensity image and Figures 3.6(b) and 3.6(c) are the outputs of M_1 and M_2, respectively. As expected, the result of M_1 have higher contrast in the F-region than M_2. This is evident when comparing the facial details of the man in Figures 3.6(b) and 3.6(c). On the other hand, high radiance is suppressed in the output of M_2, for example, in areas such as the pavement and the sky.

(a) (b) (c)
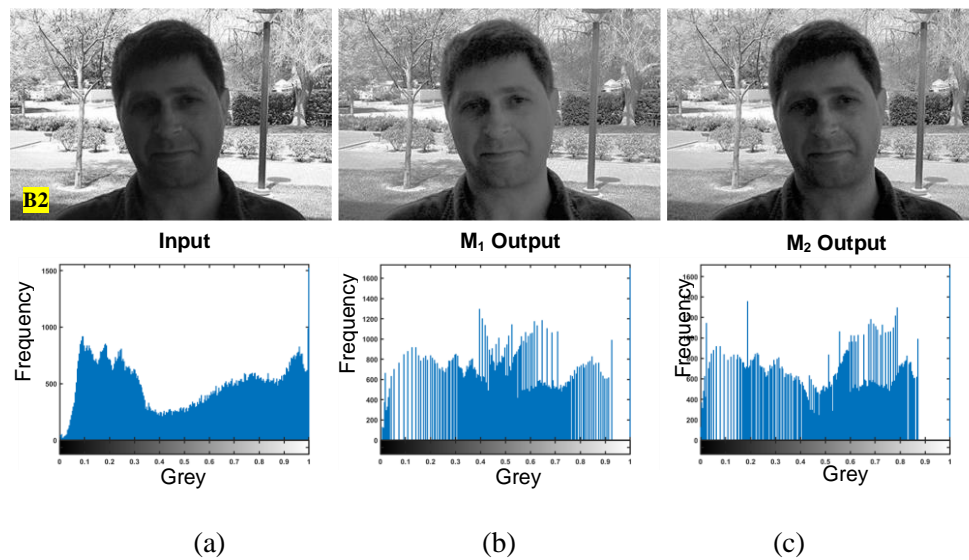
Figure 3.6. RBHS on sample backlit image (a) Intensity image (b) M1 output (c) M2 output

(d) Adaptive brightness control

The histogram specification of the input masks can result in low brightness problems in the final enhancement stages. This problem occurs due to the shifting of pixel intensity values in the lightest tones to darker shades of grey as shown in the output histograms of Figures 3.6(b) and 3.6(c). Therefore, to compensate for this loss, an adaptive brightness control (ABC) mechanism is employed. The term "adaptive brightness control" or "automatic brightness control" is often associated with the automatic adjustment of a display panel's brightness level based on the ambient light environment [64]. This method is used mostly as an energy-saving feature in smartphones, tablets, and digital television systems [64],[65]. On the contrary, ABC is defined in this thesis as a method of automatically compensating for low brightness in the input masks after RBHS is performed. Though the nomenclatures are the same, the differences rest within the methods and applications.

Figure 3.7 describes the proposed ABC algorithm. The algorithm addresses the problem of low brightness in an input mask by increasing pixel intensity values by a factor α, known as the adaptation factor. The value of α is determined by the brightness level of the input. Currently, there is no conventional method for measuring brightness levels in digital images, despite the various approaches suggested [41],[66],[67]. Furthermore, brightness, as defined by Wyszecki et. al [68], is subjective as well as its perception by a human viewer. Taking these two accounts into consideration, the proposed algorithm selects a value of α based on the subjective judgment of the input's illumination.
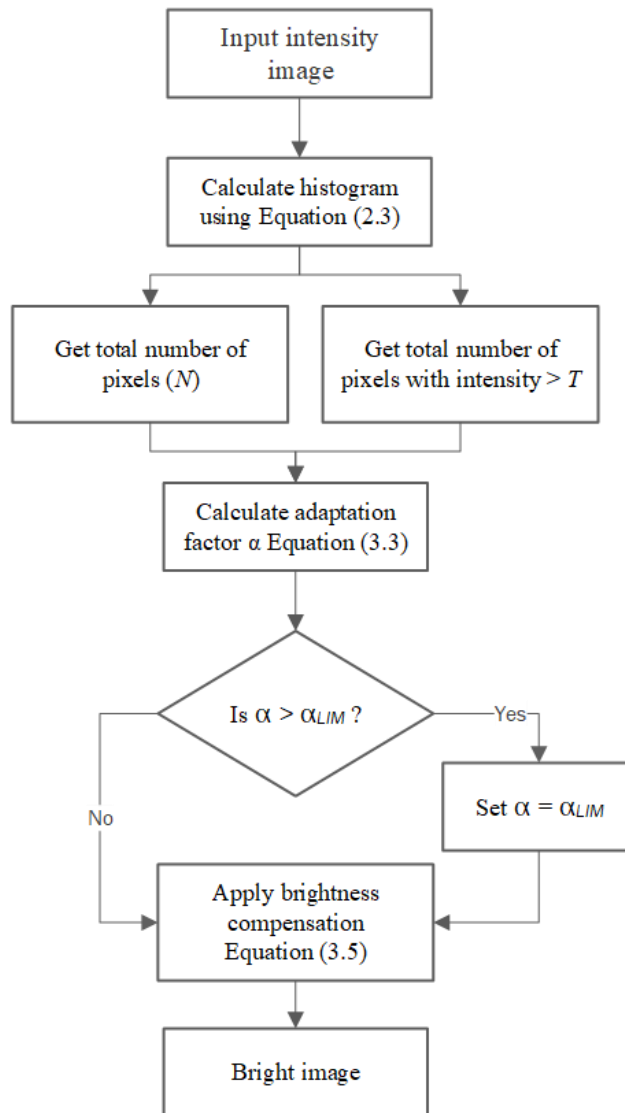
Figure 3.7. Adaptive Brightness Control (ABC)

(i) Brightness threshold

In Figure 3.7, the threshold T defines a minimal point of perceived brightness on the intensity spectrum of an input's histogram. A pixel with an intensity value greater than T is considered a bright element, denoted as ϕ^b. i.e., it contributes primarily to the lightness of the image. Mathematically, a bright element is defined by equation (3.2).

$$\phi^b = \begin{cases} 1, & if\ L - 1 \geq I_v'(x,y) > T \\ 0, & if\ I_v'(x,y) \leq T \end{cases} \tag{3.2}$$

where $I_v'(x,y)$ is an input intensity value and $L = 2^n$ is the maximum grey level of the input determined by its bit-depth (n). The value of T must correlate with the range of grey levels in I_v' since it depends on the bit-depth of the input.

To assign a weight to the variable T, the threshold methods proposed by Otsu [41] and Trongtirakul [1] were investigated. These methods provide a basis for image segmentation, but they proved inadequate for the nature of brightness compensation because they extend to a broader range of grey levels beyond the lightest tones. As a result, this thesis employed a simple but intuitive approach to obtain the value T.

According to digital imagery, the luminous scale in a histogram estimates the brightness level of each pixel as a percentage [69]. A normalized histogram will scale from 0% brightness (black) to 100% brightness (white) with the shadow region comprising 0% to 25%, while the highlights range from 75% to 100%, approximately [68]. Since high-intensity values localize in the highlight region, T can be defined by experimenting with various thresholds in the range of $[75\% - 100\%]$. The effects of various values of T are depicted in Figure 3.8.

$T = 75\%,$	$T = 78\%$	$T = 81\%$	$T = 84\%$
$T = 87\%$	$T = 90\%$	$T = 94\%$	$T = 96\%$
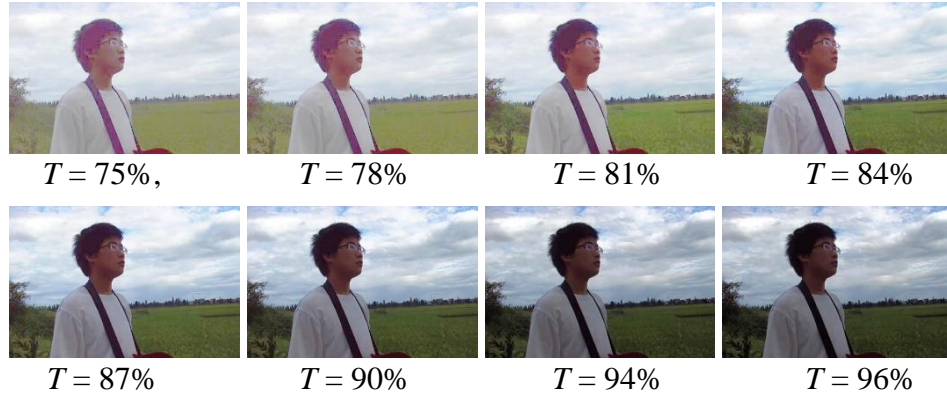
Figure 3.8. Some selected values for brightness threshold

As shown in Figure 3.8, the values of $T > 94\%$ cause no significant improvement in the perceptual quality of the backlit image, while values below 90% lead to noise and washed-out hues in the enhanced output. These observations indicate that high values of T result in better image quality. Therefore, after performing a series of experiments with values between [90%, 94%], the brightness threshold T was desired at 94% brightness. This is given as $hsv(0°, 0\%, 94\%)$ and $rgb(240,240,240)$ in the HSV and RGB colour models, respectively. Therefore, on the histogram spectrum, pixels with intensity levels greater than $T = 240$ are considered bright elements.

(ii) Adaptation factor

The adaptation factor determines the magnitude of brightness compensation, and it is computed using equation (3.3). Given the additive nature of the ABC procedure, values of α must occur between $0 \leq \alpha < 1$ to correspond to the input mask's normalized intensity values.

$$\alpha = \frac{N}{(N-n)} - 1 \qquad (3.3)$$

$$n = \sum_{k=0}^{L-1} H_v(r_k > T) \tag{3.4}$$

where H_v is the histogram of I'_v, N is the total number of pixels in the input; r_k is an input intensity in the range $[0, L-1]$; and n, given by equation (3.4), is the sum of pixels within bins $H_v(r_k > T) = \phi^b$.

Table 3.1 shows the values of α for some selected backlit images which are shown in Figure 3.1.

Table 3.1. Adaptation factor for selected backlit input

No.	Test Image	Size	n	α
01	Backlit 2.jpg	448 x 296	16,627	0.1434
02	Backlit 5.jpg	375x300	23,411	0.2628
03	Backlit 7.jpg	480x316	9,559	0.0673
04	Backlit 10.jpg	600x450	75,177	0.3959
05	Backlit 15.jpg	480x320	45,239	0.4175
06	Backlit 124.jpg	1120x700	951	0.0012

(iii) Brightness compensation

Brightness compensation is achieved in an input mask by shifting pixel intensity values to the right (highlight region) of the histogram by the adaptation factor α obtained in equation (3.3). The relationship is given in equation (3.5).

$$G'_k(x,y) = \alpha + \sum_{i=1}^{x} \sum_{j=i}^{y} G_k(x,y), for\ k = 1,2 \tag{3.5}$$

where $G_k(x,y)$ is the histogram-specified image of an input mask M_k, and $G'_k(x,y)$ is the ABC output image that is coupled with the hue and saturation channels of the backlit input. The RGB output image for M_k is obtained by the HSV to RGB transformation [63] of $G'_k(x,y)$.

54

(iv) Alpha-clipping

Brightness over-compensation was observed to be a common problem in images with many bright elements. The overcompensation is caused by relatively high α values, which frequently results in colour oversaturation in the input masks. To address this problem, the concept of alpha-clipping is introduced in the ABC process. Letting α_{LIM} be a limiting parameter, all values from equation (3.3) greater than α_{LIM} are clipped, as shown in Figure 3.7. The parameter α_{LIM} is desired at 0.23. Values of α greater than 0.23 may result in excessive brightness for backlit images containing many bright elements. This phenomenon can be observed in Figure 3.9 which shows the α values for the various brightness thresholds displayed in Figure 3.8.

| $\alpha = 0.99$ | $\alpha = 0.88$ | $\alpha = 0.68$ | $\alpha = 0.51$ |
| $\alpha = 0.33$ | $\alpha = 0.21$ | $\alpha = 0.07$ | $\alpha = 0.04$ |
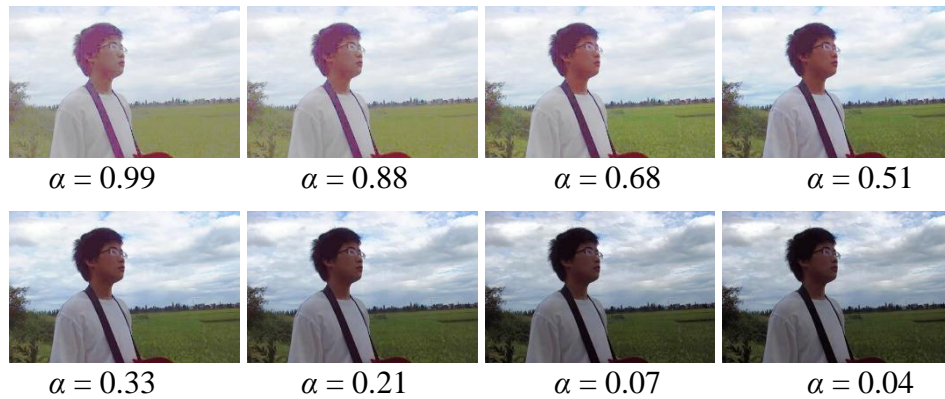
Figure 3.9. Brightness compensation for various values of α

(e) Fusion of F- and B- masks with backlit input

The input masks M_1 and M_2 can also be referred to as the foreground (F) and background (B) masks, respectively. This is because M_1 contains the desired foreground information to be extracted from the backlit input, whereas M_2, the improved background details. The combination of M_1 and M_2 with the backlit input is achieved using the discrete wavelet transform method of image fusion.

This method is preferred because it has proven effective in suppressing colour artefacts [70]. In the next section, a straightforward single-stage DWT fusion is presented followed by the proposed two-stage DWT process that yields the final enhanced image.

(i) Single-stage DWT fusion

Figure 3.10 is a pseudo-code that illustrates a straightforward fusion of two RGB images, I_1 and I_2, based on a given wavelet function $\psi_{a,b}(x, y)$. The procedure begins with the 2-D wavelet decomposition of the input channels z^i as given by equation (3.6).

$$[cA_k, cH_k, cV_k, cD_k]^i = DWT\{I_k(z^i), \psi_{a,b}(x, y)\} \qquad (3.6)$$

where cA_k is the approximation coefficient matrix; cH_k, cV_k, and cD_k, are the horizontal, vertical, and diagonal detail coefficient matrices, respectively. The variable $k \in \{1, 2\}$ and $i \in \{R, G, B\}$. Each input I_k will yield a sum of 12 wavelet coefficients, 4 obtained from each colour channel and their combined sum equivalent to 24. Following equation (3.6), the mean $\bar{X} = \frac{\Sigma X}{N}$ is computed for each I_1 and I_2 channel pair as shown in Figure 3.10. This procedure yields an average feature vector $\bar{X}^i \leftarrow [cA, cH, cV, cD]^i$ for each colour channel $[i]$, reducing the total number of wavelet coefficients to 12. Using equation (3.7), the composite image for each colour channel is obtained.

$$\theta^i = IDWT\{\bar{X}^i, \psi_{a,b}(x, y)\} \qquad (3.7)$$

where $\bar{X}^i$ is the mean vector of the coefficient matrices $[cA, cH, cV, cD]^i$; $\psi_{a,b}(x, y)$ is the wavelet type used to decompose the inputs; and θ^i is a

greyscale output image. Finally, merging the RGB channels $(\theta^R, \theta^G, \theta^B)$

produces the fused image θ.

% Pseudo code for a single-stage dwt fusion

Input: $I_1 = (x^R, x^G, x^B)$; $I_2 = (y^R, y^G, y^B)$;
Wavelet-type: $\psi_{a,b}(x, y)$;
Result: $\theta(rgb)$;
for each Input $k \in \{I_1, I_2\}$:

   for each channel z^i of I_k:

      get the $DWT\{I_k(z^i), \psi_{a,b}(x, y)\}$;

      output$\rightarrow [cA_k, cH_k, cV_k, cD_k]^i$;

   end;

end;

for each channel $i \in \{R, G, B\}$ pair of $I_1 \cdot I_2$:

   get the mean $\bar{X}^i \leftarrow [cA, cH, cV, cD]^i$;

     $cA = \bar{X}(cA_1, cA_2)$;

     $cH = \bar{X}(cH_1, cH_2)$;

     $cV = \bar{X}(cV_1, cV_2)$;

     $cD = \bar{X}(cD_1, cD_2)$;

   compute $\theta^i = IDWT\{\bar{X}^i, \psi_{a,b}(x, y)\}$;

   end;

Result: set $\theta = (\theta^R, \theta^G, \theta^B)$;

Figure 3.10. Single-stage DWT fusion

(ii) Two-stage DWT fusion process

The two-stage DWT fusion process illustrated in Figure 3.11 is used to combine the salient features of the enhanced histogram-specified images G_1' and G_2' with the backlit RGB input. The procedure involves the cascading of two single-stage fusions. In the first stage, the outputs of M_1 and M_2 are fused. The resultant image $F_1(x, y)$ is fused with the backlit input $I(x, y)$ in the second stage to produce the final enhanced image $F_2(x, y)$.
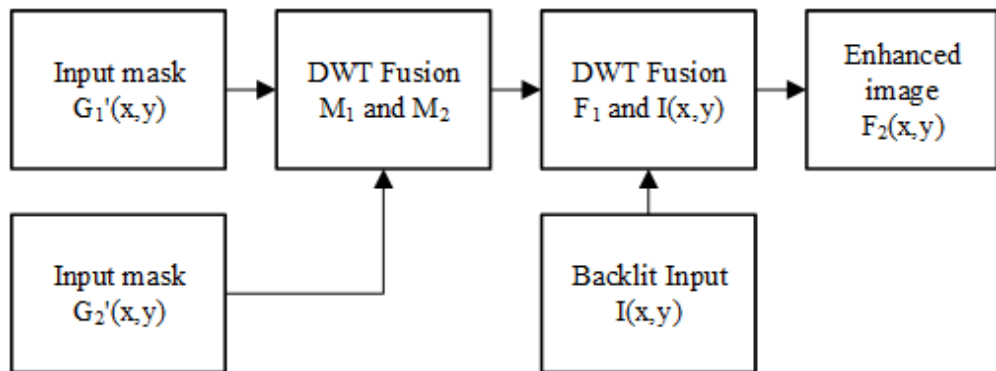
Figure 3.11. Two-stage RBHF fusion Process

(iii) Optimization of DWT fusion

The single-stage DWT fusion shown in Figure 3.10 uses a nested *for* loop to perform an element-wise operation in computing the mean feature vector $\bar{X}^i$. As a result, the time complexity of the proposed algorithm increases significantly by $O(n^2)$ for a given input. A vectorized approach is proposed in this section to accelerate the algorithm, particularly the DWT fusion (DWT-F). Vectorization is the process of converting loop-based, scalar-oriented code to matrix or vector operations [71]. The MATLAB R2018a [21] platform supports vectorized computing.

From equation (3.6), the wavelet coefficients for each input channel z^i yields the matrices $[cA_k, cH_k, cV_k, cD_k]^i$, where $k \in \{1, 2\}$ and $i \in \{R, G, B\}$. The mean feature vector $\bar{X}^i \leftarrow [cA, cH, cV, cD]^i$ is then obtained by summing each pair of the coefficient matrix and dividing the resultant elements by 2, as given in equations (3.8) to (3.11).

$$cA = (cA_1 + cA_2)^i/2 \tag{3.8}$$

$$cH = (cH_1 + cH_2)^i/2 \tag{3.9}$$

$$cV = (cV_1 + cV_2)^i/2 \tag{3.10}$$

$$cD = (cD_1 + cD_2)^i/2 \tag{3.11}$$

3.2.2. Multiple RBHF process

The enhancement quality of the proposed method can further be improved through an iterative process known as multiple RBHF. This process is established by configuring the proposed method in a feedback loop with a counter defined by the parameter *Iter*, as shown in Figure 3.12. The value of *Iter* determines the number of iterations. An *Iter* of 1 will yield the outcomes of a single RBHF process.
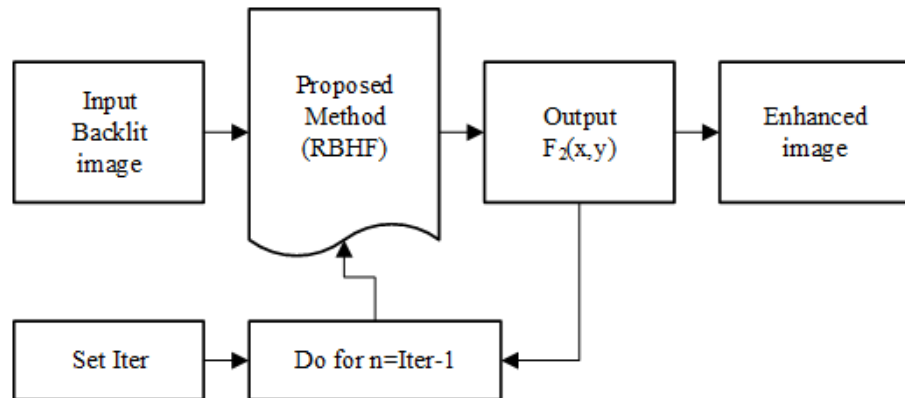
Figure 3.12. Proposed Multiple RBHF process

3.3. Measures

This section presents the image quality metrics used to evaluate the performance of the proposed method. The presentation begins with a discussion on the three objective measures, i.e., Peak Signal-to-Noise Ratio (PSNR), Structural Similarity (SSIM) index, and the Natural Image Quality Evaluator (NIQE), followed by a subjective assessment based on the International Telecommunication Union (ITU) framework.

3.3.1. Objective Measures

The PSNR is a well-known image quality metric that compares the maximum pixel intensity, L, of an image to the power of corrupting noise. It is defined as a ratio given by equation (3.12) [71].

$$PSNR = 10log_{10}\frac{L^2}{MSE} \tag{3.12}$$

$$where, \quad MSE = \frac{1}{M \text{x} N}\sum_{x=0}^{M-1}\sum_{y=0}^{N-1}[I(x,y) - K(x,y)]^2 \tag{3.12}$$

where $I(x,y)$ is an input or reference image with sizes M x N, and $K(x,y)$ is the enhanced image. High values in PSNR tend to suggest good image quality. However, this assessment is not consistent with human perception of quality [72].

The SSIM is another popular quality metric that measures the structural similarity between two images. The SSIM index is a single score that combines local image structure, luminance, and contrast and it can be expressed as given in (3.13) [72],[73]:

$$SSIM(x,y) = \frac{(2\mu_x\mu_y + c_1)(2\sigma_{xy} + c_2)}{(\mu_x^2 + \mu_y^2 + c_1)(\sigma_x^2 + \sigma_y^2 + c_2)} \qquad (3.13)$$

where μ_x and μ_y are the means of x and y, respectively; σ_x^2 is the variance of x; σ_y^2, the variance of y; σ_{xy} is the covariance of x and y; the variable $c_1 = (k_1 L)^2$ and $c_2 = (k_2 L)^2$; L is the maximum pixel intensity; $k_1 = 0.01$ and $k_2 = 0.03$ by default [73]. The SSIM score range from 0 to 1. High values indicate high image quality.

The NIQE is a no-reference image quality model that measures the naturalness of an image based on only observable deviations from statistical regularities detected in natural photographs, with no training or exposure to distorted images [74]. The NIQE can be expressed as a simple distance metric between the model statistics and that of the distorted image as given in equation (3.14).

$$D(V_1, V_2, \Sigma_1, \Sigma_2) = \sqrt{\left((V_1 - V_2)^T \left(\frac{(\Sigma_1 + \Sigma_2)^{-1}}{2} \right) (V_1 - V_2) \right)} \qquad (3.14)$$

where V_1, V_2 and Σ_1, Σ_2 represent the mean vectors and covariance matrices of a natural multivariate Gaussian (MVG) model and the MGV model of the distorted image, respectively. Images with high quality are expected to have a lower NIQE value [74].

3.3.2. Subjective Measures

The radio communication sector of the International Telecommunication Union (ITU-R) recommends the ITU-R BT.500-14 [75] image quality assessment framework. The framework employs human observers to judge

image quality. It specifies the number of observers, viewing conditions, and grading scales to be utilized during each subjective test [75].

The framework recommends a minimum of 15 observers for each evaluation. The observers are expected to be non-experts with no prior knowledge of the backlit image artefacts that the proposed method may introduce. Before each test session, they are examined for normal visual acuity and colour vision. They are also informed about the nature of the test, image sequence, time interval, and the grading scheme of 1 to 5, as shown in Table 3.2 [75]. Each level is designed to reflect the judgment of the observer.

Table 3.2. ITU-R BT.500-14 subjective quality assessment metric [75]

Level	Distortion in the image	Quality
5	Imperceptible	Excellent
4	Perceptible but not annoying	Good
3	Slightly annoying	Fair
2	Annoying	Poor
1	Very annoying	Bad

CHAPTER 4

EXPERIMENTAL RESULTS AND DISCUSSION

Various experiments were conducted on a dataset of 162 backlit images using MATLAB R2018a on a PC with 32GB RAM and a 2.6GHz Intel Core i7 processor. The parameters of the ABC and fusion stages in all simulations were defined as follows: $T = 240$; $\alpha_{LIM} = 0.23$; and $\psi_{a,b}(x,y) = sym5$. The results are presented in this chapter as follows: section 4.1 gives the results of the proposed method for images with low backlit sectors. In section 4.2, the results for the high backlit sector category are presented, followed by those of the low and high background highlight categories in sections 4.3 and 4.4, respectively. Next, section 4.5 gives a computational analysis of the proposed algorithm before and after the DWT-F optimization. Following this, section 4.6 presents the results of applying multiple RBHF processes on several backlit images to improve enhancement quality.

In section 4.7, the proposed method's performance is compared to existing enhancement techniques such as Histogram Equalization [4], Multiscale Retinex (M-Retinex) [76], and Low-Light Image Enhancement via Illumination Map Estimation (LIME) [77]. Section 4.8 compares some properties of the backlit inputs to the enhanced output images. Finally, the impact of the wavelet parameter $\psi_{a,b}(x,y)$ on the enhancement quality of the final output image is discussed in section 4.9.

4.1. Enhancement of images with low backlit sector

Figures 4.1(a) to 4.1(t) display the results of 20 selected backlit inputs characterized by soft "shadows" in the foreground. In each Figure, the first image from left to right is the backlit image, and the second is the enhancement result. Overall, the proposed method significantly improved the visual quality of the backlit images without any noticeable distortion or colour artefacts. More particularly, the outcomes of images B7, B11, B21, B24, and B125 demonstrate that the proposed method can effectively correct exposure disparities between the F- and B- regions and provide a more uniformly lit picture scene.

(a) Image B7

(b) Image B8

(c) Image B12

(d) Image B18

(e) Image B19

(f) Image B21

(g) Image B24

(h) Image B65
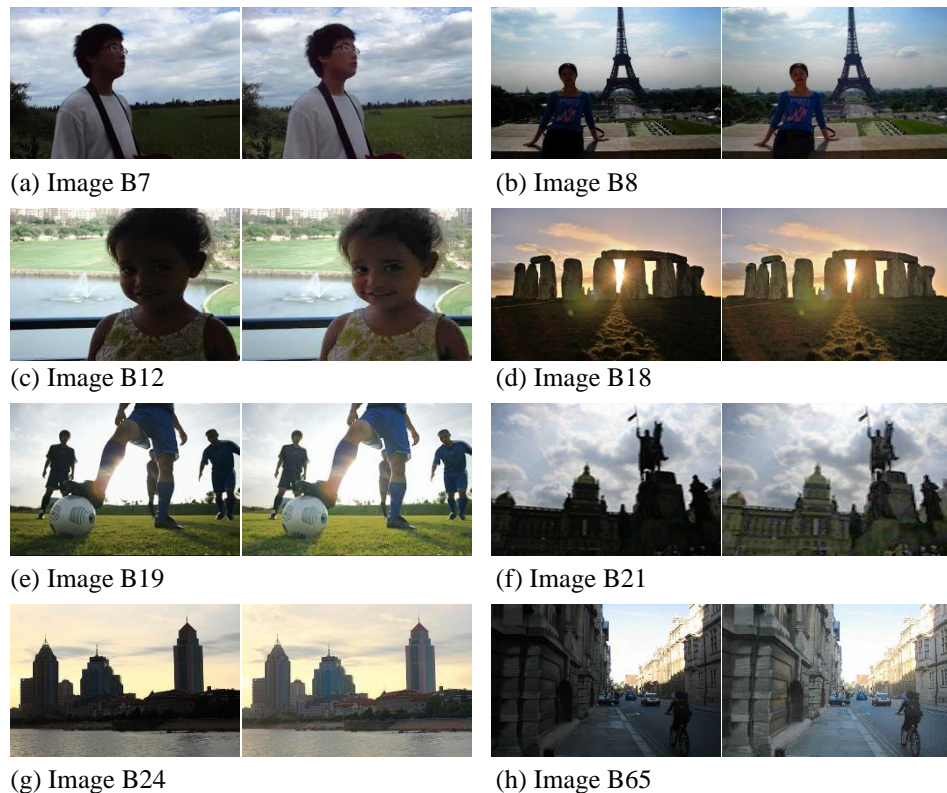
Figure 4.1. Enhancement of images with low backlit sectors

(i) Image B84

(j) Image B98

(k) Image B102

(l) Image B105

(m) Image B113

(n) Image B125

(o) Image B11

(p) Image B63

(q) Image B27

(r) Image B131

(s) Image B133

(t) Image B132

Figure 4.1. *(continued)* Enhancement of images with low backlit sectors

4.1.1. Objective assessment

In this section, the PSNR, SSIM, and NIQE image quality metrics are used to evaluate the results in Figure 4.1. Table 4.1 displays the outcomes of each evaluation, and the results are plotted in Figures 4.2, 4.3, and 4.4. The proposed method obtained high PSNR for most test images. The average value achieved from the dataset in Table 4.1 was 19.2 dB, with more than half the images having values above or slightly below the average, as shown in Figure 4.2. However, due to a relatively higher backlit degradation, five outcomes, including B63, B65, B98, B102, and B131, yielded low PSNR, more than 3 dB lower than the average.

Figure 4.3 displays the SSIM quality scores in Table 4.1. By expressing the values as percentages, the proposed method tends to maintain more than (60-70) % structural similarity with the backlit inputs. Image B65, for example. Despite having the lowest PSNR, it realized an SSIM index of 0.67. Outcomes such as images B102, B98, B113, and B131, with values below 0.5, are characteristic of high backlit degradation (noise) in the input image, as seen in Figure 4.1.

The results of the NIQE assessment are displayed in Figure 4.4. For each test image, the NIQE score of the input (I/P) is compared to that of the output (O/P). As shown in the graph, the proposed method preserves or slightly improves the naturalness quality of the backlit input. This result is consistent with the non-appearance of artefacts in the enhanced images in Figure 4.1.

Table 4.1. Objective test for images with low backlit sector

S/N	Test Image	Descriptor	Size	PSNR (dB)	SSIM	NIQE I/P	NIQE O/P
1	B7	Man Outdoor	480 x 316	23.7	0.91	2.26	2.15
2	B8	Woman Outdoor	399 x 299	24.8	0.84	2.62	2.46
3	B11	Office Building	360 x 480	19.0	0.72	2.63	2.40
4	B12	Girl	260 x 194	23.4	0.87	3.99	3.56
5	B18	Sunset Rocks	480 x 319	22.6	0.84	2.49	2.88
6	B19	Football	400 x 266	20.4	0.91	5.01	4.51
7	B21	Building Statue	212 x 209	21.1	0.75	3.01	3.34
8	B24	Cityscape	600 x 400	19.1	0.84	2.64	2.34
9	B27	Outdoor Yard	189 x 250	17.3	0.77	4.83	4.85
10	B63	Broad Street	478 x 640	16.4	0.73	2.64	2.82
11	B65	City Street	2048 x 1536	14.0	0.65	1.81	1.60
12	B84	Sunset Mountain	640 x 425	18.0	0.67	2.82	2.50
13	B98	Dark Room Block	1024 x 586	15.3	0.47	1.69	1.91
14	B102	Dark Room Table	640 x 427	15.3	0.37	2.74	2.45
15	B105	Living Room	500 x 335	19.8	0.69	3.29	2.73
16	B113	Dark Room Bed	1024 x 685	15.2	0.39	2.54	2.61
17	B125	City Road	704 x 518	21.2	0.82	3.92	3.20
18	B131	KICC Building	424 x 540	15.0	0.47	5.36	5.45
19	B132	Hilton Hotel	436 x 572	20.1	0.69	4.79	4.38
20	B133	National Archives	510 x 680	22.1	0.87	3.42	3.59
	Average			19.2	0.71	3.22	3.09

Peak Signal-to-Noise Ratio by Test Image
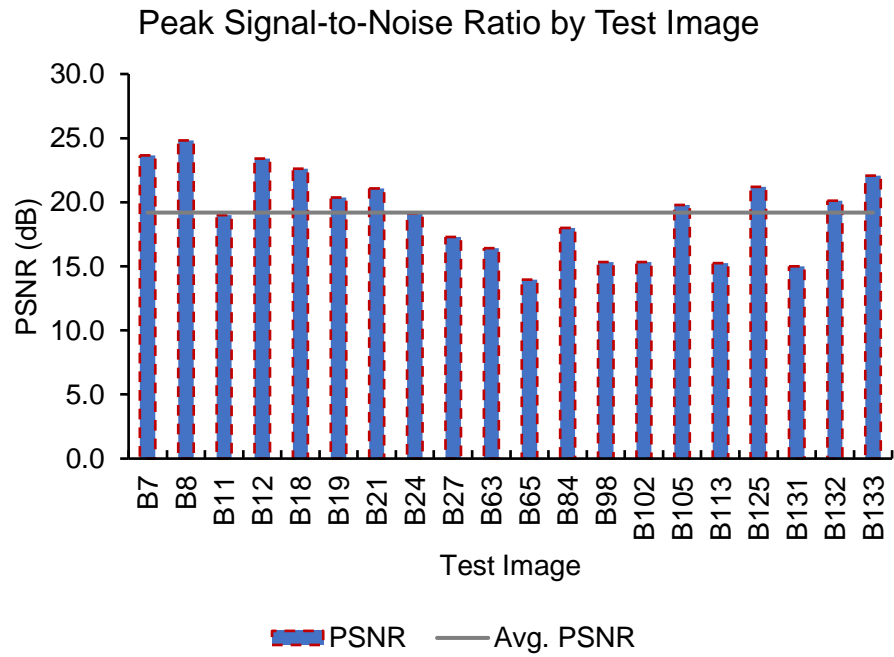
Figure 4.2. PSNR evaluation of images with low backlit sector

Structural Similarity Index by Test Image
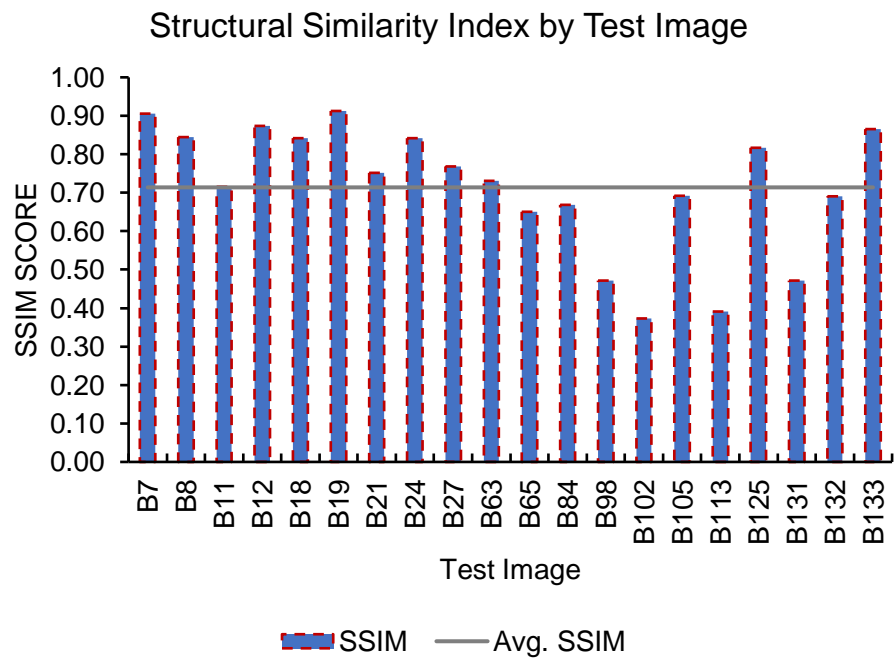
Figure 4.3. SSIM assessment of images with low backlit sector

NIQE Assessment of Input vs Output Image
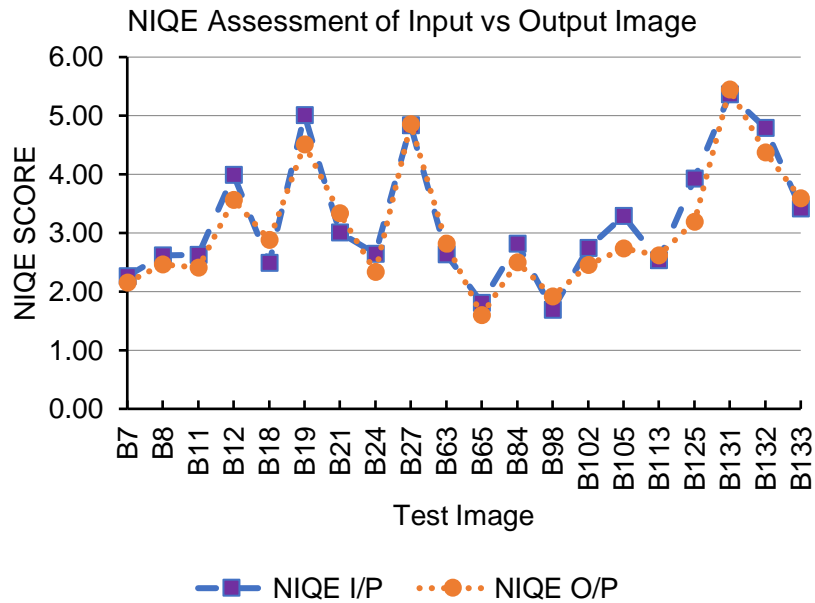
Figure 4.4. NIQE assessment of images with low backlit sector

4.1.2. Subjective assessment

A subjective evaluation of the enhancement results in Figure 4.1 was conducted by 16 subjects using the ITU-R BT.500-14 image quality framework. The test subjects included 6 students from the Railway training institute in Nairobi and 10 residents of the Plainsview community in South B with no exposure to image processing technology. Initially, they were tested for visual acuity and colour vision, then briefed on the experiment's parameters and asked to rank the quality of each image in Figure 4.1 using the recommended scale in section 3.3.2. Table 4.2. gives the results of their evaluations.

Table 4.2 presents each image's ranking by the number of test subjects. The average quality score per image was calculated by weighting every quality level: Bad=1, Poor=2, Fair=3, Good=4, and Excellent=5. On average, the proposed method achieved values ranging from 3.56 to 4.88, with many images scoring

"good" or "excellent." Image B63 ranked the highest, followed by images B133,

B24, B27, and B132.

Table 4.2. Subjective test for images with low backlit sector

S/N	Test Image	Descriptor	Number of test subjects per quality score					Average Quality
			Bad	Poor	Fair	Good	Excellent	
1	B7	Man Outdoor	0	0	3	8	5	4.13
2	B8	Woman Outdoor	0	0	3	5	8	4.31
3	B11	Office Building	0	0	1	3	12	4.69
4	B12	Girl	2	1	3	6	4	3.56
5	B18	Sunset Rocks	0	1	3	4	8	4.19
6	B19	Football	1	0	1	8	6	4.13
7	B21	Building Statue	0	2	3	8	3	3.75
8	B24	Cityscape	0	0	0	4	12	4.75
9	B27	Outdoor Yard	0	0	0	4	12	4.75
10	B63	Broad Street	0	0	1	0	15	4.88
11	B65	City Street	0	0	1	3	12	4.69
12	B84	Sunset Mountain	0	0	2	2	12	4.63
13	B98	Dark Room Block	0	0	3	2	11	4.50
14	B102	Dark Room Table	0	0	1	5	10	4.56
15	B105	Living Room	0	0	2	6	8	4.38
16	B113	Dark Room Bed	0	1	0	5	10	4.50
17	B125	City Road	0	4	3	5	4	3.56
18	B131	KICC Building	0	1	1	4	10	4.44
29	B132	Hilton Hotel	0	0	1	2	13	4.75
20	B133	National Archives	0	0	1	1	14	4.81

4.2. Enhancement of images with high backlit sector

Figure 4.5(a) to 4.5(l) show the enhancement results for 12 backlit images characterized by hard shadows in the foreground. In each figure, the first image (left to right) is the backlit input, and the second is the enhanced output. The overall result shows significant improvement in the perception of details in the highly under-exposed foreground. A few examples can be found in the outcomes of images B4, B5, B20, B100, B124, and B116. However, the enhancement quality of images B33, B91, and B129 was impacted by shadow clipping. As a result, shadow-clipped areas in the input are seen to have no visual information in the enhanced output. This is evident in the boy's facial features in Figure 4.5(f) or the dining floor in Figure 4.5(e).

(a) Image B4

(b) Image B5

(c) Image B14

(d) Image B20

(e) Image B91

(f) Image B33
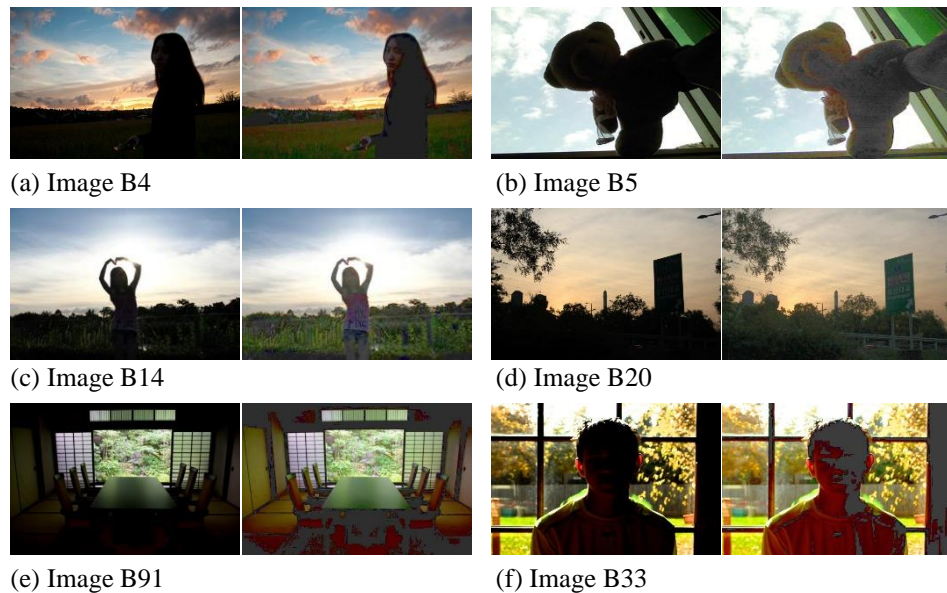
Figure 4.5. Enhancement of images with high backlit sector

(g) Image 100   (h) Image B114

(i) Image B124   (j) Image B116

(k) Image B120   (l) Image B129
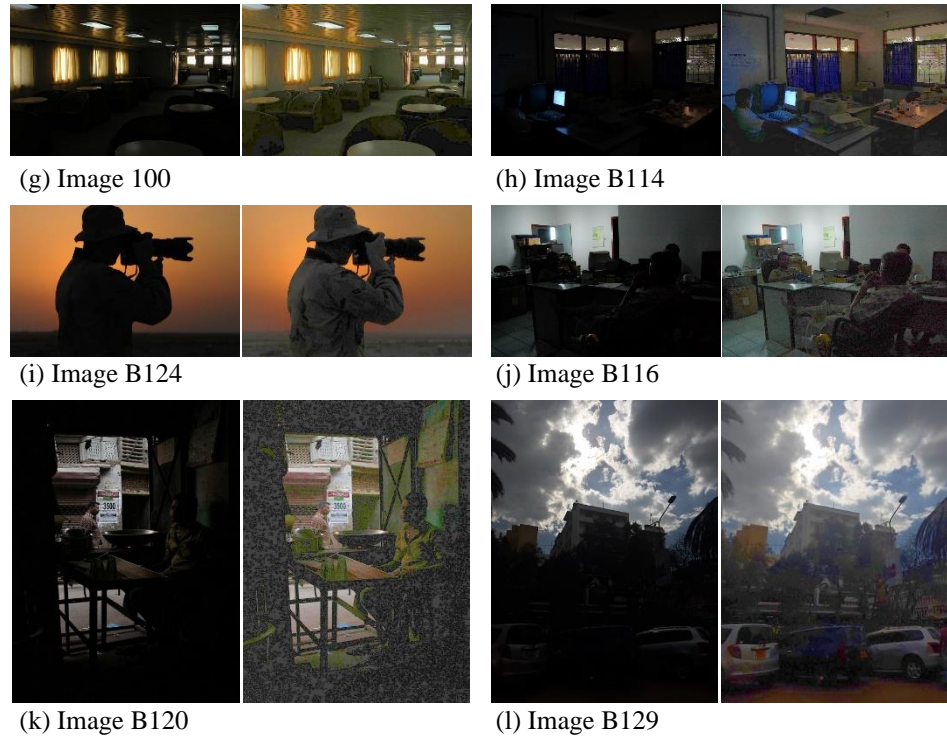
Figure 4.5. *(continued)* Enhancement of images with high backlit sector

4.2.1. Objective assessment

The quality metrics in section 3.3.1 are used to evaluate the results of Figure 4.5. The PSNR, SSIM, and NIQE measurements are given in columns (4), (5), and (6) of Table 4.3, respectively. Their values are also plotted in Figures 4.6 to 4.8. On average, the proposed method achieved a PSNR quality of 16.9 dB. This value is about 3 dB less than the average for images with low backlit sectors. However, this is a significant gain given the high backlit degradation in the inputs of Figure 4.5.

Figure 4.7 displays the SSIM results in Table 4.3. For most test images, the proposed method achieved more than (40-60) % structural similarity. However, photos such as B114 and B120 realized the least SSIM scores. Such outcomes

72

are expected because the enhanced images of B114 and B120 contained more salient features than their backlit inputs.

According to Table 4.3 and Figure 4.8, the proposed method tends to preserve or slightly improve the naturalness quality of the backlit inputs in terms of NIQE. This can be seen in the outcomes of B5, B20, B91, and B124. The result of image B120, on the other hand, shows a significant decrease in the NIQE value. This is consistent with the output in Figure 4.5(k), which is less naturally appealing compared to other results in Figure 4.5.

Table 4.3. Objective test for images with high backlit sector

S/N	Test Image	Descriptor	Size	PSNR (dB)	SSIM	NIQE I/P	NIQE O/P
1	B4	Woman Fields	452 x 300	21.2	0.64	2.71	2.57
2	B5	Teddy bear	375 x 300	16.5	0.63	4.66	4.30
3	B14	Woman Fields 2	329 x 220	19.2	0.72	3.17	3.61
4	B20	Signboard	694 x 460	20.5	0.69	2.95	2.41
5	B33	Boy at Window	1400 x 1049	15.8	0.53	3.80	3.44
6	B91	Dining Room	506 x 338	15.9	0.37	3.67	3.49
7	B100	Dining Hall	640 x 480	15.0	0.33	3.01	3.47
8	B114	Office 1	640 x 426	13.4	0.16	3.07	3.52
9	B116	Photographer	640 x 426	15.3	0.40	3.92	3.50
10	B120	Office 2	427 x 640	13.3	0.15	3.39	4.94
11	B124	Street Kitchen	1120 x 700	20.0	0.70	4.40	3.25
12	B129	Parking Lot	440 x 586	16.4	0.48	3.23	3.49
	Average			16.9	0.48	3.50	3.50

Peak Signal-to-Noise Ratio by Test Image
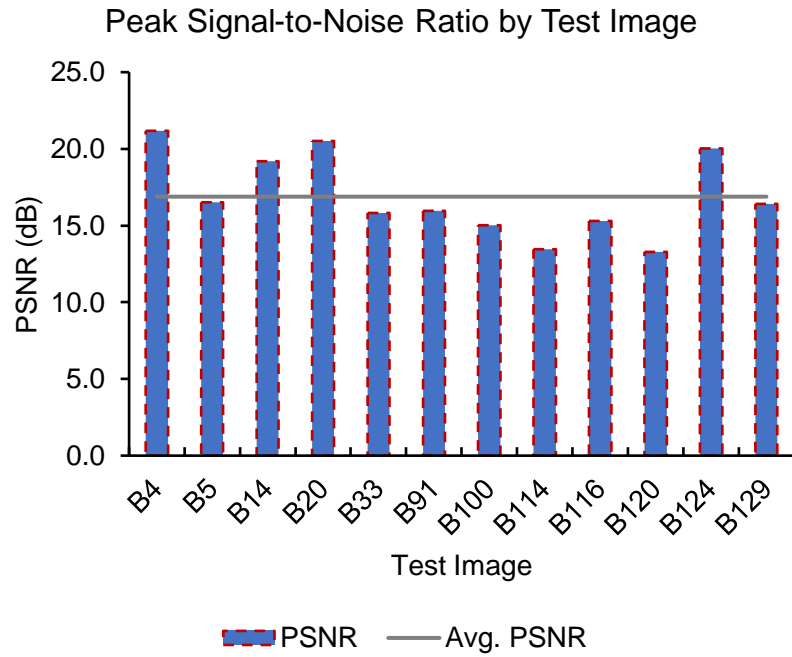
Figure 4.6. PSNR evaluation of images with high backlit sector

Structural Similarity Index by Test Image
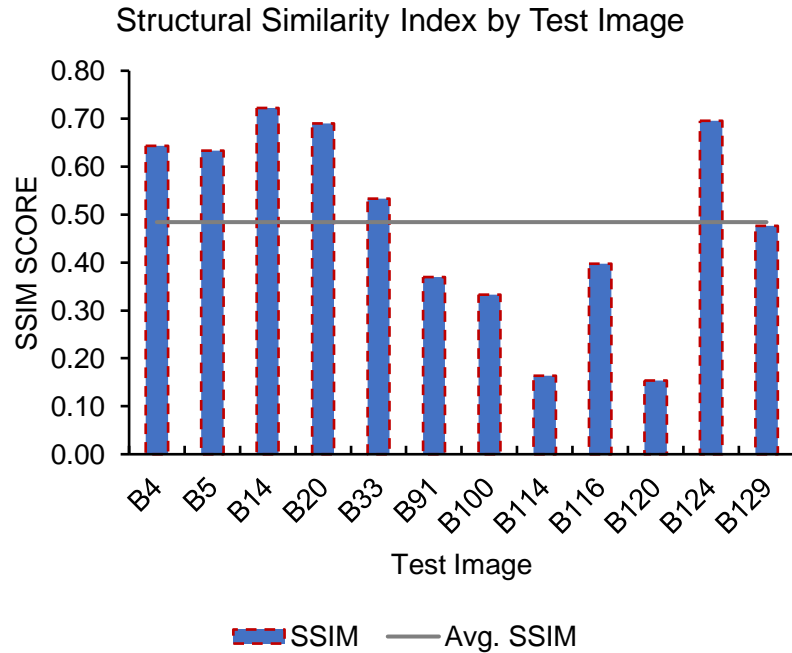
Figure 4.7. SSIM evaluation of images with high backlit sector
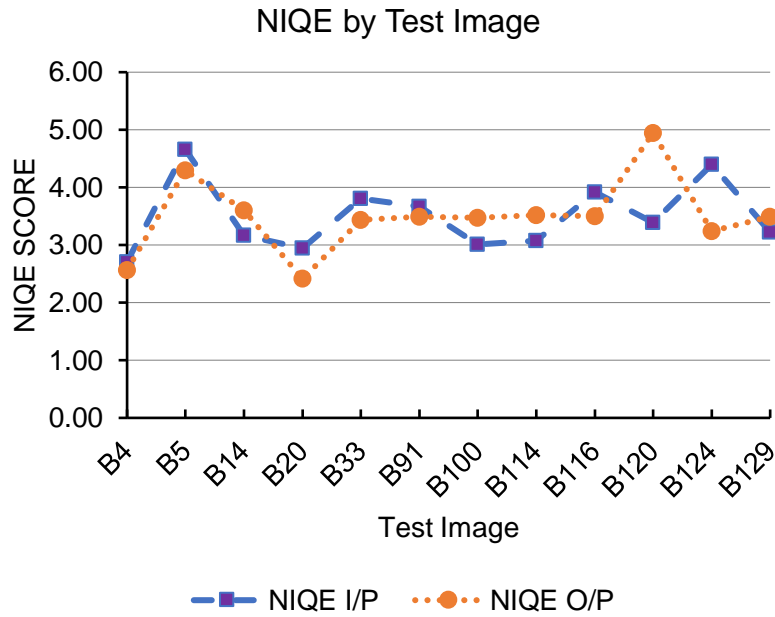
Figure 4.8. NIQE evaluation of images with high backlit sector

4.2.2. Subjective assessment

A group of 16 people, as referenced in section 4.1.2, were asked to judge the results in Figure 4.5 following the ITU-R BT.500-14 image quality framework. Table 4.4 shows the outcome of their assessments. The average quality score per image was calculated by weighting every quality level: Bad=1, Poor=2, Fair=3, Good=4, and Excellent=5.

The results in Table 4.4 show that the proposed method achieved lower enhancement quality for the images with a high backlit sector which is consistent with the PSNR evaluation in Table 4.3. Except for images B20 and B116, many images realized values in the range of 2.13 to 3.88 on average.

Table 4.4. Subjective test for images with high backlit sector

S/N	Test Image	Descriptor	Bad	Poor	Fair	Good	Excellent	Average
1	B4	Woman Fields	2	5	4	3	2	2.88
2	B5	Teddy bear	3	4	5	2	2	2.75
3	B14	Woman Fields 2	3	3	2	4	4	3.19
4	B20	Signboard	0	0	2	5	9	4.44
5	B33	Dining Room	3	9	3	1	0	2.13
6	B91	Boy at Window	3	4	4	4	1	2.75
7	B100	Dining Hall	1	5	3	2	5	3.31
8	B114	Office 1	0	3	2	5	6	3.88
9	B116	Photographer	1	1	3	2	9	4.06
10	B120	Office 2	5	1	4	3	3	2.88
11	B124	Street Kitchen	3	2	2	1	8	3.56
12	B129	Parking Lot	3	1	2	5	5	3.50

4.3. Enhancement of images with low background highlight

Images in the low background highlight category are grouped based on lower radiance in the B-regions. However, these images differ in terms of their backlit degradation. Figures 4.9(a) to 4.9(n) displays the enhancement results for some selected inputs with low background highlights. In each figure, the first image from left to right is the backlit input, and the second is the enhanced output. The results in Figure 4.9 show significant improvements in the visual quality of the backlit inputs without noticeable distortion or colour artefacts. Furthermore, the outcomes of images B55, B119, and B121 versus B54, B75, and B79, demonstrate how the proposed method dynamically adjusts the exposure for various inputs while maintaining their natural scenery.

(a) Image B37

(b) Image B48

(c) Image B54

(d) Image B55

(e) Image B119

(f) Image B121

(g) Image B66

(h) Image B71

(i) Image 74

(j) Image B75

(k) Image B79

(l) Image B101
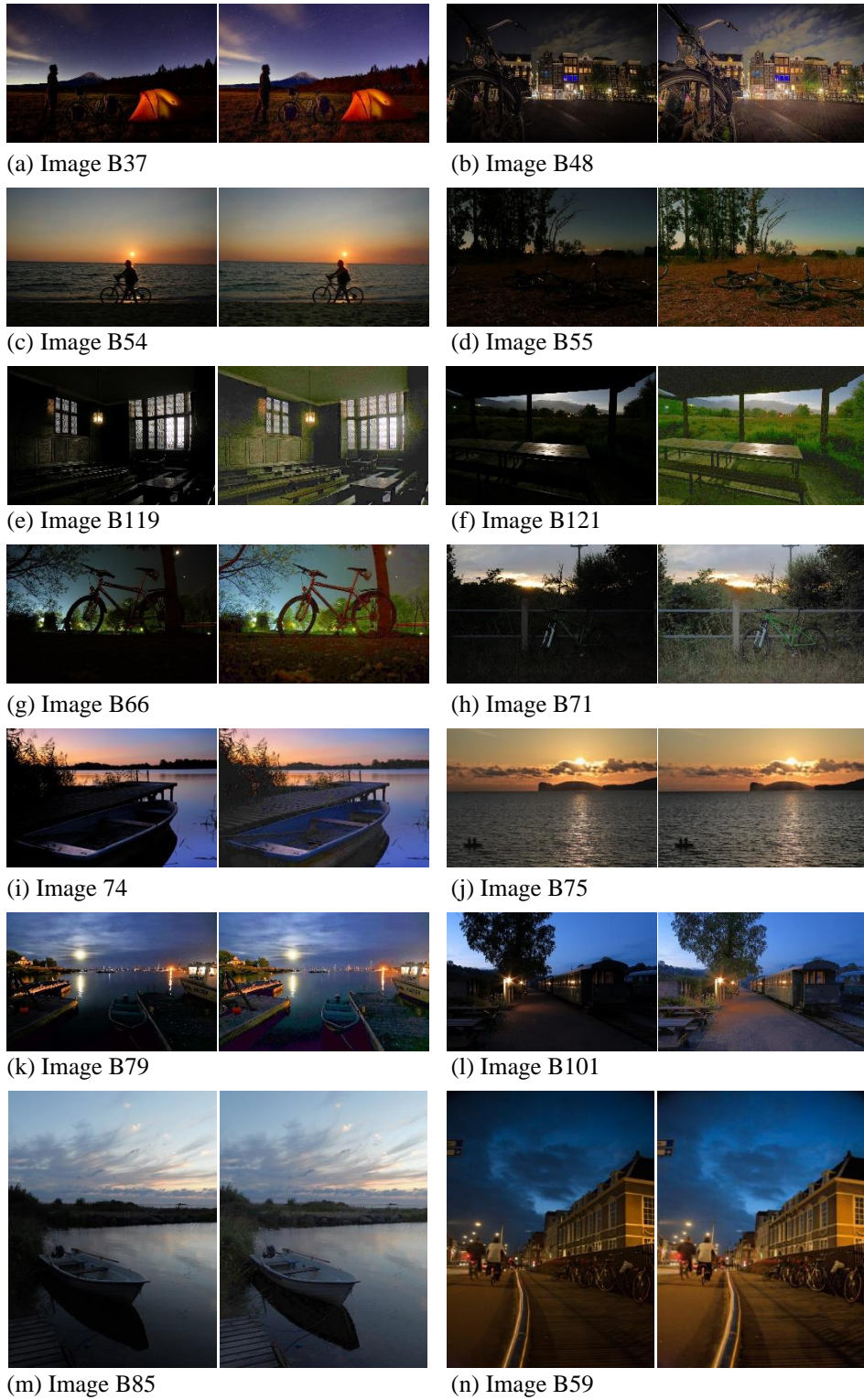

(m) Image B85

(n) Image B59

Figure 4.9. Enhancement of images with low background highlights

4.3.1. Objective assessment

Table 4.5 gives the objective measures for the enhancement results of Figure 4.9. The PSNR measurements are provided in column (4), followed by the SSIM scores in column (5). Columns (6) and (7) give the NIQE measurements for the input and output images, respectively. Figures 4.10 to 4.12 further illustrate the results. On average, the proposed method achieved a PSNR quality of 18.1 dB. Images with high backlit degradation such as B119, B121, B71, B48, B66, and B55 tend to have low PSNR values up to 5 dB less than the average, as seen in Figure 4.10. These images in Figure 4.11 also seem to have a lower structural similarity index. Such outcomes were observed in sections 4.1.1 and 4.2.1 and appear consistent with severely degraded backlit images. Finally, in terms of the NIQE assessment, in many instances, the proposed method improved the naturalness quality of the inputs, as seen in Figure 4.12.

Table 4.5. Objective test for images with low background highlight

S/N	Test Image	Descriptor	Size	PSNR (dB)	SSIM	NIQE I/P	NIQE O/P
1	B85	Boat Morning	774 x 1032	23.3	0.82	2.00	2.10
2	B79	Boat Sundown	1023 x 633	20.3	0.65	4.00	3.37
3	B75	Ocean Sunset	512 x 334	25.0	0.95	4.45	4.74
4	B74	Boat Night	507 x 338	19.0	0.56	4.41	4.48
5	B71	Bush Bicycle	900 x 602	14.9	0.40	1.95	2.47
6	B66	Woods Bicycle	789 x 504	15.4	0.34	2.11	2.02
7	B59	Street Night	338 x 507	19.8	0.83	2.75	2.42
8	B55	Fields Bicycle	640 x 480	14.9	0.31	3.44	3.42
9	B54	Ocean Cycling	500 x 333	22.2	0.82	5.82	4.04
10	B48	Residential	640 x 424	15.1	0.48	2.54	2.24
11	B37	Camping	640 x 427	18.6	0.60	5.17	4.03
12	B121	Fields Table	1600 x 1067	14.4	0.14	2.66	2.15
13	B119	Court Room	925 x 692	13.6	0.20	2.84	3.15
14	B101	Dawn Train	640 x 480	17.2	0.54	2.35	2.34
	Average			18.1	0.54	3.32	3.07

Peak Signal-to-Noise Ratio by Test Image

Figure 4.10. PSNR evaluation of images with low background highlights

Structural Similarity Index by Test Image
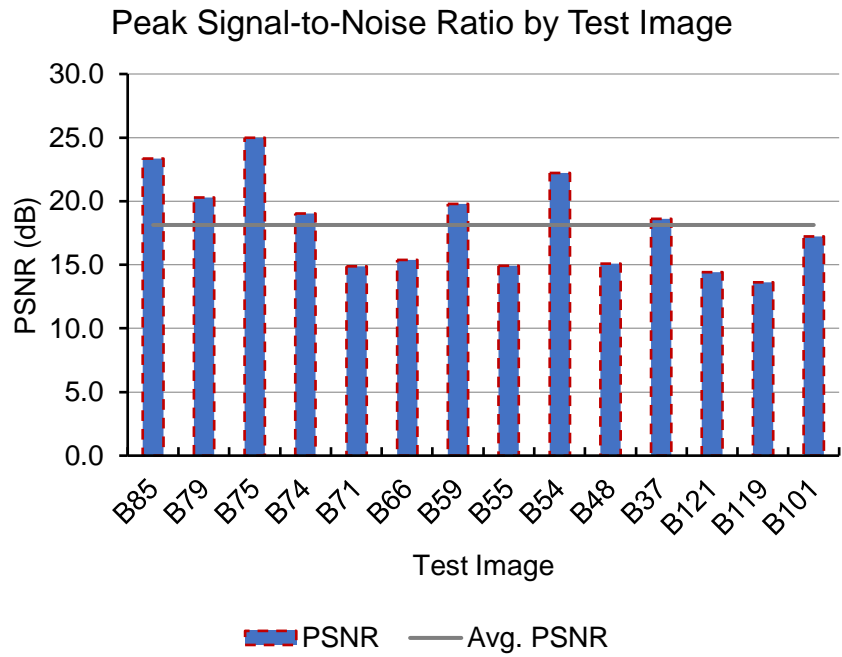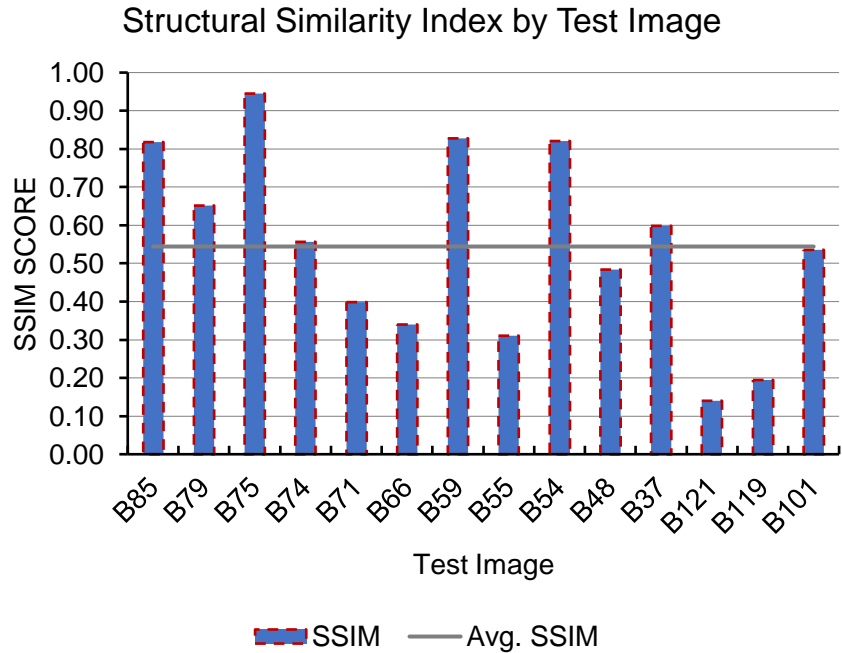

Figure 4.11. SSIM evaluation of images with low background highlights
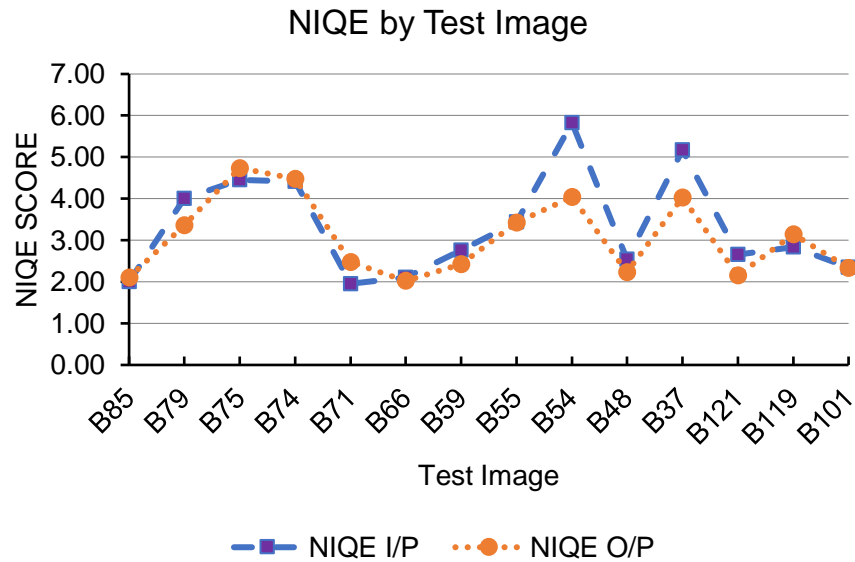
Figure 4.12. NIQE evaluation of images with low background highlights

4.3.2. Subjective assessment

Table 4.6 gives the subjective evaluation of the results in Figure 9. In each test, a group of 16 people, as referenced in section 4.1.2, were asked to judge the image enhancement quality according to the ITU-R BT.500-14. A weight was assigned to each quality level, i.e. Bad=1, Poor=2, Fair=3, Good=4, and Excellent=5, and the average quality score per image was calculated.

In Table 4.6, the proposed method achieved high-quality scores for many test images. The average quality per image ranged from 4.0 to 4.94 except for image B119 which received the lowest score of 3.38. The best enhancement quality, according to Table 4.6, was achieved by image B101 and the second best was B85.

Table 4.6. Subjective test for images with low background highlight

S/N	Test Image	Descriptor	Bad	Poor	Fair	Good	Excellent	Average
1	B85	Boat Morning	0	0	0	2	14	4.88
2	B79	Boat Sundown	0	0	2	5	9	4.44
3	B75	Ocean Sunset	0	0	1	5	10	4.56
4	B74	Boat Night	2	0	1	6	7	4.00
5	B71	Bush Bicycle	0	0	0	4	12	4.75
6	B66	Woods Bicycle	0	0	4	5	7	4.19
7	B59	Street Night	0	0	1	4	11	4.63
8	B55	Fields Bicycle	0	0	2	2	12	4.63
9	B54	Ocean Cycling	0	0	0	5	11	4.69
10	B48	Residential	0	0	2	0	14	4.75
11	B37	Camping	0	0	0	6	10	4.63
12	B121	Fields Table	0	0	1	7	8	4.44
13	B119	Court Room	1	1	7	5	2	3.38
14	B101	Dawn Train	0	0	0	1	15	4.94

4.4. Enhancement of images with high background highlights

Images in the high background highlight category are characterized by high radiance in the B-regions. Nevertheless, these images differ with respect to their backlit degradation. Figures 4.13(a) to 4.13(l) show the enhancement results of some selected backlit inputs. The first image in each figure (left to right) is the backlit image and the second is the enhancement results. Overall, the proposed method significantly improved visibility in the under-exposed foreground despite the high radiance in background areas. Some examples can be seen in the results of B10, B25, B89, B31, B93, and B111. The outcomes of B15 and B31 in Figure 4.13(d) and 4.13(g), respectively, show the proposed method

82

attempting to reclaim details of the sky from the over-exposed areas around the sun. However, this created noticeable fluctuations in the intensity level of neighbouring pixels.

(a) Image B6

(b) Image B10

(c) Image B13

(d) Image B15

(e) Image B17

(f) Image B25

(g) Image B31

(h) Image B89

(i) Image 93

(j) Image B110

(k) Image B111

(l) Image B117
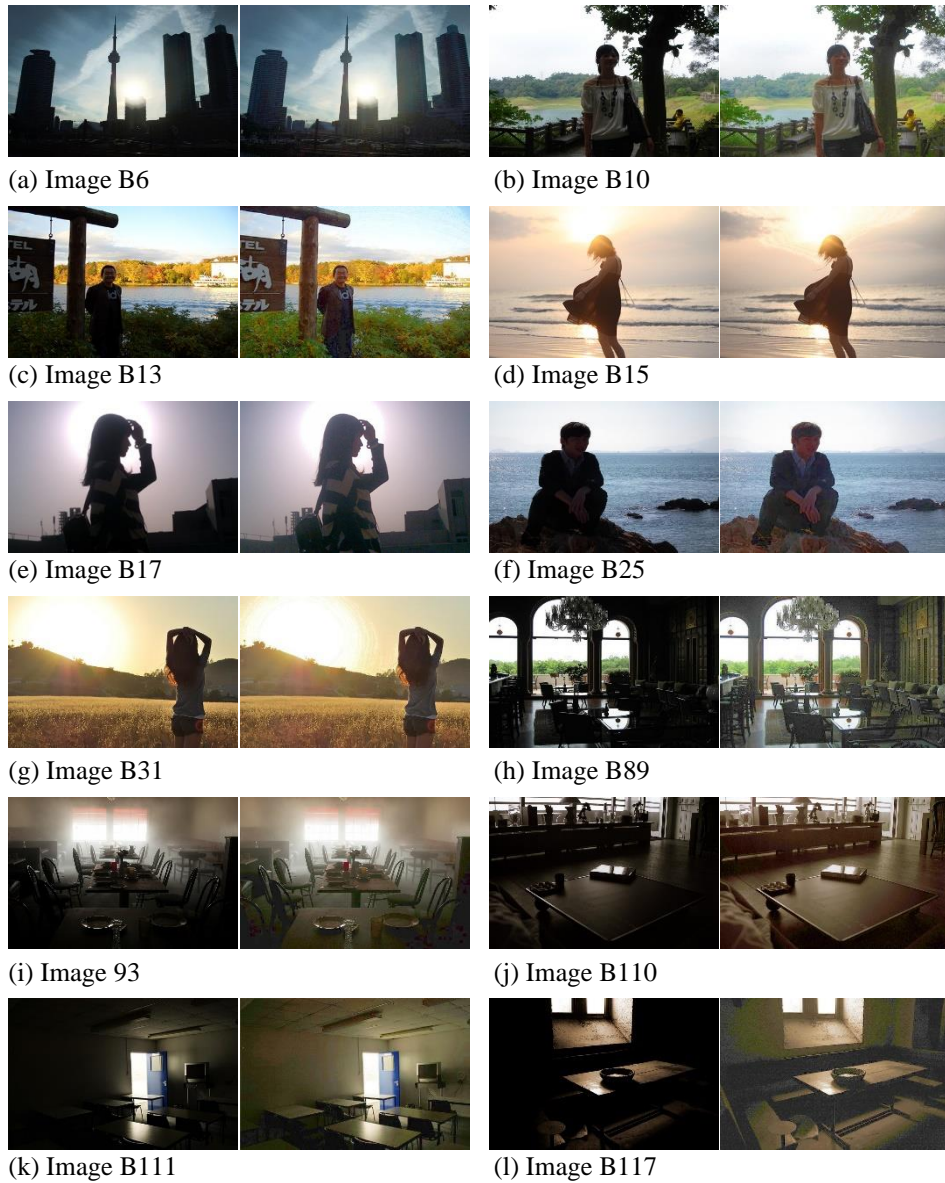
Figure 4.13. Enhancement of images with high background highlights

4.4.1. Objective assessment

Table 4.7 shows the performance of the proposed method on the test images in Figure 4.13. In column (4) are the PSNR quality measurements plotted in Figure 4.14, followed by the SSIM scores in column (5) and displayed in Figure 4.15. Columns (6) and (7) provide the NIQE metrics for the input and output images, respectively. Their collective results are displayed in Figure 4.16. The proposed method yielded high PSNR for many of the test images. Images with high backlit degradation such as B89, B117, and B111 tend to have low PSNR, more than 3 dB less than the average. As for the SSIM index, Figure 4.15 shows that the proposed method achieved more than (40-60) % structural similarity for many test images. Low SSIM scores, however, were also frequent with highly degraded inputs. The NIQE results in Figure 4.16 show improvements in the naturalness quality of several backlit inputs, including B93, B6, B25, B15, B111, B110, and B10. A slight decrease was reported in the outcomes of B13 and B17.

Table 4.7. Objective test for images with high background highlight

S/N	Test Image	Descriptor	Size	PSNR (dB)	SSIM	NIQE I/P	NIQE O/P
1	B93	Restaurant 1	1021 x 732	17.8	0.58	2.41	2.08
2	B89	Restaurant 2	500 x 375	13.4	0.39	4.54	4.66
3	B6	Cityscape	514 x 385	21.8	0.77	3.56	2.78
4	B31	Girl 1 Field	500 x 328	25.8	0.97	3.84	3.71
5	B25	Boy Sea	400 x 300	20.4	0.79	3.92	3.70
6	B17	Girl Outside	320 x 212	22.3	0.82	4.43	4.56
7	B15	Girl Sea	480 x 320	25.6	0.98	4.18	3.54
8	B13	Lakeside	400 x 300	17.7	0.65	2.20	2.90
9	B117	Eating Room	640 x 427	13.4	0.18	4.29	4.90
10	B111	Classroom	493 x 331	14.7	0.32	4.23	3.48
11	B110	Sitting Room	1024 x 663	15.7	0.36	2.34	1.85
12	B10	Damside	600 x 450	16.6	0.70	2.25	2.19
	Average			18.7	0.62	3.51	3.36

Peak Signal-to-Noise Ratio by Test Image

Figure 4.14. PSNR evaluation of images with high background highlight
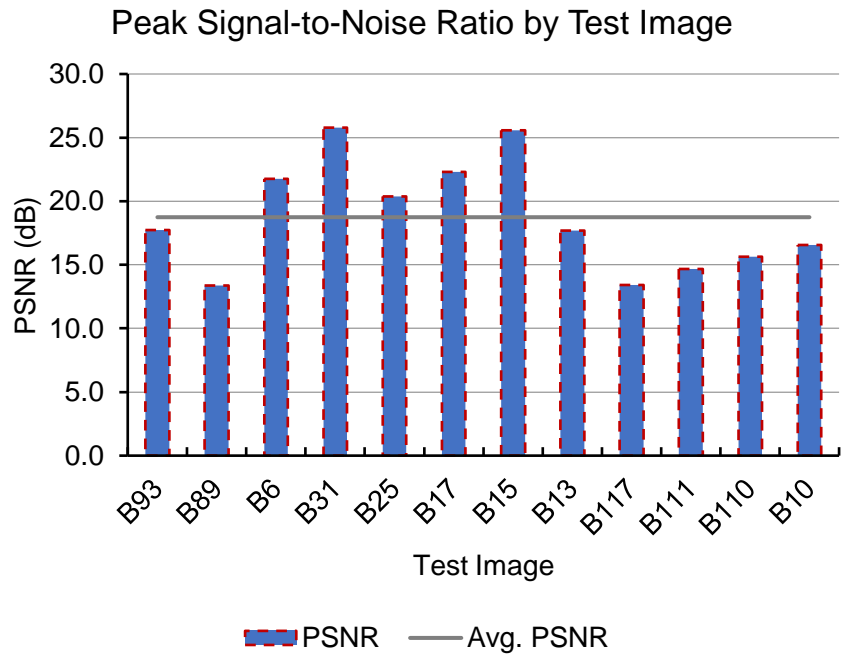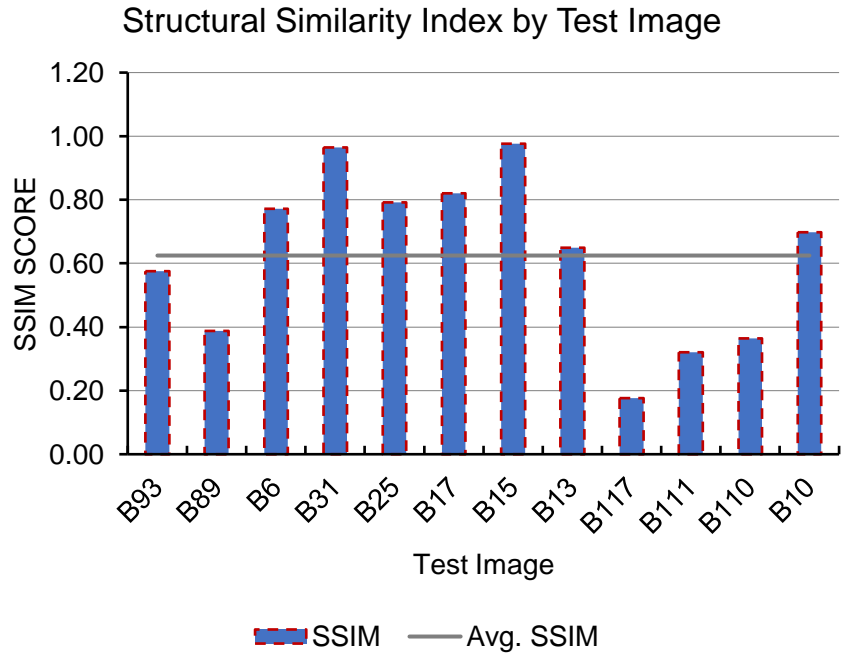
Structural Similarity Index by Test Image

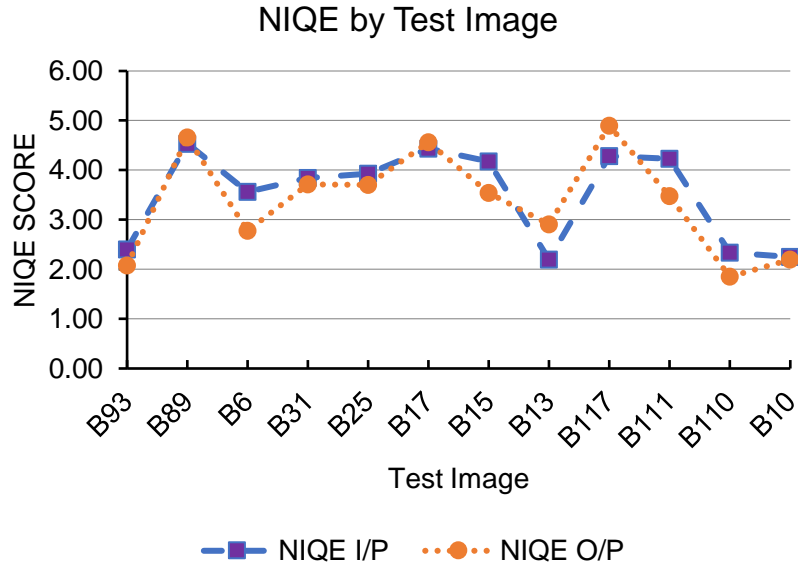Figure 4.15. SSIM evaluation of images with high background highlight

Figure 4.16. NIQE evaluation of images with high background highlights

4.4.2. Subjective assessment

Table 4.8 gives the subjective measurements for the results in Figure 4.13. In each experiment, a group of 16 people, as referenced in section 4.1.2, were asked to judge the image enhancement quality according to the ITU-R BT.500-14. A weight was assigned to each quality level, i.e., Bad=1, Poor=2, Fair=3, Good=4, and Excellent=5, and the average quality score per image was calculated.

Overall, the proposed method achieved high-quality scores for many test images. The average quality per image ranged from 4.06 to 4.56 except for images B15 and B117 which received the lowest scores of 2.19 and 3.63, respectively. According to Table 4.8, the highest quality was achieved in images B110 and B10, followed by images B111, B89, and B17.

Table 4.8. Subjective test for images with high background highlight

S/N	Test Image	Descriptor	Bad	Poor	Fair	Good	Excellent	Average
1	B110	Sitting Room	0	1	2	0	13	4.56
2	B10	Damside	0	0	2	3	11	4.56
3	B111	Classroom	0	0	3	2	11	4.50
4	B89	Restaurant 2	0	0	1	7	8	4.44
5	B17	Girl Outside	0	0	2	5	9	4.44
6	B31	Girl 1 Field	0	0	3	4	9	4.38
7	B25	Boy Sea	0	0	3	5	8	4.31
8	B93	Restaurant 1	0	1	3	5	7	4.13
9	B15	Girl Sea	3	9	2	2	0	2.19
10	B6	Cityscape	1	0	2	6	7	4.13
11	B13	Lakeside	0	0	3	9	4	4.06
12	B117	Eating Room	1	1	5	5	4	3.63

4.5. Computation time analysis of the proposed method

This section discusses the runtime of the proposed algorithm in section 3.2.1. The runtime analysis is based on the results of Figure 4.1. All findings can be applied to the dataset in sections 4.2, 4.3, and 4.4.

Table 4.9 presents the computation time obtained for the 20 simulations in Figure 4.1 using the *tik* and *tok* functions in MATLAB. The data is organized from the lowest picture resolution to the highest. The computation time before the DWT-F optimization is given by CTBO, and CTAO is the time measurement after optimization. The average computation time was found to be 5.33 seconds before optimization. However, it took roughly twice the average time to enhance images like B98 and B113 with a resolution of more than 600,000 pixels. Furthermore, photos with higher resolution, such as B65, required approximately eight times the average score.

Comparing the results of CTBO to CTAO, a significant reduction in the computation time was achieved. Precisely, the optimization of the DWT-F process reduced the computation time by 92.5%, as shown in Table 4.9, with a standard deviation of 0.82. As a result, the average time required to enhance each backlit input in Figure 4.1 was reduced from 5.33s to 0.4s. Such improvement in performance can be seen in the outcome of image B65.

Table 4.9. Computation time analysis of the proposed method

S/N	Test Image	Descriptor	Size	Time (s) CTBO	Time (s) CTAO
1	B21	Building Statue	212 x 209	0.62	0.04
2	B27	Outdoor Yard	189 x 250	0.67	0.04
3	B12	Girl	260 x 194	0.78	0.04
4	B19	Football Outdoor	400 x 266	1.61	0.07
5	B8	Woman Outdoor	399 x 299	1.65	0.07
6	B7	Man Outdoor	480 x 316	2.11	0.12
7	B18	Sunset Rocks	480 x 319	1.98	0.11
8	B105	Living Room	500 x 335	2.16	0.13
9	B11	Office Building	360 x 480	3.15	0.14
10	B131	KICC Building	424 x 540	2.63	0.16
11	B24	Cityscape	600 x 400	3.19	0.18
12	B132	Hilton Hotel	436 x 572	2.95	0.20
13	B84	Sunset Mountain	640 x 425	4.47	0.26
14	B102	Dark Room Table	640 x 427	4.64	0.26
15	B63	Broad Street City	478 x 640	4.23	0.31
16	B133	National Archives	510 x 680	4.15	0.34
17	B125	City Road	704 x 518	4.48	0.34
18	B98	Dark Room	1024 x 586	10.47	0.63
19	B113	Dark Room	1024 x 685	9.59	0.77
20	B65	City Street	2048 x 1536	41.16	3.79
	Average			5.33	0.40

Figure 4.17 further illustrates the results in Table 4.9. The runtime of the proposed algorithm is seen to increase with the input size. As a result, for larger image resolutions like B98 or B113, the practicality of the proposed algorithm is limited. However, with the DWT-F optimization, the time complexity is improved, thus making the algorithm computationally efficient.
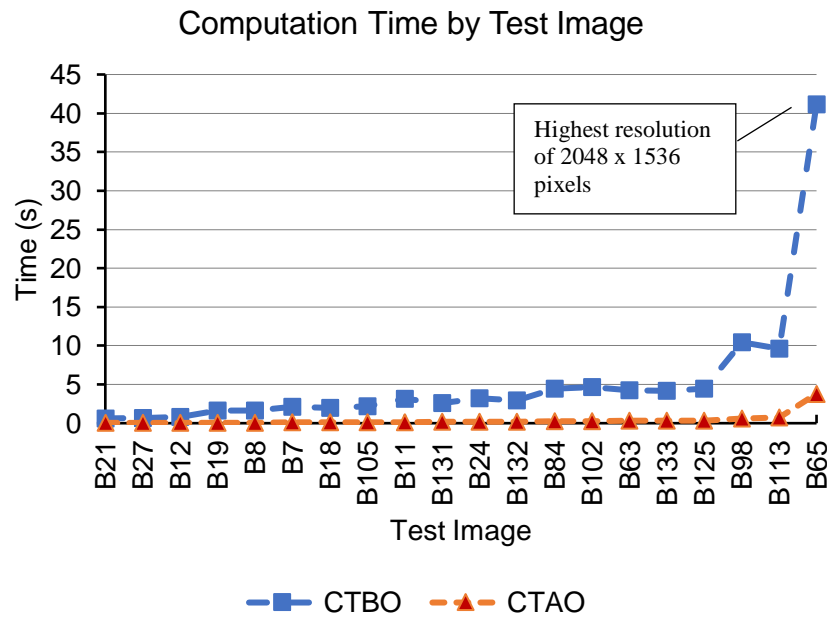
Computation Time by Test Image

Figure 4.17. Proposed method's computation time analysis

4.6. Multiple RBHF Process for improving enhancement quality

The experimental results in sections 4.1 to 4.4 show that the proposed method significantly improves the visual quality of the backlit image. These results were validated using objective and subjective measurements. On many occasions, the proposed method achieved high PSNR, SSIM, and NIQE quality. However, test images like B55, B71, B98, and B114 often realized low PSNR and SSIM index. These images were consistent with high backlit degradation. Therefore, to further improve their PSNR quality, the multiple RBHF process in section 3.2.3

was proposed. In theory, it is a valid approach since the proposed method has demonstrated the ability to preserve details and colour in the enhanced output. This section evaluates the impact of multiple RBHF process on some selected backlit inputs.

Figure 4.18 displays the results of applying ten (10) iterations of the proposed algorithm on sample backlit images. The backlit inputs are shown in Figure 4.18(a). Figures 4.18(b) to 4.18(k) are the enhancement results per iteration. The number of iterations was set at ten because, after ten iterations, there is no structural difference between the input and output images, as given by the SSIM index. Overall, the algorithm seems to improve the exposure of the backlit input with each iteration. Significant improvements in perceptual quality can be seen after the second and third iterations in Figures 4.18(c) and 4.18(d), respectively.

The proposed method also maintains the natural or original hues of the backlit input, even for ten iterations. Details such as edges and textures are preserved without underlining artefacts. A few examples can be seen in the outcomes of images B7, B11, B37, B55, B98 and B132. However, during the second iteration of B114, the effect of shadow clipping became visible in the enhanced image. Also, over-exposure tends to occur in the results of B65 by the 5th iteration. This problem occurs when the exposure level is higher than the amount required to illuminate the scene.
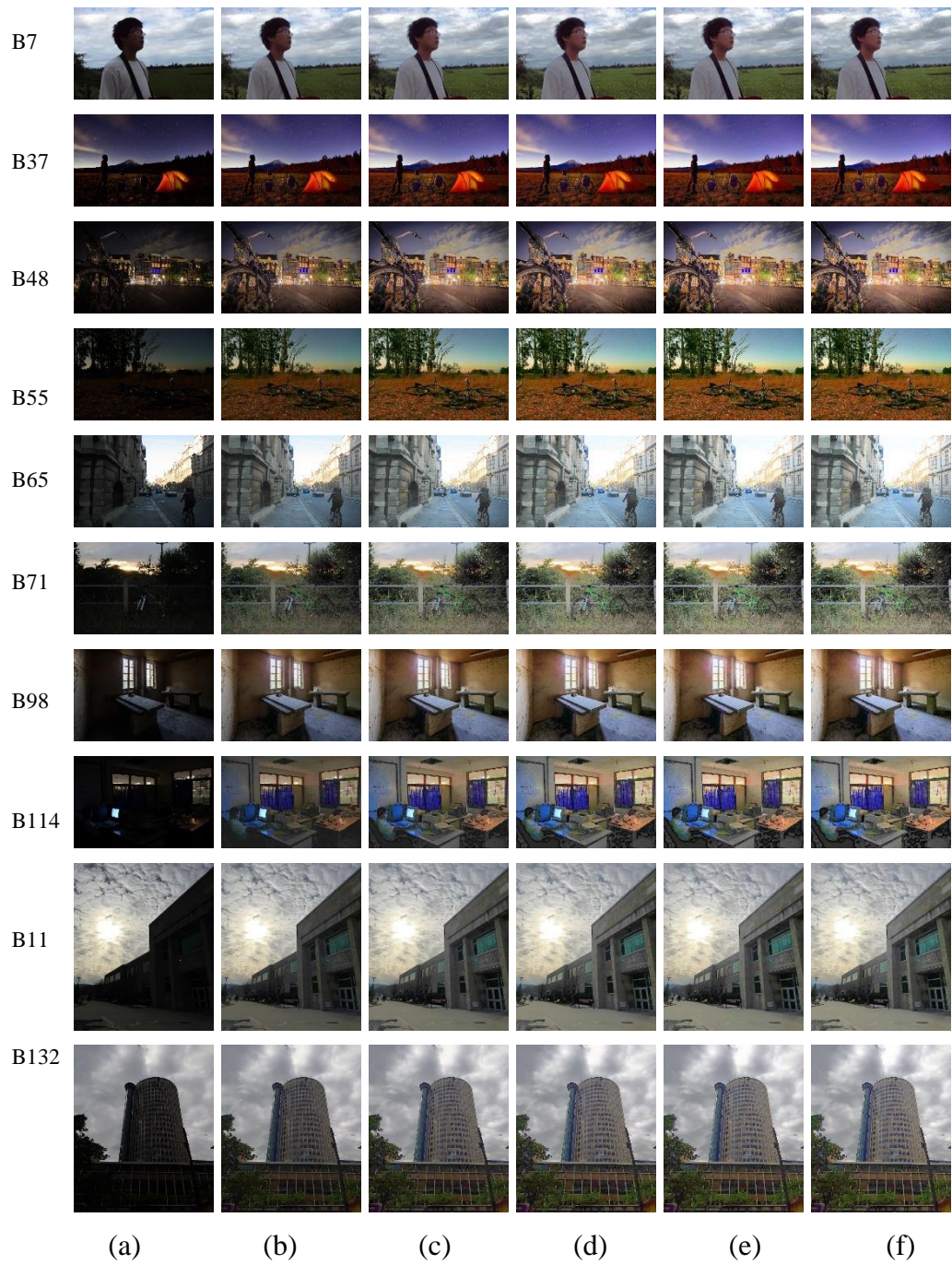
Figure 4.18. Performance of multiple RBHF (a) Backlit input (b) iter =1
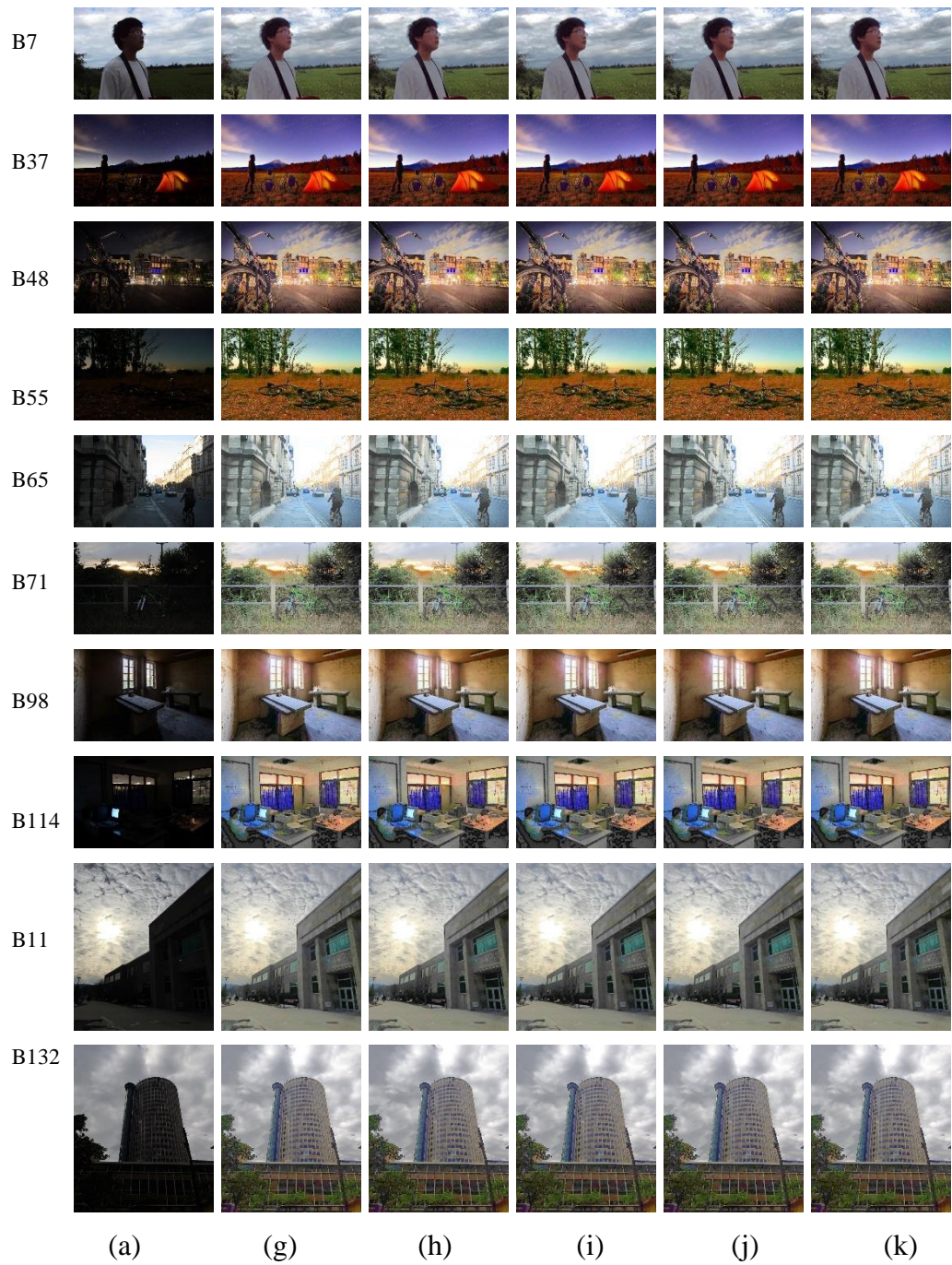(c) iter =2 (d) iter =3 (e) iter =4 (f) iter =5

Figure 4.18. *(continued)* Performance of multiple RBHF (a) Backlit input (g) iter =6 (h) iter =7 (i) iter =8 (j) iter =9 (k) iter =10

4.6.1. Objective assessment

The PSNR, SSIM, and NIQE quality metrics are used to evaluate the results in Figure 4.18. The PSNR measurements in Figures 4.19 and 4.20 show that multiple iterations of the proposed method significantly increase the PSNR quality of the backlit image. For many test inputs, up to a 12 dB increase was realized during the first three iterations. Some examples can be seen in the outcomes of B11, B48, and B55 in Figure 4.19 and B65, B114, and B98 in Figure 4.20. The PSNR values for inputs B7 and B65 tend to increase steadily for the ten iterations, while other inputs such as B37, B11, B48, and B114 appear to converge. The results of B7 and B65 also suggest that the PSNR quality can be improved beyond ten iterations.

Figures 4.21 and 4.22 display the SSIM measurements for the simulation results in Figure 4.18. For each iteration (*n*), the output image is compared to the enhanced image of the previous iteration (*n-1*), except for the first iteration, where the output image is compared to the original input. Figures 4.21 and 4.22 show a high increase in the backlit inputs' SSIM index within the first three iterations. After the third iteration, the SSIM values converged to absolute similarity. Beyond this point, there is no apparent difference between the input and output images.

The SSIM scores in Figures 4.23 and 4.24 measure the structural similarity between the original backlit image and the output for each iteration. The results show that the multiple iterations of the proposed method do not improve the enhanced image's structural similarity with the degraded backlit input. About a 10% reduction in the SSIM index occurred after the 2nd iteration. The decrease

in the SSIM values of Figures 4.23 and 4.24 is expected because as the backlit degradation is reduced by each iteration, more salient features are revealed in the enhanced images. Nevertheless, the proposed method maintained 80% structural similarity on average in the outcome of image B7 and (40-50) % in that of B11, B37, B65, and B132.

Figures 4.25 and 4.26 give the results of the NIQE assessment of the multiple RBHF process. Slight changes in the NIQE scores are observed for images B7, B55, B11, B48, and B132. However, the graphs suggest a noticeable drop in the naturalness quality of backlit inputs B37, B65, and B98 after each iteration.
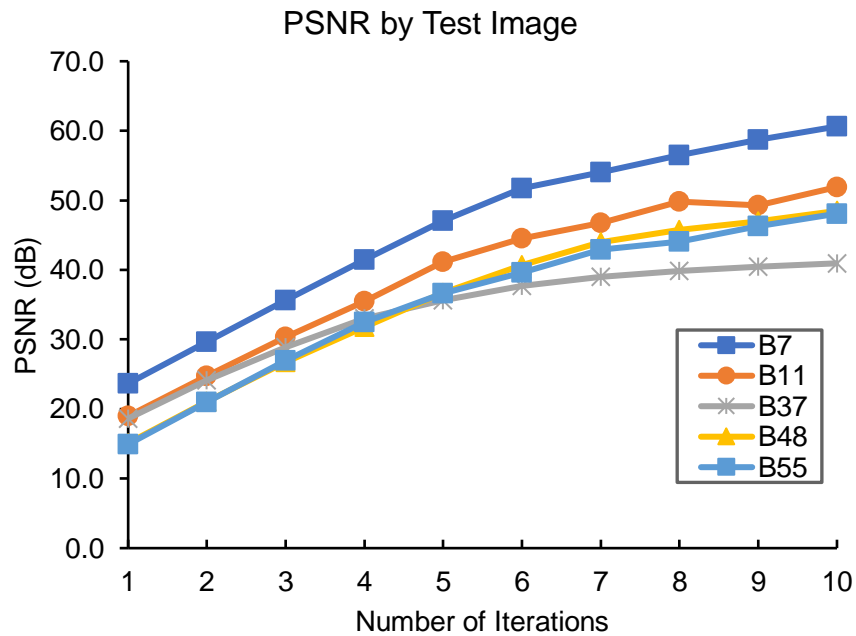
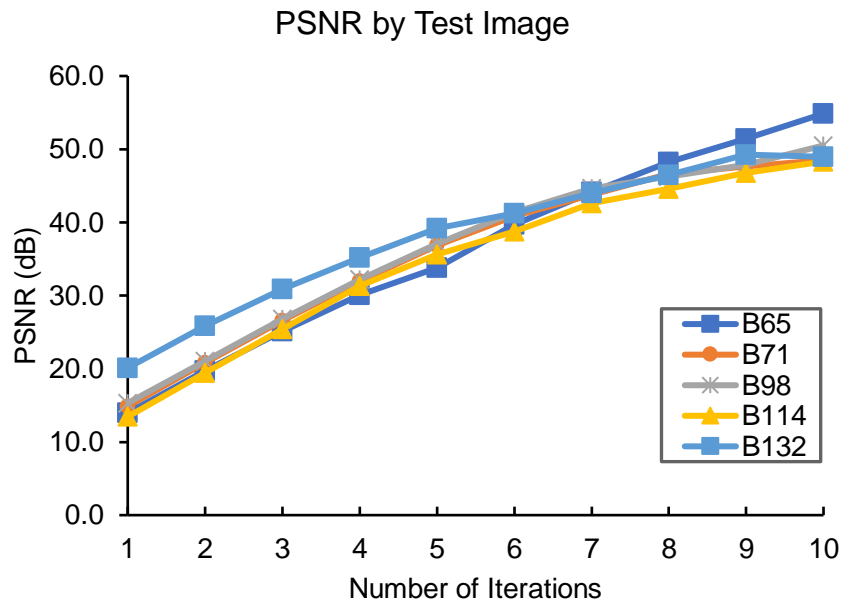

Figure 4.19. PSNR Evaluation of Multiple RBHF (Set 1)

PSNR by Test Image

Figure 4.20. PSNR Evaluation of the Multiple RBHF (Set 2)
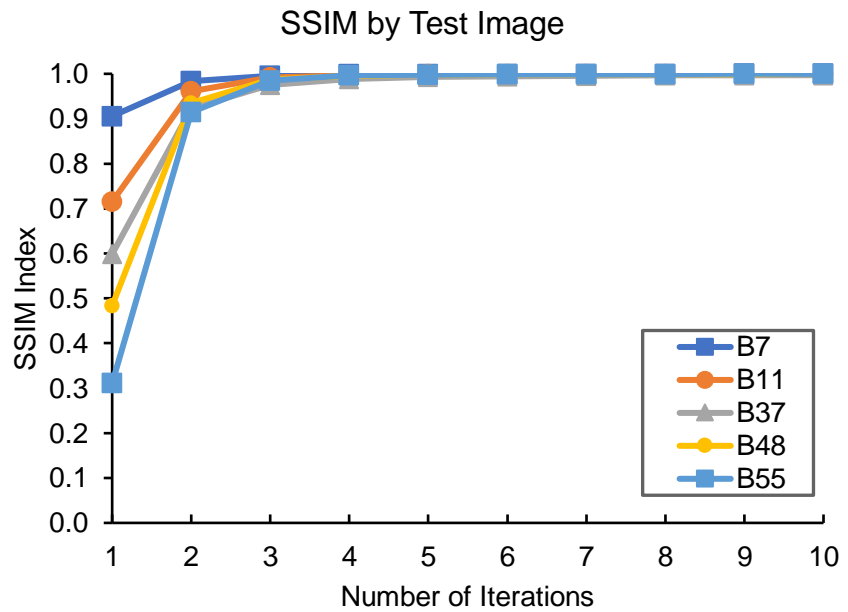
SSIM by Test Image

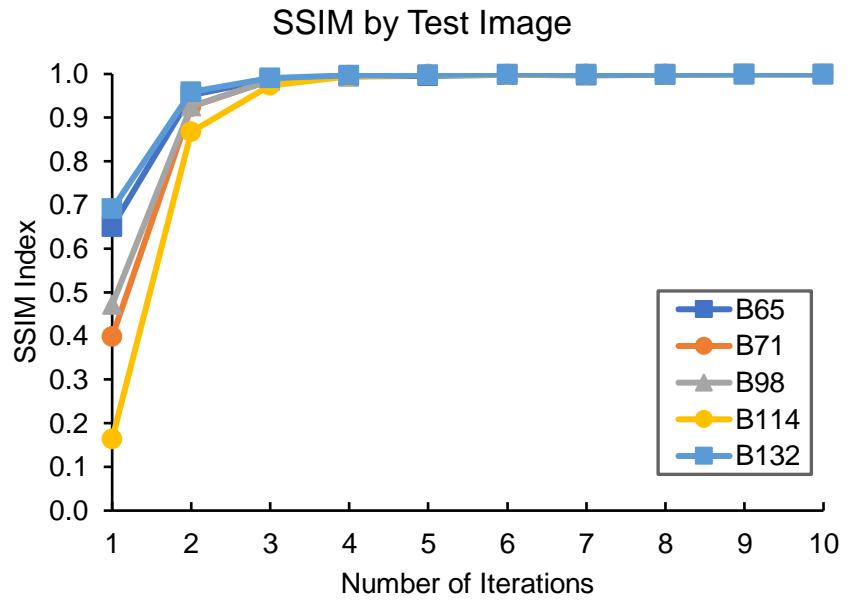Figure 4.21. SSIM Evaluation 1 of Multiple RBHF (Set 1)

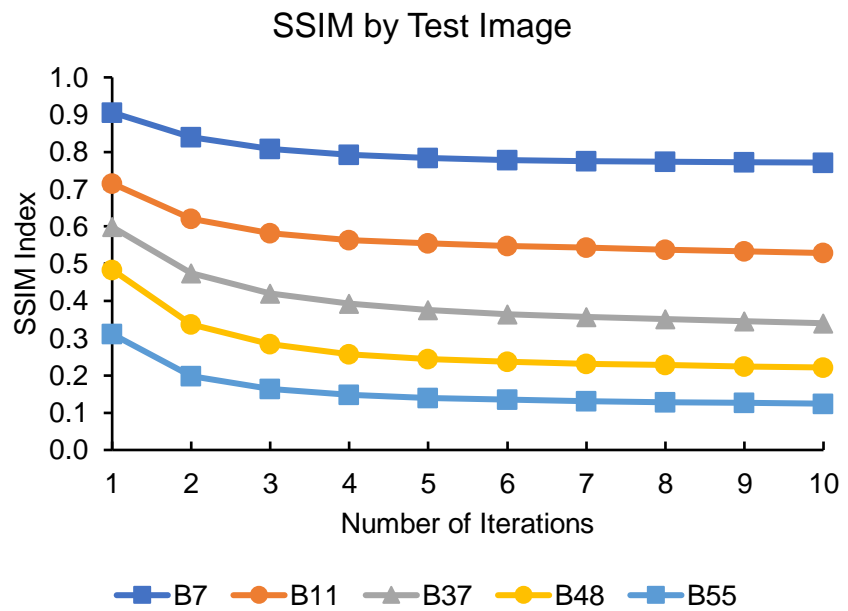Figure 4.22. SSIM Evaluation 1 of Multiple RBHF (Set 2)

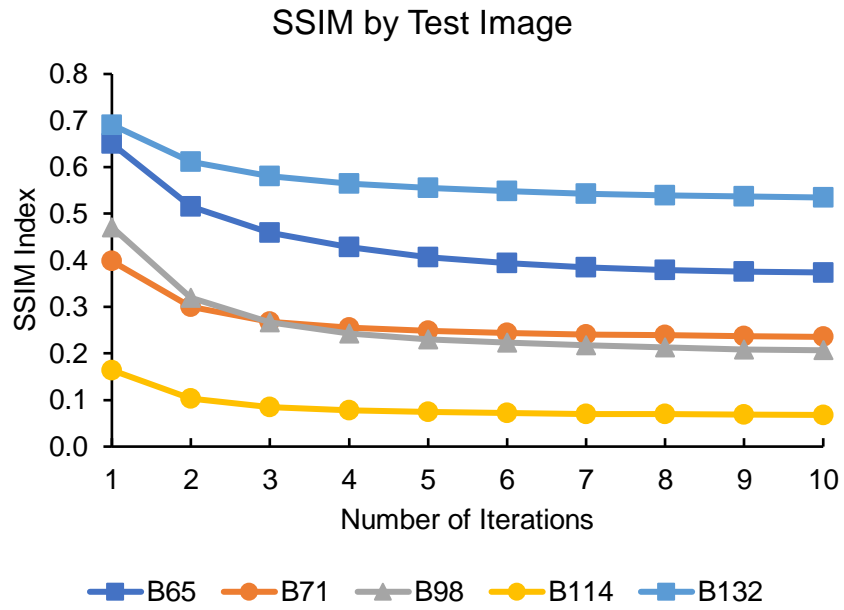Figure 4.23. SSIM Evaluation 2 of Multiple RBHF (Set 1)

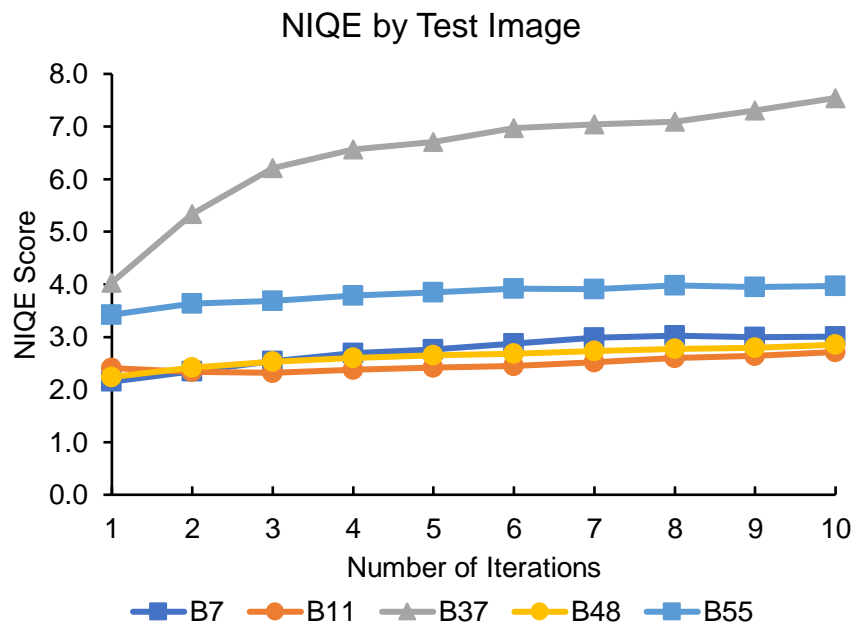Figure 4.24. SSIM Evaluation 2 of Multiple RBHF (Set 2)

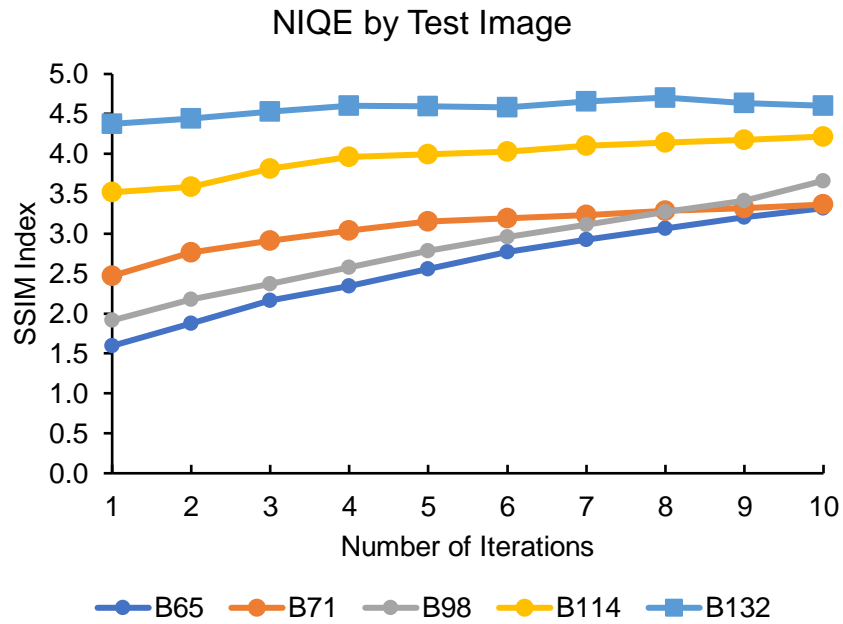Figure 4.25. NIQE Evaluation of Multiple RBHF (Set 1)

Figure 4.26. NIQE Evaluation of Multiple RBHF (Set 2)

4.6.2. Subjective assessment

Following the ITU-R BT.500-14, 16 people, consisting of 10 residents from the Plainsview community in South B and 6 students from the Railways Training Institute, Nairobi, were asked to judge the enhancement result for each iteration in Figure 4.18. They were also required to choose the outcome having the best picture quality. Table 4.10 gives the result of their subjective assessments, which is further illustrated in Figure 4.23.

Table 4.10 and Figure 4.23 demonstrate that two iterations of the proposed algorithm are often sufficient in producing a significantly higher image quality. However, for some inputs like B48 and B114, one iteration was deemed sufficient while others such as B55 required three iterations. These results are consistent with the SSIM evaluation in Figure 4.20.

Table 4.10. Subjective evaluation for multiple RBHF

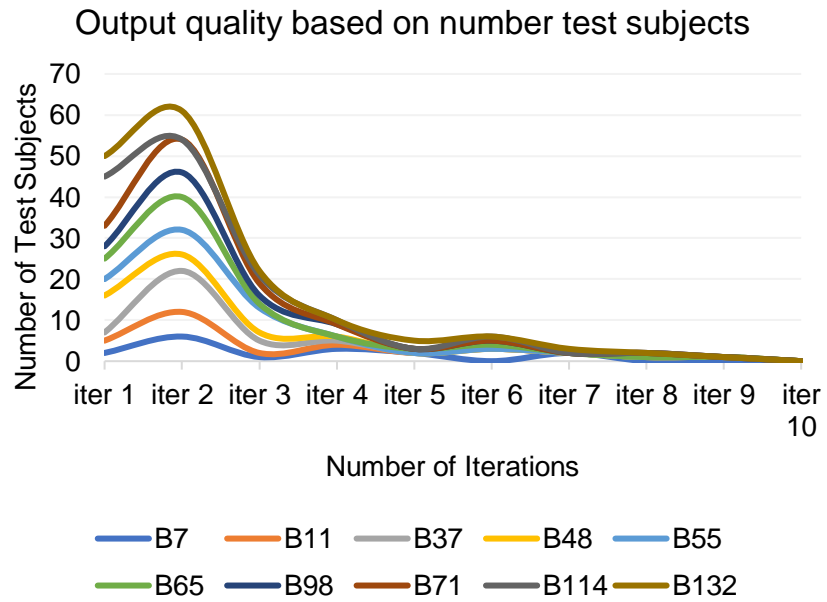| S/N	Iterations	Number of test subjects per image									
		B7	B11	B37	B48	B55	B65	B98	B71	B114	B132
1	iter 1	2	3	2	9	4	5	3	5	12	5
2	iter 2	6	6	10	4	6	8	6	8	0	7
3	iter 3	1	1	3	2	6	1	2	3	2	1
4	iter 4	3	1	1	1	0	0	3	0	1	0
5	iter 5	2	0	0	0	0	1	0	0	0	2
6	iter 6	0	3	0	0	0	1	1	0	1	0
7	iter 7	2	0	0	0	0	0	0	0	0	1
8	iter 8	0	1	0	0	0	0	1	0	0	0
9	iter 9	0	1	0	0	0	0	0	0	0	0
10	iter 10	0	0	0	0	0	0	0	0	0	0

Figure 4.27. Subjective evaluation of Multiple RBHF output quality

101

4.6.3. Computational Time Analysis

Figure 4.28 shows the average runtime per iteration. The results are limited to the computation after the DWT-F optimization. Image B65, with a resolution of 2048 x 1536 pixels, had the highest time cost, as expected. However, low-resolution images such as B7, B11, B114, B37, and B132, were enhanced in about 0.65 seconds per iteration.
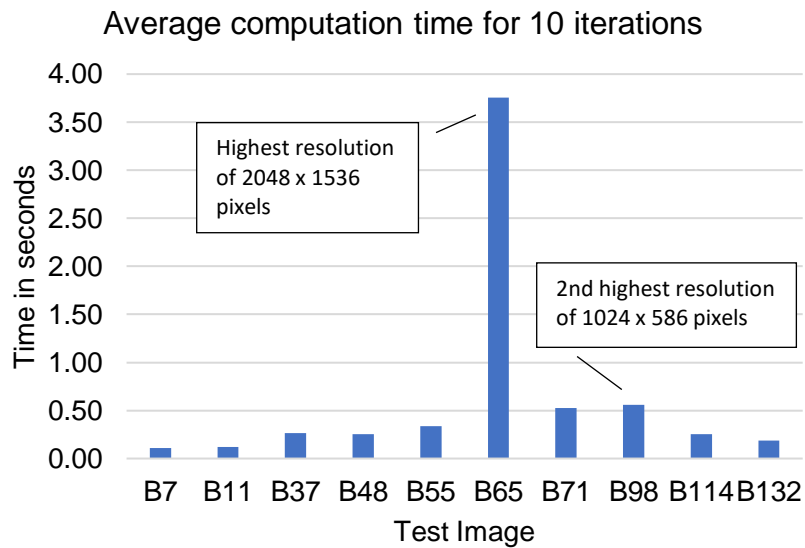

Figure 4.28. Time analysis for the Proposed Multiple RBHF Process

4.7. Comparative analysis with existing methods

In this section, the proposed method's performance is compared to existing enhancement algorithms such as Histogram Equalization [4], Retinex [76], and LIME [77]. The performance of each algorithm is evaluated both qualitative and quantitative in sections 4.7.1 and 4.7.2, respectively.

4.7.1. Qualitative evaluation

Figure 4.29 compares the enhanced results of the proposed method to that of existing image enhancement algorithms. The test images are displayed in Figure

102

4.29(a). The outcomes for Histogram Equalization [4], Retinex [76], and LIME [77] are shown in Figures 4.29(b), 4.29(c), and 4.29(d), respectively, whereas the proposed method in Figures 4.29(e) and 4.29(f).

The results in Figure 4.29 show that the proposed method outperforms existing image enhancement methods in terms of visual quality. Histogram Equalization, for example, enhanced visual perception of backlit inputs while distorting or washing out hues. Consider the outcome in Figure 4.29(a). The sky in image B7 appears to have shifted from a light blue to a purple tint, whereas the colours in images B48 and B55 are clearly washed-out. Figure 4.29(d) shows a similar colour distortion.

In most simulations, M-Retinex and LIME produced slightly better results than Histogram Equalization. However, M-Retinex frequently caused an unnatural appearance in the inputs, as seen in the outcomes of B7, B65, and B11 in Figure 4.25(c). LIME, in contrast, exaggerated image details, as shown in B7 and B11 of Figure 4.29(d). As a result, the proposed method outperforms Histogram Equalization, M-Retinex, and LIME by achieving higher visual quality while avoiding colour distortion, over-enhancement, or hue washing-out.
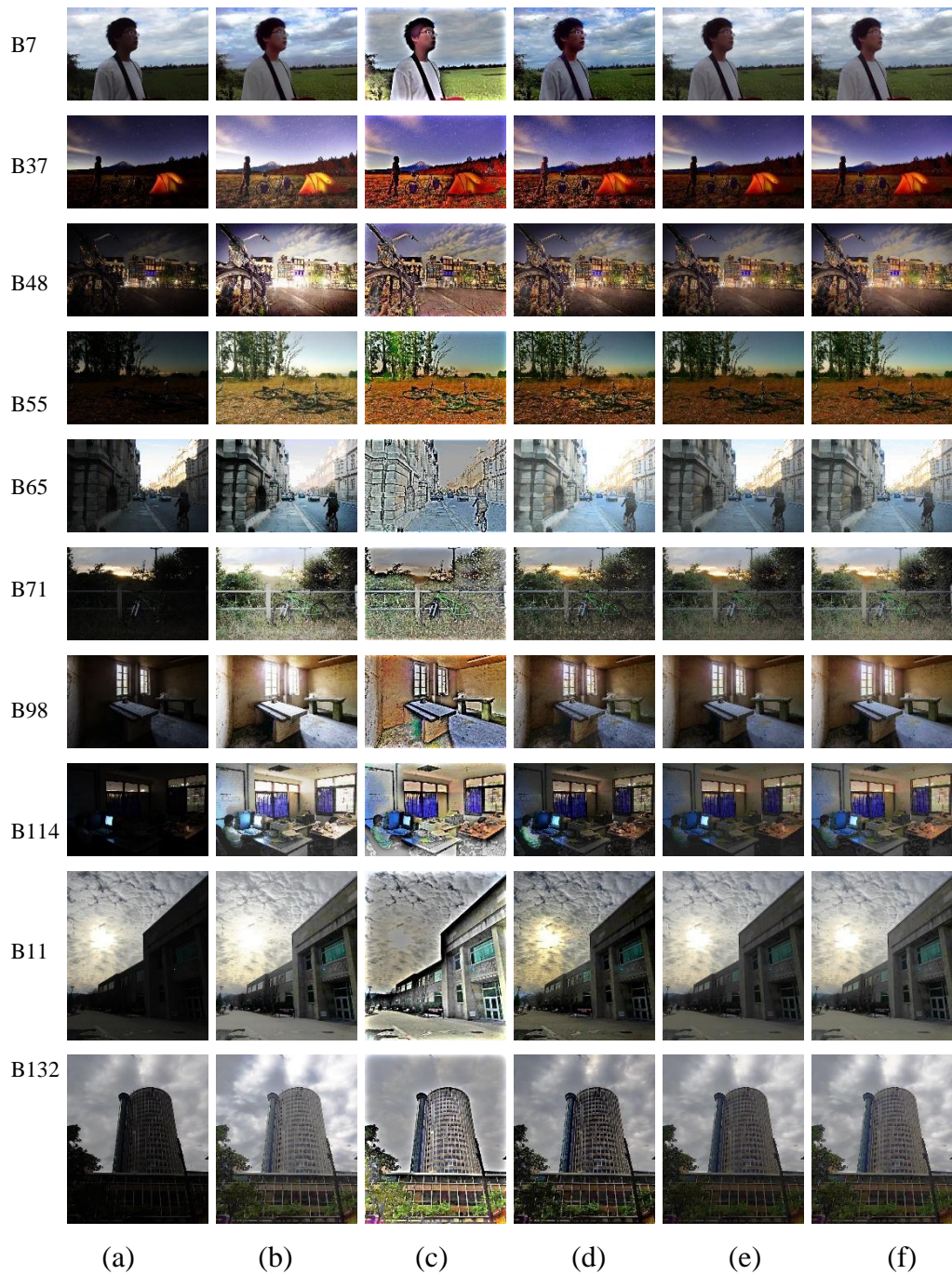
Figure 4.29. Comparison of various methods (a) Backlit input (b) HE [4] (c) M-Retinex [76] (d) LIME [77] (e) Proposed method iter=1 (f) Proposed method iter=2

4.7.2. Quantitative evaluation

(a) PSNR Assessment

Table 4.11 gives the PSNR assessment for the results in Figure 4.29. The first iteration of the proposed method achieved the highest PSNR quality in 8 out of 10 simulations when compared to histogram equalization, M-Retinex, and LIME. The second iteration, on the other hand, outperformed these methods completely in all simulations.

Table 4.11. Comparison of PSNR for various methods

S/N	Test Image	Descriptor	HE	M-Retinex	LIME	Proposed iter=1	Proposed iter=2
1	B7	Man Outdoor	20.9	10.7	18.8	23.7	29.6
2	B11	Office Building	14.2	8.1	18.9	19.0	24.8
3	B37	Camping	8.4	10.1	13.6	18.6	24.1
4	B48	Residential	6.9	8.4	12.8	15.1	21.1
5	B55	Fields Bicycle	6.4	8.2	12.3	14.9	20.9
6	B65	City Street	11.3	7.1	14.7	14.0	19.7
7	B71	Bush Bicycle	8.1	7.3	4.6	14.9	20.8
8	B98	Dark Room	7.2	7.7	14.0	15.3	21.0
9	B114	Office 1	5.7	5.3	14.6	13.4	19.5
10	B132	Hilton Hotel	13.6	9.7	17.8	20.1	25.9

(b) SSIM Assessment

Table 4.12 measures the structural similarity between the backlit input and the enhanced results in Figure 4.29. In 9 out of 10 simulations, the first iteration of the proposed method obtained the highest structural similarity compared to histogram equalization, M-Retinex, and LIME. It also achieved the second-best

SSIM quality for many test images in the second iteration, outperforming histogram equalization and M-Retinex.

Table 4.12. Comparison of SSIM index for various methods

S/N	Test Image	Descriptor	HE	M-Retinex	LIME	Proposed iter=1	Proposed iter=2
1	B7	Man Outdoor	0.79	0.65	0.75	0.91	0.84
2	B11	Office Building	0.59	0.45	0.66	0.72	0.62
3	B37	Camping	0.33	0.37	0.43	0.60	0.47
4	B48	Residential	0.21	0.25	0.37	0.48	0.34
5	B55	Fields Bicycle	0.13	0.14	0.23	0.31	0.20
6	B65	City Street	0.57	0.34	0.58	0.65	0.52
7	B71	Bush Bicycle	0.22	0.23	0.35	0.40	0.30
8	B98	Dark Room	0.22	0.20	0.37	0.47	0.32
9	B114	Office 1	0.06	0.09	0.20	0.16	0.10
10	B132	Hilton Hotel	0.55	0.48	0.61	0.69	0.61

(c) NIQE Assessment

Table 4.13 gives the NIQE assessment for the enhanced results in Figure 4.29. Overall, the first iteration of the proposed method realized the best quality scores in 7 out of 10 simulations, nearly outperforming the methods by histogram equalization, M-Retinex, and LIME.

Table 4.13. Comparison of NIQE scores for various methods

S/N	Test Image	Descriptor	HE	M-Retinex	LIME	Proposed iter=1	Proposed iter=2
1	B7	Man Outdoor	1.99	1.96	2.02	2.15	2.34
2	B11	Office Building	2.90	2.93	2.99	2.40	2.34
3	B37	Camping	4.84	4.73	5.25	4.03	5.34
4	B48	Residential	2.87	3.07	2.59	2.24	2.42
5	B55	Fields Bicycle	4.03	4.48	4.07	3.42	3.63
6	B65	City Street	1.69	2.09	2.11	1.60	1.88
7	B71	Bush Bicycle	3.49	3.07	2.78	2.47	2.77
8	B98	Dark Room	2.56	2.81	2.27	1.91	2.18
9	B114	Office 1	5.19	4.67	3.67	3.52	3.59
10	B132	Hilton Hotel	4.31	4.74	4.94	4.38	4.44

4.8. Input and Output characteristics

An exposure correction algorithm based on histogram processing and image fusion was proposed in the previous chapter. The proposed algorithm was evaluated using objective and subjective metrics on several backlit inputs with varying exposure levels. This chapter discusses the input and output characteristics of the grey-level images in terms of their illumination map, intensity mappings, and histogram properties. For simplicity, 12 images, three from each category within the dataset, are presented in Table 4.14 to facilitate the discussions. The categories are represented in column (4) as follows: LBS = low backlit sector; HBS = high backlit sector; LBH = low background highlight; HBH = high background highlight.

Table 4.14. Selected backlit images for input-output analysis

S/N	Test Image	Descriptor	Category	PSNR	SSIM	NIQE I/P	NIQE O/P
1	B24	Cityscape	LBS	19.1	0.84	2.64	2.34
2	B84	Sunset Mountain	LBS	18.0	0.67	2.82	2.50
3	B102	Dark Room Table	LBS	15.3	0.37	2.74	2.45
4	B4	Woman Fields	HBS	21.2	0.64	2.71	2.57
5	B33	Boy at Window	HBS	15.8	0.53	3.80	3.44
6	B114	Office 1	HBS	13.4	0.16	3.07	3.52
7	B37	Camping	LBH	18.6	0.60	5.17	4.03
8	B55	Fields Bicycle	LBH	14.9	0.31	3.44	3.42
9	B74	Boat Night	LBH	19.0	0.56	4.41	4.48
10	B15	Girl Sea	HBH	25.6	0.98	4.18	3.54
11	B31	Girl 1 Field	HBH	25.8	0.97	3.84	3.71
12	B89	Restaurant 2	HBH	13.4	0.39	4.54	4.66

4.8.1. Illumination map comparison

Figure 4.30 compares the illumination of the backlit images in Table 4.14 to their output images obtained by one iteration of the proposed method in sections (4.1) to (4.4), respectively. The first image in each figure is the illumination map of the backlit input, and the second is that of the enhancement result. The illumination maps were calculated in MATLAB R2018a by converting the colour profiles of intensity images in the HSV space to the one shown in Figure 4.30. In the new colour scheme, the grey value at each pixel position is coded black, red, orange, yellow, or white based on luminance. Black represents hard shadows, and white represents excessive highlights.

The results in Figure 4.30 shows how the backlit degradation in each input varies with different exposure levels. Images with soft shadows such as B24,

B84, B102, B37, and B55 have higher visibility in the F-region than those degraded by hard shadows like images B4, B33, B14, B74, and B89. Similarly, backlit inputs B37, B55, and B74 with low background radiance have higher visibility in the B-region than B15, B31, and B89. The region-based histogram specification scheme of the proposed method accounts for such variations by mapping output intensity values based on the luminance profile in the input.

For example, when comparing the results of image B24 to that of B84, in Figures 4.30(a) and 4.30(b), respectively, the proposed method tends to increase exposure more in the B-region of B24 than B84 despite the two images having soft shadows in the foreground. This is because, in the context of exposure correction, more contrast is required in the F-region of image B24 to balance the high radiance in the over-exposed B-region. Another example can be seen when comparing the results of images B37 and B55 in Figures 4.30(g) and 4.30(h), respectively. In other instances, the proposed algorithm tends to reduce the high radiance in the input to improve contrast in over-exposed sectors as seen in Figure 4.30(j).
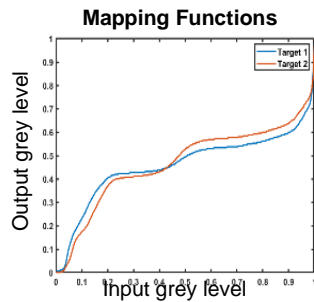
(a) Image B24

(b) Image B84

(c) Image B102

(d) Image B4

(e) Image B33

(f) Image B114

(g) Image B37

(h) Image B55

(i) Image 74

(j) Image B15

(k) Image B31

(l) Image B89
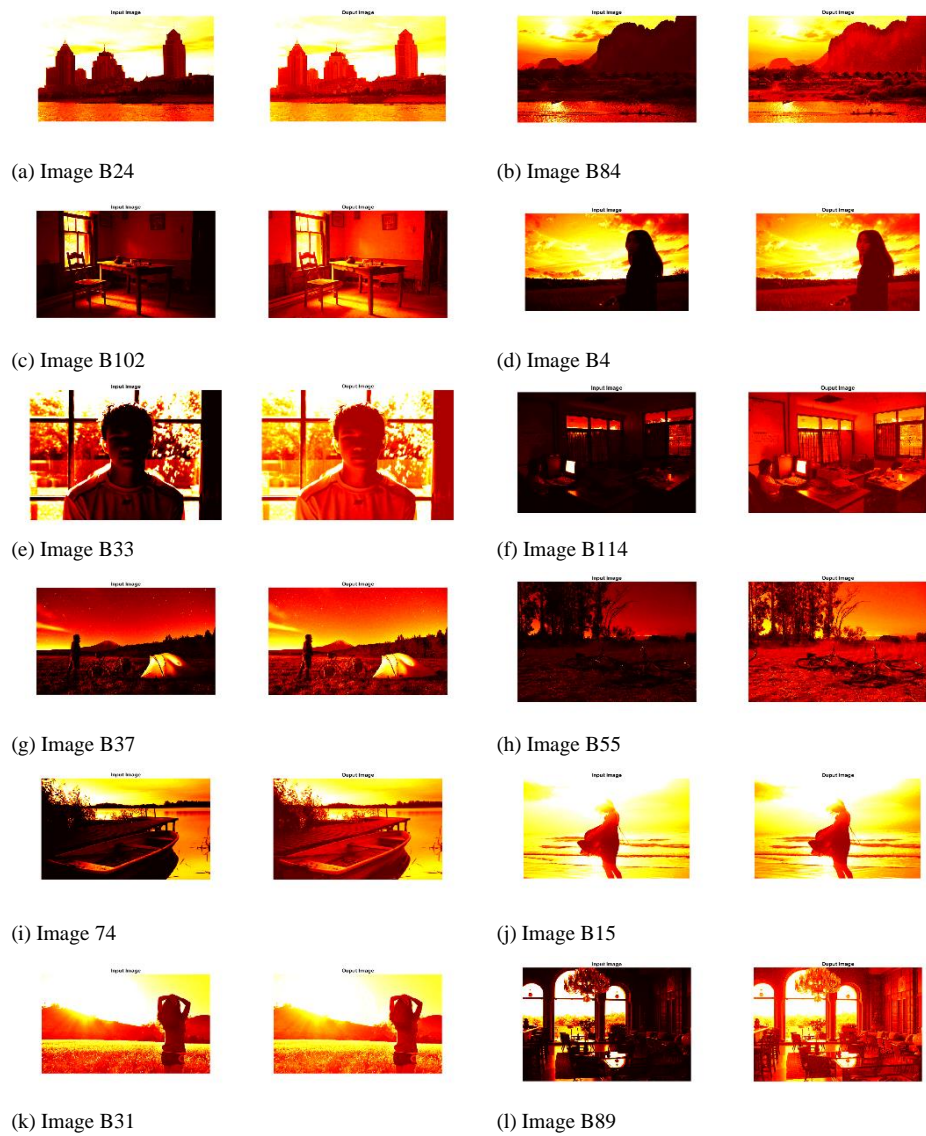
Figure 4.30. Illumination maps for various inputs and outputs

4.8.2. Intensity mappings

Figures 4.31(a) to 4.31(l) display the transformation functions derived from equation (3.1) for the set of images in Table 4.14, using the results of one iteration of the proposed method given in sections (4.1) to (4.4), respectively. The blue line in all figures represents the transformation function used in M_1 to map the input intensity values to Target 1, whereas the orange line is used in M_2 to map the input values to Target 2. As seen in Figure 4.31, the mapping

110

functions for foreground and background contrast enhancement automatically adapt to changes in the luminance profile of the backlit input as opposed to the "one size fits all" approach used in several related works [1],[49],[50],[43],[53], and [54].
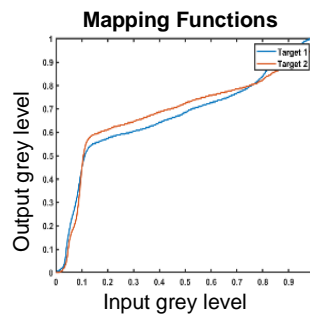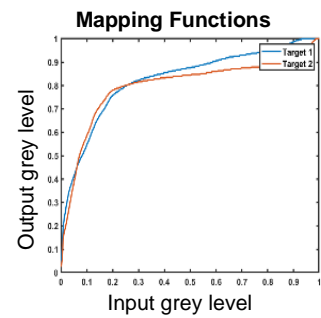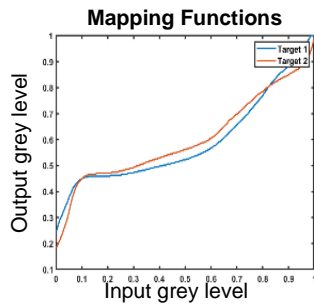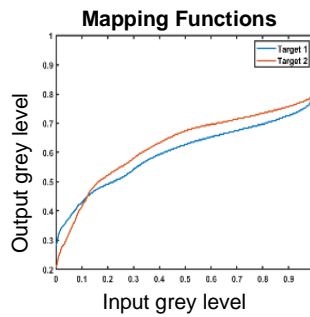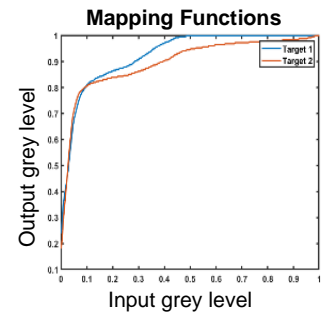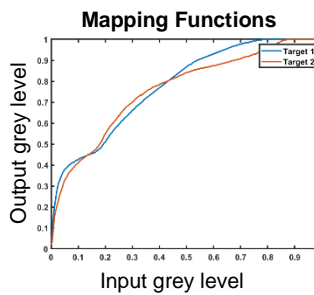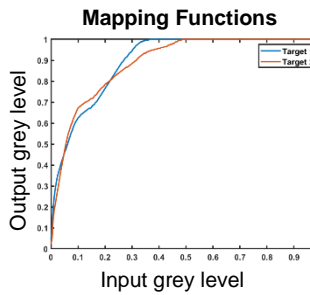
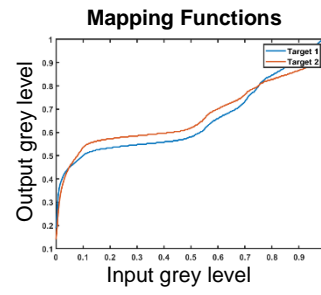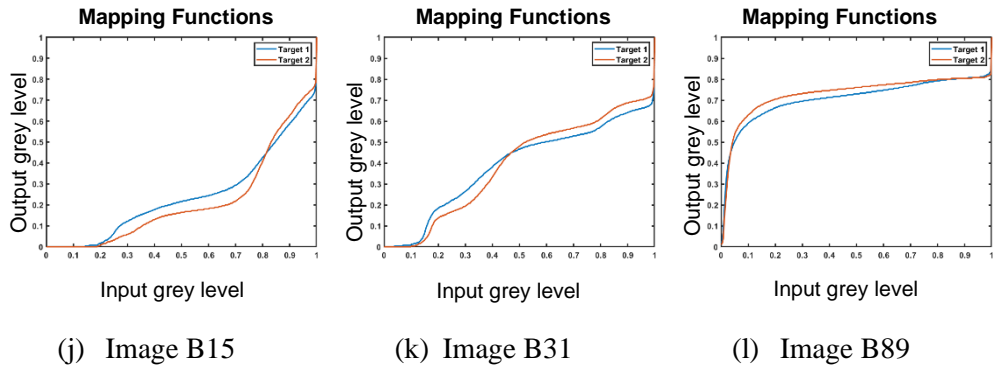| (a) Image B24	(b) Image B84	(c) Image B102
(d) Image B4	(e) Image B33	(f) Image B114
(g) Image B37	(h) Image B55	(i) Image B74

Figure 4.31. Mapping functions for various backlit inputs

4.8.3. Histogram properties

Figures 4.32(a) to 4.32(l) depicts the input and output histograms for the set of images in Table 4.14, using the results of one iteration of the proposed method given in section (4.1) to (4.4), respectively. Figure 4.32 demonstrates how the proposed method improves contrast in the backlit inputs by shifting pixel values away from the hard shadows. Some examples can be seen in the outcomes of images B24, B84, B102, and B4. In other instances, like the one shown in Figure 4.32(f), the algorithm improved contrast by expanding the dynamic range of the image. Figure 4.32(j) is another outcome worth mentioning. The proposed method seems to suppress the high radiance in the input by shifting pixel values to the left side of the histogram.
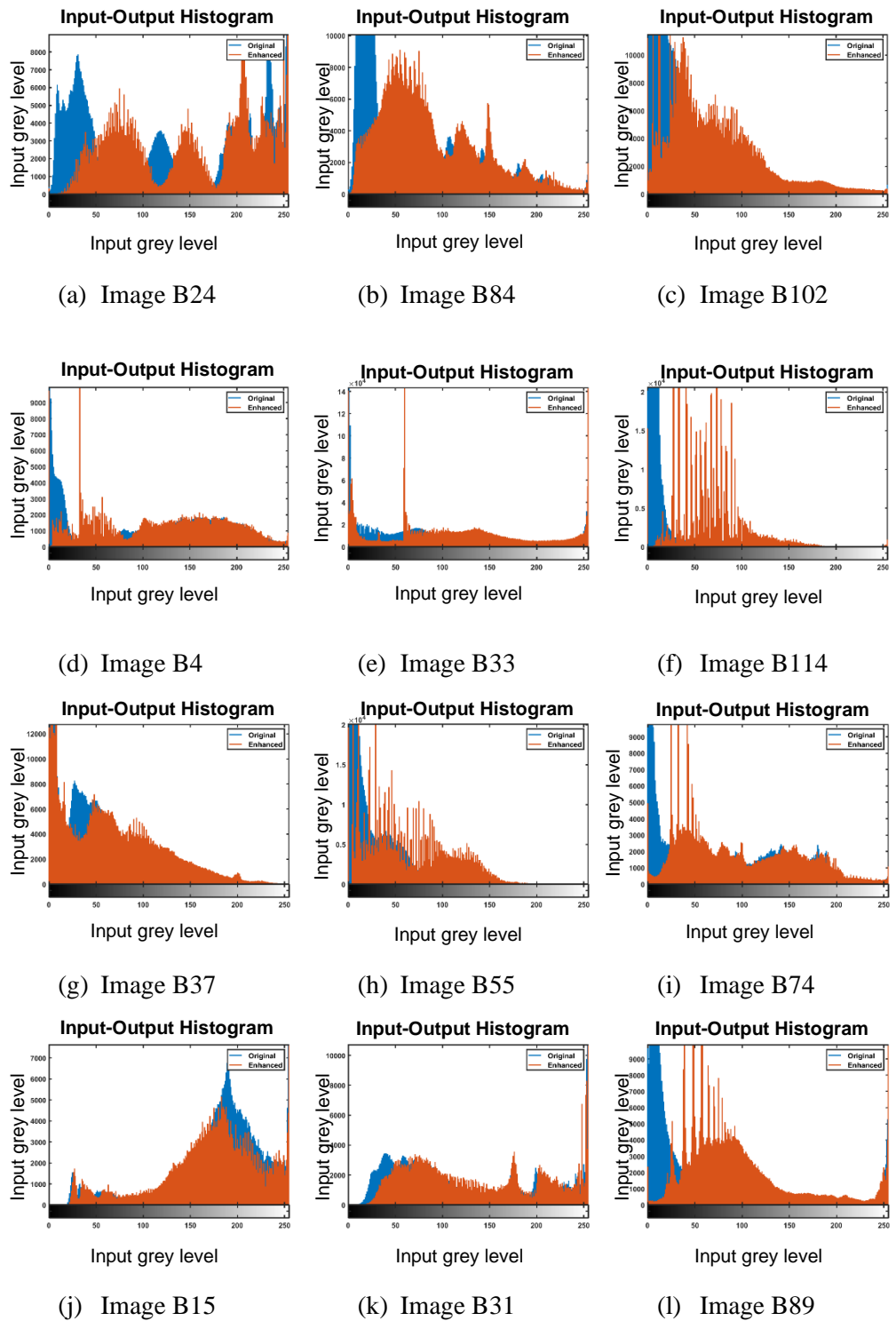
(a) Image B24 (b) Image B84 (c) Image B102

(d) Image B4 (e) Image B33 (f) Image B114

(g) Image B37 (h) Image B55 (i) Image B74

(j) Image B15 (k) Image B31 (l) Image B89

Figure 4.32. Input and output histogram for various backlit inputs

4.9. Impact of wavelet function

The proposed method uses a two-stage DWT-F process that extracts and combines features of the input masks with the backlit input to produce the final enhanced image. The low-pass and high-pass filters used in the decomposition and reconstruction phases are determined by the wavelet parameter $\psi_{a,b}(x,y)$. This section discusses the selection of wavelet function impact on the enhancement quality of the final output image. The discussion is limited to the Haar, Daubechies, Symlets, and Coiflets families. Four daughter wavelets from each family—except the Haar family, which has only a single wavelet—are arbitrarily selected to simulate the algorithm's performance in MATLAB. The output of the experiments is evaluated qualitatively and quantitatively in sections 4.9.1 and 4.9.2, respectively.

4.9.1. Qualitative evaluation

In Figure 4.33, two sample backlit images are enhanced by various wavelet functions from the Daubechies (dbN), Symlets (symN), and Coiflets (coifN) families. The four daughter wavelets selected from each family are distinguished by their number of vanishing moment *N*, as shown in Figure 4.33. Overall, the choice of wavelet function tends to have no significant difference in the perceptual quality of the backlit inputs. This can be seen by comparing the enhancement results of images B7 and B75 using sym4, sym5, coif2 or Haar, db5, and sym3.
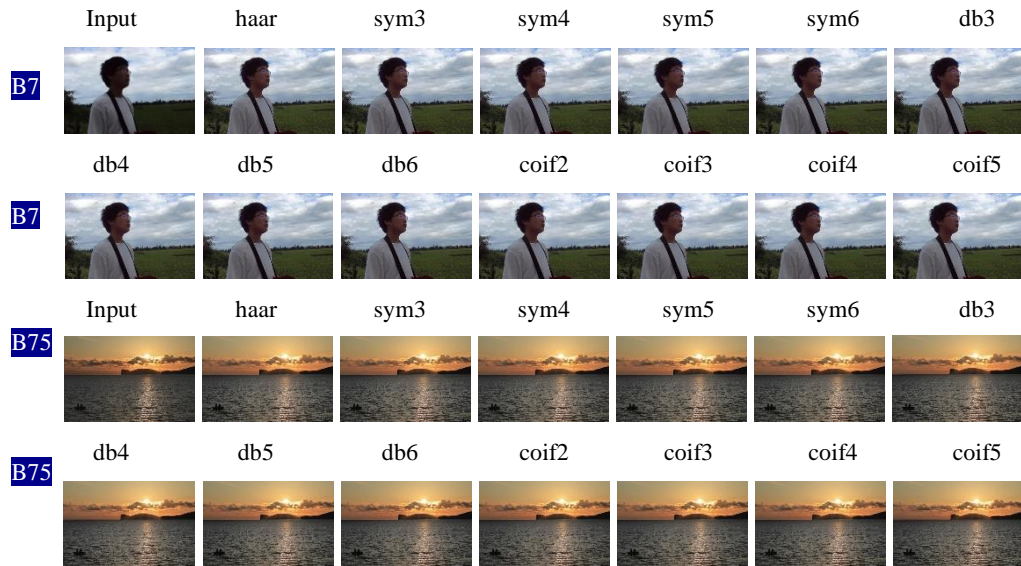
Figure 4.33. Comparison of multiple wavelet functions

4.9.2. Quantitative evaluation

Table 4.15 shows the PSNR, SSIM, and NIQE quality assessments for the results in Figure 4.33. The PSNR measurements are given in column (3). The SSIM scores are provided in columns (4), and columns (5) and (6) are the NIQE measures for the input and output images, respectively. Table 4.15 reveals that the choice of a particular wavelet slightly impacts the PSNR and SSIM index by ±0.1 dB and ±1%, respectively. In contrast, the NIQE results show multiple variations for each experiment. For example, the outcomes of B7 show significant improvements in the NIQE quality by the Haar, sym3, db3, db5, db6, coif3, coif4, and coif5 wavelets despite them having the lowest PSNR. Therefore, there exists a direct relationship between the choice of Wavelet transform and the naturalness quality of the enhanced image.

115

Table 4.15. Quantitative evaluation of various wavelet functions

S/N	Test Image	Wavelet	PSNR (dB)	SSIM	NIQE I/P	NIQE O/P
1	B7	Haar	23.6	0.90	2.26	1.85
		sym3	23.6	0.90	2.26	1.65
		sym4	23.6	0.90	2.26	2.57
		sym5	23.7	0.91	2.26	2.15
		sym6	23.6	0.90	2.26	2.73
		db3	23.6	0.90	2.26	1.65
		db4	23.7	0.91	2.26	2.20
		db5	23.6	0.90	2.26	1.67
		db6	23.6	0.90	2.26	1.73
		coif2	23.7	0.91	2.26	2.59
		coif3	23.6	0.90	2.26	1.88
		coif4	23.6	0.90	2.26	1.87
		coif5	23.6	0.90	2.26	1.84
2	B75	Haar	24.8	0.94	4.45	4.51
		sym3	24.9	0.94	4.45	4.52
		sym4	25.0	0.94	4.45	4.90
		sym5	25.0	0.95	4.45	4.74
		sym6	24.9	0.94	4.45	4.88
		db3	24.9	0.94	4.45	4.52
		db4	25.0	0.95	4.45	4.79
		db5	24.9	0.94	4.45	4.48
		db6	25.0	0.94	4.45	4.49
		coif2	25.0	0.95	4.45	4.79
		coif3	25.0	0.94	4.45	4.65
		coif4	25.0	0.94	4.45	4.90
		coif5	25.0	0.94	4.45	4.86

CHAPTER 5

CONCLUSION AND RECOMMENDATIONS

5.1. Conclusion

In this thesis, a novel backlit image enhancement algorithm has been proposed. The algorithm uses a region-based histogram specification scheme in combination with the discrete wavelet transform image fusion to improve the visual quality of a single backlit image. The performance of the algorithm was tested on standard backlit images from Li's database and the Exclusively Dark dataset. Both objective and subjective image quality assessment results validate the superior performance of the proposed method in terms of improving perceptual quality at a low computation cost with no distortion or colour artefacts.

The enhancement results for images with low backlit sectors demonstrate that the proposed algorithm can correct exposure disparities between an under-exposed foreground and a well-lit background in a picture scene with more than (60-70) % structural similarity retained in the enhanced image.

Images with high backlit sectors were consistent with low PSNR and SSIM index despite significant improvements in their visual perception by the proposed method. Furthermore, the effects of shadow clipping become apparent in the enhanced output for some test images within the high backlit sector category. However, experimental results show that multiple iterations of the proposed method can improve the PSNR quality up to 12 dB after the first three iterations with no distortion or colour artefacts.

Images from the high and low background highlight categories showed similar outcomes in the PSNR, SSIM, and NIQE assessments to those in the low and high backlit sector categories. The reason is that despite variations in background luminance, the degree of under-exposure in the foreground always constitutes either a hard or soft shadow.

The performance of the proposed method was compared to existing image enhancement methods such as Histogram Equalization, Retinex, and Low-Light Image Enhancement via Illumination Map Estimation. Experimental results demonstrated the superiority of the proposed method in improving the perceptual quality of the backlit image with no colour distortion or artefacts. Two iterations of the proposed method significantly outperformed existing methods in terms of PSNR, SSIM, and NIQE quality metrics.

Finally, global contrast stretching techniques were widely known to be ineffective in solving the problem of backlit image enhancement. However, the findings in this report demonstrate the efficacy of a histogram-based approach when combined with image fusion.

5.2. Recommendations

The following recommendations are provided to guide the use of the proposed method and support further research.

(i) Multiple iterations can be used to improve the performance of the proposed algorithm in a situation where the PSNR or visual quality of the enhanced image is perceived to be low by the observer.

Typically, two to three iterations are sufficient to produce a better image quality.

(ii) The wavelet parameter in the DWT fusion stages mainly contributes to the naturalness quality of the enhanced image. High values of NIQE alone are not a determinant for better image quality. Therefore, an appropriate choice of wavelet function should maintain the NIQE score of input but with high PSNR, such as sym5.

(iii)The algorithm proposed in this thesis only addresses the problem of exposure correction in backlit images. Applying the classical unsharp masking algorithm on the output of the second DWT fusion stage could improve sharpness in the enhanced image.

(iv)As the research aimed to develop a backlit image enhancement method for cell phone applications, developing and prototyping the algorithm on a PC using MATLAB offered a more flexible and efficient environment for testing and optimizing key parameters. Future works shall consider the practical translation of the proposed algorithm to Android devices, by rewriting the code in Java, the primary programming language for Android app development, identifying or developing custom Java libraries for the DWT fusion, and conducting performance optimizations and memory management to ensure efficient execution. Additionally, user interface design tailored to cell phone screens and interactions could be explored to enable intuitive usage of the backlit image enhancement algorithm on mobile devices.

REFERENCES

[1] T. Trongtirakul, W. Chiracharit and S. S. Agaian, "Single Backlit Image Enhancement," in IEEE Access, vol. 8, pp. 71940-71950, 2020, doi: 10.1109/ACCESS.2020.2987256

[2] Li's Database. Accessed: October 18, 2021. [Online]. Available: https://github.com/7thChord/backlit

[3] A. Gay, "How to Take Silhouette Photos in 7 Easy Steps," Pretty Presets for Lightroom.https://www.lightroompresets.com/blogs/pretty-presets-blog/6162254-how-tophotograph-a-silhouette (accessed Apr. 10, 2021)

[4] S. M. Pizer, E. P. Amburn, J. D. Austin., "Adaptive histogram equalization and its variations," Computer vision, graphics, and image processing, vol. 39, no. 3, pp. 355–368, 1987

[5] D. J. Jobson, Z.U. Rahman and G.A. Woodell, "Properties and performance of a center/surround retinex," IEEE Transactions on Image Processing, vol. 6, no. 3,pp. 451–462, 1997

[6] D. J. Jobson, Z. U. Rahman and G. A. Woodell, "A multiscale retinex for bridging the gap between color images and the human observation of scenes," IEEE Transactions on Image Processing, vol. 6, no. 7, pp. 965–976, 1997.

[7] M. Elad, R. Kimmel, D. Shaked and R. Keshet, "Reduced complexity retinex algorithm via the variational approach," Journal of visual communication and image representation, vol. 14, no. 4, pp. 369–388, 2003.

[8] J. Bernacki, "Automatic exposure algorithms for digital photography," Multimedia Tools and Applications, vol. 79, May 2020, doi: 10.1007/s11042-019-08318-1.

[9] P. E. Debevec and J. Malik, "Recovering high dynamic range radiance maps from photographs," in Proceedings Association of Computing Machinery's Special Interest Group on Computer Graphics and Interactive Techniques. Classes, 2008, Art. no. 31.

[10] G. Cecere, N. Corrocher, and R. Battaglia, "Innovation and competition in the smartphone industry: Is there a dominant design?," Telecommunications Policy, vol. 39, Aug. 2014, doi: 10.1016/j.telpol.2014.07.002.

[11] "Cell phone sales worldwide," Statista, Mar. 31, 2021. https://www.statista.com/statistics/263437/global-smartphone-sales-to-end-users-since-2007/ (accessed Apr. 09, 2021).

[12] R. C. Gonzales and R. E. Woods, Digital Image Processing (4th Ed., Global Ed.). Pearson Publishing Co., Inc. New Jersey, USA, 2018.

[13] J. D. Cressler, "Let There Be Light: The Bright World of Photonics". Silicon Earth: Introduction to Microelectronics and Nanotechnology, Second Edition 2017. CRC Press. p. 29. ISBN 978-1-351-83020-1.

[14] "CCD and CMOS sensors". Canon Professional Network. Archived from the original on 28 April 2018. Retrieved 9 March 2022.

[15] M. Tom, December 29, 2011. "CMOS Is Winning the Camera Sensor Battle, and Here's Why". Archived from the original on 25 September 2015. Retrieved 10 March 2022.

[16] "CCD vs CMOS - Difference and Comparison | Differ." https://www.diffen.com/difference/CCD_vs_CMOS (accessed March. 18, 2022).

[17] U. Optics, "Cell Phone Cameras | CMOS Imaging," *Universe Optics*, September 12, 2014. https://www.universeoptics.com/cell-phone-camera-technologies-incorporate-cmos-imaging/ (accessed Mar 18, 2022).

[18] "About Bayer Cameras - NI IMAQ White Balancing Utility Documentation." [Available online] https://documentation.help/NI-IMAQ-White-Balancing-Utility/About%20Bayer%20Cameras.html (accessed March. 24, 2022).

[19] K. Wachira, "A Hybrid Heuristic-Base Localised Area Demosaicking Technique for Panchromatic Colour Filter Arrays," MSc thesis, University of Nairobi, Nairobi, Kenya, 2018

[20] Pantone, "What are the Different Color Models?" https://www.pantone.com/articles/color-fundamentals/color-models-explained (accessed March. 24, 2022).

[21] "MATLAB - MathWorks." https://www.mathworks.com/products/matlab.html (accessed Jul. 25, 2022).

[22] "Understanding Color Spaces and Color Space Conversion - MATLAB & Simulink." https://www.mathworks.com/help/images/understanding-color-spaces-and-color-space-conversion.html (accessed Mar. 24, 2022).

[23] "Photo Sizes And 7 Other Factors That Influence Image Quality," Depositphotos Blog, Nov. 07, 2019. https://blog.depositphotos.com/photo-sizes-image-quality.html (accessed Mar. 24, 2022).

[24] "Understanding Dynamic Range in Digital Photography." https://www.cambridgeincolour.com/tutorials/dynamic-range.htm (accessed Mar. 24, 2022).

[25] "A Beginners Guide to Dynamic Range in Photography." https://shotkit.com/dynamic-range/ (accessed Mar. 25, 2022).

[26] "Sony A7R IV camera is here: 61MP, 15 stops of dynamic range, 5-axis IBIS and 10fps! | Digital Camera World." https://www.digitalcameraworld.com /news/sony-a7r-iv-camera-is-here-61mp-15-stops-of-dynamic-range-5-axis-ibis-and-10fps (accessed Mar. 25, 2022).

[27] U.Dawood, "If your eyes were cameras, what would the specs be?," digitalcameraworld, Dec. 08, 2020.https://www.digitalcameraworld.com/news/ /if-your-eyes-were-cameras-what-would-the-specs-be (accessed March 25, 2022).

[28] J. Artaius, "What is exposure?," digital cameraworld, May 07, 2020.https://www.digitalcameraworld.com/tutorials/what-is-exposure (accessed Jul. 25, 2022).

[29] M. Rehan, "Photography" http://mayarehan.weebly.com/photography. html (accessed Jul. 25, 2022).

[30] "How to manually change your camera's exposure settings? Exposure tips to ensure your photographs are properly exposed every time. – SLR Photography Guide." https://www.slrphotographyguide.com/exposure-tips/ (accessed Jul. 25, 2022).

[31] K. Sharma, "Entry-Level Android Phones Can Now Take HDR Photos with Camera Go Update," MySmartPrice, Dec. 18, 2020. https://www.mysmartprice.com/gear/entry-level-android-phones-can-now-take-hdr-photos-camera-go-update/ (accessed Jul. 25, 2022).

[32] "How to use your HDR camera settings | Adobe." https://www.adobe.com/creativecloud/photography/hub/guides/learn-about-hdr-camera-settings (accessed Jul. 25, 2022).

[33] "When to use HDR," duendevisual, Aug. 26, 2015. https://duendevisual.wordpress.com/2015/08/26/when-to-use-hdr/ (accessed July. 26, 2022).

[34] TheAILearner, "What is Contrast in Image Processing?," https://theailearner.com/2019/01/30/what-is-contrast-in-image-processing/ (accessed Jul. 25, 2022).

[35] TheAILearner, "Contrast Stretching," https://theailearner.com/2019/01/30/contrast-stretching/ (accessed Jul. 25, 2022).

[36] M. Roomi and G. M. Ganesan, "Review of Image Contrast Enhancement Methods and Techniques.," Research Journal of Applied Sciences, Engineering and Technology, vol. 2, no. 11, pp. 309–326, Feb. 2015, doi: 10.19026/rjaset.9.1409.

[37] L. B. Toh, M. Y. Mashor, P. Ehkan, H. Rosline, A. K. Junoh, and N. H. Harun, ''Implementation of high dynamic range rendering on acute leukemia slide images using contrast stretching,'' in Proceedings, 3rd Int. Conf. Electron. Design (ICED), Phuket, Thailand, Aug. 2016, pp. 491–496.

[38] H. Moradmand, S. Setayeshi, A. Karimian, M. Sirous, and M. Akbari, "Comparing the performance of image enhancement methods to detect microcalcification clusters in digital mammography," Iran J Cancer Prev. Spring;5(2):61-8., 2012. PMID: 25628822; PMCID: PMC4299620.

124

[39] Y. Ueda, D. Moriyama, T. Koga and N. Suetake, "Histogram Specification-Based Image Enhancement for Backlit Image," 2020 IEEE International Conference on Image Processing (ICIP), United Arab Emirates, 2020, pp. 958-962, doi: 10.1109/ICIP40778.2020.9190929.

[40] C.-M. Tsai and Z.-M. Yeh, "Contrast compensation by fuzzy classification and image illumination analysis for back-lit and front-lit color face images," IEEE Trans. Consum. Electron., vol. 56, no. 3, pp. 1570–1578, Aug. 2010.

[41] N. Otsu, "A threshold selection method from graylevel histograms," IEEE Trans. Syst., Man, Cybern., vol. SMC-9, pp. 62–66, (1979)

[42] "What is a Wavelet? - MATLAB & Simulink." https://www.mathworks .com/help/wavelet/gs/what-is-a-wavelet.html (accessed April 03, 2022).

[43] K. Amolins, Y. Zhang, and P. Dare, "Wavelet based image fusion techniques — An introduction, review and comparison," ISPRS Journal of Photogrammetry and Remote Sensing 62(4), pp. 249–263, doi: 10.1016/j.isprsjprs.2007.05.009.

[44] C. Chui, An Introduction to Wavelets. USA: Academic Press, New York, 1992

[45] A. Achim, A. Łoza, D. Bull, and N. Canagarajah, "5 - Statistical modelling for wavelet-domain image fusion," in Image Fusion, T. Stathaki, Ed. Oxford: Academic Press, 2008, pp. 119–138. doi: 10.1016/B978-0-12-372529-5.00001-9.

[46] "Introduction to Wavelet Families - MATLAB & Simulink." https://www.mathworks.com/help/wavelet/gs/introduction-to-the-wavelet-families.html (accessed May. 08, 2022).

[47] Q. Wang, X. Fu, X.-P. Zhang, and X. Ding, ''A fusion-based method for single backlit image enhancement,'' in Proceedings IEEE International Conference Image Processing (ICIP), Phoenix, Arizona, USA, Sep. 2016, pp. 4077–4081.

[48] V. Patil, D. Sale, and M. A. Joshi, "Image Fusion Methods and Quality Assessment Parameters," Asian Journal of Engineering and Applied Technology, vol. 2, no. 1, pp. 40–46, May 2013.

[49] C. Solomon and T. Breckon, Fundamentals of Digital Image Processing: A Practical Approach with Examples in Matlab, 1st ed. Wiley Publishing, 2011.

[50] F. Yi and I. Moon, "Image segmentation: A survey of graph-cut methods," in 2012 International Conference on Systems and Informatics (ICSAI2012), Yantai, China, 2012, pp. 1936–1941. doi: 10.1109/ICSAI.2012.6223428.

[51] S. Yelmanov and Y. Romanyshyn, ''Image contrast enhancement in automatic mode by nonlinear stretching,'' in Proceedings, 14th International Conference Perspective Technology Methods MEMS Design (MEMSTECH), Lviv, Ukraine, 2018, pp. 104–108

[52] A. Achim, A. Łoza, D. Bull, and N. Canagarajah, "5 - Statistical modelling for wavelet-domain image fusion," in Image Fusion, T. Stathaki, Ed. Oxford: Academic Press, 2008, pp. 119–138. doi: 10.1016/B978-0-12-372529-5.00001-9.

[53] P. Burt and E. Adelson, "The Laplacian Pyramid as a Compact Image Code," in IEEE Transactions on Communications, vol. 31, no. 4, pp. 532-540, April 1983, doi: 10.1109/TCOM.1983.1095851.

[54] A. Buades, J.-L. Lisani, A. B. Petro, and C. Sbert, ''Backlit images enhancement using global tone mappings and image fusion,'' IET Image Process., vol. 14, no. 2, pp. 211–219, Feb. 2020.

[55] C. Li, S. Tang, J. Yan and T. Zhou, "Low-Light Image Enhancement via Pair of Complementary Gamma Functions by Fusion," in IEEE Access, vol. 8, pp. 169887-169896, 2020, doi: 10.1109/ACCESS.2020.3023485.

[56] Z. Li and X. Wu, "Learning-Based Restoration of Backlit Images," in IEEE Transactions on Image Processing, vol. 27, no. 2, pp. 976-986, Feb. 2018, doi: 10.1109/TIP.2017.2771142.

[57] "Dell XPS 15 Laptop | Dell USA," Dell. https://www.dell.com/en-us/shop/dell-laptops/xps-15-laptop/spd/xps-15-9500-laptop (accessed Jul. 25, 2022).

[58] "Galaxy A7 2018 | SM-A750GZBJTPA | LATIN_EN," Samsung latin_en. https://www.samsung.com/latin_en/smartphones/galaxy-a/samsung-galaxy-a7-blue-64gb-sm-a750gzbjtpa/ (accessed Jul. 29, 2022).

[59] "GitHub - cs-chan/Exclusively-Dark-Image-Dataset: Exclusively Dark (ExDARK) https://github.com/cs-chan/Exclusively-Dark-Image-Dataset (accessed Jul. 29, 2022).

[60] "World Photography Day Wallpaper." http://hotcore.info/babki/world-photography-day-wallpaper.htm (accessed Jul. 25, 2022).

[61] Uhuru Park monument, Nairobi, Kenya - Google Search." https://www.google.com/ (accessed Jul. 29, 2022).

[62] N. Delaunay, "In Seychelles, nature is prized above mass tourism." https://phys.org/news/2020-01-seychelles-nature-prized-mass-tourism.html (accessed Jul. 25, 2022).

[63] A. R. Smith, "Colour Gamut Transform Pairs". SIGGRAPH 78 Conference Proceedings. 1978, pp. 12–19.

[64] T. Ma, C. Lin, S. Hsu, C. Hu and T. Hou, "Automatic brightness control of the handheld device display with low illumination," 2012 IEEE International Conference on Computer Science and Automation Engineering (CSAE), 2012, pp. 382-385, doi: 10.1109/CSAE.2012.6272797.

[65] M. Schuchhardt, S. Jha, R. Ayoub, M. Kishinevsky and G. Memik, "Optimizing mobile display brightness by leveraging human visual perception," 2015 International Conference on Compilers, Architecture and Synthesis for Embedded Systems (CASES), 2015, pp. 11-20, doi: 10.1109/CASES.2015.7324538.

[66] S. Bezryadin, P. Bourov, and D. Ilinih, "Brightness Calculation in Digital Image Processing," International Symposium on Technologies for Digital Photo Fulfilment, vol. 2007, pp. 10–15, January 2007, doi: 10.2352/ISSN.2169-4672.2007.1.0.10.

[67] S. Bezryadin and P. Bourov, "Color coordinate system for accurate colour image editing software," in The International Conference Printing Technology SPb, 2006, vol. 6, pp. 145–148.

[68] G. Wyszecki, W. S. Stiles, "Colour Science. Concepts and Methods, Quantitative Data and Formulae", Second Edition, John Wiley & Sons, USA, (2000)

[69] "Understanding Histograms in Photography," Photography Life, Feb. 22, 2013. https://www.photographylife.com/understanding-histograms-in-photography (accessed March 08, 2022).

[70] K. Amolins, Y. Zhang, and P. Dare, "Wavelet based image fusion techniques -An introduction, review and comparison," 2007.

[71] "Vectorization - MATLAB & Simulink." https://www.mathworks.com /help/matlab/matlab_prog/vectorization.html (accessed Jul. 25, 2022).

[72] "Image Quality Metrics - MATLAB & Simulink." https:// www.mathworks.com/help/images/image-quality-metrics.html (accessed Jul. 25, 2022).

[73] "SSIM/MS-SSIM." https://vicuesoft.com/glossary/term/ssim-ms-ssim/ (accessed Jul. 25, 2022).

[74] A. Mittal, R. Soundararajan, and A. Bovik, "Making a 'Completely Blind' Image Quality Analyzer," Signal Processing Letters, IEEE, vol. 20, pp. 209–212, Mar. 2013, doi: 10.1109/LSP.2012.2227726.

[75] RECOMMENDATION ITU-R BT.500-14, "Methodologies for the subjective assessment of the quality of television images," p. 102., October 2019

[76] A.-B. Petro, C. Sbert, and J.-M. Morel, "Multiscale Retinex," Image Processing On Line, vol. 4, pp. 71–88, April 2014, doi: 10.5201/ipol.2014.107.

[77] X. Guo, Y. Li, and H. Ling, ''LIME: Low-light image enhancement via illumination map estimation,'' IEEE Trans. Image Process., vol. 26, no. 2, pp. 982–993, Feb. 2017

APPENDICES

A1. Turnitin Report

Turnitin Originality Report

Processed on: 22-Jul-2023 13:46 EAT
ID: 2134935690
Word Count: 23105
Submitted: 1

Thesis Corrections 1 By Shaffa Kokro Jr.

Similarity Index
8%

Similarity by Source

Internet Sources:	6%
Publications:	5%
Student Papers:	2%

1% match (Thaweesak Trongtirakul, Werapon Chiracharit, Sos S. Agaian. "Single Backlit Image Enhancement", IEEE Access, 2020)
Thaweesak Trongtirakul, Werapon Chiracharit, Sos S. Agaian. "Single Backlit Image Enhancement", IEEE Access, 2020

< 1% match (Internet from 10-Nov-2022)
http://erepository.uonbi.ac.ke/bitstream/handle/11295/153164/macharia%20Hf.pdf?isAllowed=y&sequence=4

< 1% match (Internet from 17-Dec-2022)
http://erepository.uonbi.ac.ke/bitstream/handle/11295/104383/Sewe%20Stephen.pdf?isAllowed=y&sequence=2

< 1% match (Internet from 17-Dec-2022)
http://erepository.uonbi.ac.ke/bitstream/handle/11295/104381/Wachira%20Kinyua.pdf?isAllowed=y&sequence=2

< 1% match (Internet from 29-Oct-2003)
http://www.ino.qc.ca/en/PDF/Low-Light%20Level%20Recognition%20Using%20COTS%20Optical%20Correlator.pdf

< 1% match (Internet from 10-Nov-2022)
https://dokumen.pub/digital-image-processing-3rd-edition-3rdnbsped-0-13-168728-x-978-0-13-168728-8.html

< 1% match (Internet from 01-Feb-2023)
https://www.researchgate.net/publication/324645690_LECARM_Low-Light_Image_Enhancement_using_Camera_Response_Model

< 1% match (Internet from 10-May-2023)
https://www.researchgate.net/publication/275029203_Noninvasive_Real-Time_Automated_Skin_Lesion_Analysis_System_for_Melanoma_Early_Detection_and_Prevention

< 1% match (Internet from 14-May-2023)
https://www.arxiv-vanity.com/papers/2010.12347/

< 1% match (Internet from 18-Apr-2023)
https://www.arxiv-vanity.com/papers/1807.11014/

< 1% match (Yoshiaki Ueda, Daiki Moriyama, Takanori Koga, Noriaki Suetake. "Histogram Specification-Based Image Enhancement for Backlit Image", 2020 IEEE International Conference on Image Processing (ICIP), 2020)
Yoshiaki Ueda, Daiki Moriyama, Takanori Koga, Noriaki Suetake. "Histogram Specification-Based Image Enhancement for Backlit Image", 2020 IEEE International Conference on Image Processing (ICIP), 2020

< 1% match (Internet from 08-May-2010)
http://www.utdallas.edu/~dxa081000/IMAGEFILTERING.ppt

< 1% match ("Neural Information Processing", Springer Science and Business Media LLC, 2017)
"Neural Information Processing", Springer Science and Business Media LLC, 2017

< 1% match (Internet from 23-Mar-2023)
https://www.science.gov/topicpages/i/image+quality+enhancement

< 1% match (Internet from 24-May-2023)
https://www.science.gov/topicpages/b/based+super-resolution+imaging

< 1% match (Visual Signal Quality Assessment, 2015.)
Visual Signal Quality Assessment, 2015.

< 1% match (Elnaz Pashaei, Elham Pashaei. "Gaussian quantum arithmetic optimization-based histogram equalization for medical image enhancement", Multimedia Tools and Applications, 2023)
Elnaz Pashaei, Elham Pashaei. "Gaussian quantum arithmetic optimization-based histogram equalization for medical image enhancement", Multimedia Tools and Applications, 2023

< 1% match (student papers from 28-Nov-2016)
Submitted to Asian Institute of Technology on 2016-11-28

< 1% match (Chris Solomon, Toby Breckon. "Fundamentals of Digital Image Processing", Wiley, 2010)
Chris Solomon, Toby Breckon. "Fundamentals of Digital Image Processing", Wiley, 2010

< 1% match (Internet from 08-Jan-2010)
http://www.comp.nus.edu.sg/~tancl/Papers/IJDAR/DocBin_IJDAR-old.pdf

< 1% match (Internet from 19-Dec-2022)
https://www.coursehero.com/file/p6mh0jep/sion-The-prevalent-paradigm-is-to-think-of-a-greyscale-image-as-a-discretization/

130

< 1% match (Internet from 11-Mar-2023)
https://WWW.coursehero.com/file/99179253/camera-modelpdf/

< 1% match (D. Vijayalakshmi, Malaya Kumar Nath, Om Prakash Acharya. "A Comprehensive Survey on Image Contrast Enhancement Techniques in Spatial Domain", Sensing and Imaging, 2020)
D. Vijayalakshmi, Malaya Kumar Nath, Om Prakash Acharya. "A Comprehensive Survey on Image Contrast Enhancement Techniques in Spatial Domain", Sensing and Imaging, 2020

< 1% match (Internet from 12-Nov-2022)
https://arxiv.org/pdf/1910.06180.pdf

< 1% match (Internet from 06-Jan-2023)
http://shodhbhagirathi.iitr.ac.in:8081/jspui/bitstream/123456789/9786/1/ECDG11251.pdf

< 1% match (Automotive Sensory Systems, 1993.)
Automotive Sensory Systems, 1993.

< 1% match (Gaiyun Wang, Zhichao Guo, Jintao Shen, Jianbin Liu, Qi Zhang. "Multi-domain Value Block Enhancement Algorithm Fused with Genetic Algorithm", 2021 IEEE 15th International Conference on Electronic Measurement & Instruments (ICEMI), 2021)
Gaiyun Wang, Zhichao Guo, Jintao Shen, Jianbin Liu, Qi Zhang. "Multi-domain Value Block Enhancement Algorithm Fused with Genetic Algorithm", 2021 IEEE 15th International Conference on Electronic Measurement & Instruments (ICEMI), 2021

< 1% match (Amina Saleem, Azeddine Beghdadi, Boualem Boashash. "A distortion-free contrast enhancement technique based on a perceptual fusion scheme", Neurocomputing, 2017)
Amina Saleem, Azeddine Beghdadi, Boualem Boashash. "A distortion-free contrast enhancement technique based on a perceptual fusion scheme", Neurocomputing, 2017

< 1% match (student papers from 03-Feb-2011)
Submitted to Nottingham Trent University on 2011-02-03

< 1% match (Weitao Deng, Lei Liu, Huateng Chen, Xiaofeng Bai. "Infrared Image Contrast Enhancement Using Adaptive Histogram Correction Framework", Optik, 2022)
Weitao Deng, Lei Liu, Huateng Chen, Xiaofeng Bai. "Infrared Image Contrast Enhancement Using Adaptive Histogram Correction Framework", Optik, 2022

< 1% match (Internet from 13-Dec-2022)
https://spectrum.library.concordia.ca/id/eprint/990150/1/Lesperance_MaSc_F2021.pdf

< 1% match (Internet from 12-Dec-2022)
https://spectrum.library.concordia.ca/id/eprint/984918/1/Ren_PhD_S2019.pdf

< 1% match (student papers from 14-Jan-2017)
Submitted to Lovely Professional University on 2017-01-14

< 1% match (Ahmad Shahrizan Abdul Ghani, Nor Ashidi Mat Isa. "Automatic system for improving underwater image contrast and color through recursive adaptive histogram modification", Computers and Electronics in Agriculture, 2017)
Ahmad Shahrizan Abdul Ghani, Nor Ashidi Mat Isa. "Automatic system for improving underwater image contrast and color through recursive adaptive histogram modification", Computers and Electronics in Agriculture, 2017

< 1% match (G. J. Awcock, R. Thomas. "Applied Image Processing", Springer Nature, 1995)
G. J. Awcock, R. Thomas. "Applied Image Processing", Springer Nature, 1995

< 1% match (Nguyen, T.T., and S. Oraintara. "The Shiftable Complex Directional Pyramid—Part I: Theoretical Aspects", IEEE Transactions on Signal Processing, 2008.)
Nguyen, T.T., and S. Oraintara. "The Shiftable Complex Directional Pyramid—Part I: Theoretical Aspects", IEEE Transactions on Signal Processing, 2008.

< 1% match (Internet from 23-Oct-2022)
http://nozdr.ru/data/media/biblio/kolxoz/Cs/CsLn/B/Bio-inspired%20Applications%20of%20Connectionism,%206%20conf.,%20IWANN%202001%28LNCS2085,%20Springer,%202001%29%

< 1% match (Internet from 05-Dec-2022)
http://amsdottorato.unibo.it/952/1/Tesi_Delia_Gianluca.pdf

< 1% match (Internet from 26-Nov-2018)
http://amsdottorato.unibo.it/885/1/Tesi_Scala_Elisa.pdf

< 1% match (Internet from 11-Jan-2023)
https://core.ac.uk/download/pdf/212687702.pdf

< 1% match (Internet from 14-Jan-2023)
https://core.ac.uk/download/pdf/232461109.pdf

< 1% match (Internet from 08-Jun-2021)
https://ir-library.ku.ac.ke/bitstream/handle/123456789/19158/A%20statistical%20investigation%20to%20determine%20the%20predisposing%isAllowed=y&sequence=1

< 1% match (student papers from 27-Apr-2021)
Submitted to Daffodil International University on 2021-04-27

< 1% match (student papers from 03-Jan-2019)
Submitted to The University of Buckingham on 2019-01-03

< 1% match (Internet from 22-Nov-2022)
https://dspace.cvut.cz/bitstream/handle/10467/73467/F1-DP-2017-Macwilliam-Krista-SaltAging.pdf?isAllowed=y&sequence=1

< 1% match (Internet from 25-Oct-2022)
https://github.com/shaffakjr/backlit-research-rbhf

< 1% match (student papers from 17-Nov-2022)
Submitted to Liverpool Hope on 2022-11-17

< 1% match (Internet from 25-Sep-2022)
http://live.ece.utexas.edu/publications/2013/mittal2013.pdf

< 1% match (student papers from 23-Apr-2020)
Submitted to Heriot-Watt University on 2020-04-23

< 1% match (student papers from 21-May-2010)
Submitted to University of Liverpool on 2010-05-21

< 1% match (Internet from 14-Feb-2023)
http://acikerisim.omu.edu.tr/xmlui/bitstream/handle/20.500.12712/33615/137876.pdf?isAllowed=y&sequence=1

< 1% match (Internet from 27-May-2023)
https://idr.l3.nitk.ac.in/jspui/bitstream/123456789/17423/1/187118MA013-Smitha%20A.pdf

< 1% match (Internet from 25-Dec-2022)
https://pure.tue.nl/ws/files/152407848/0849855_L.van_Wincoop.pdf

< 1% match (Internet from 12-Apr-2023)
https://research.chalmers.se/publication/535330/file/535330_Fulltext.pdf

< 1% match (Internet from 06-Oct-2022)
http://suaire.suanet.ac.tz/bitstream/handle/123456789/3756/Lusungu%20Essau%20Mbede.pdf?isAllowed=y&sequence=1

< 1% match (Internet from 24-Dec-2022)
https://www.igi-global.com/viewtitle.aspx?TitleId=185920&isxn=9781522527992

< 1% match (Internet from 05-Jul-2023)
https://www.proceedings.com/institute-of-electrical-and-electronics-engineers-ieee/?page=37

< 1% match (student papers from 29-Oct-2014)
Submitted to Visvesvaraya Technological University on 2014-10-29

< 1% match (Internet from 05-Feb-2016)
http://ecommons.usask.ca/bitstream/handle/10388/ETD-2015-04-2038/TORABI-ZIARATGAHI-DISSERTATION.pdf?sequence=4

< 1% match (Internet from 24-Sep-2022)
http://mapageweb.umontreal.ca/gosselif/Willenbockeletal10b.pdf

< 1% match (Internet from 27-Mar-2023)
https://api-depositonce.tu-berlin.de/server/api/core/bitstreams/b29e9091-aae6-4c3d-8185-ac9ff5308280/content

< 1% match (Internet from 20-Jul-2020)
https://drum.lib.umd.edu/bitstream/handle/1903/20302/Smith_umd_0117E_18497.pdf?isAllowed=y&sequence=1

< 1% match (Internet from 17-Jan-2023)
https://lup.lub.lu.se/luur/download?fileOId=8945376&func=downloadFile&recordOId=8945360

< 1% match (Internet from 25-Nov-2022)
https://prism.ucalgary.ca/bitstream/handle/1880/106266/ucalgary_2017_zohra_fatematuz.pdf?isAllowed=y&sequence=4

< 1% match (Internet from 16-Jan-2023)
https://ris.utwente.nl/ws/portalfiles/portal/224612125/thesis_S_Abdi.pdf

< 1% match (Dima Abi-Abdallah. BioMedical Engineering OnLine, 2006)
Dima Abi-Abdallah. BioMedical Engineering OnLine, 2006

< 1% match (F. Tirado. "Parallel wavelet transform for large scale image processing", Proceedings 16th International Parallel and Distributed Processing Symposium IPDPS-02, 2002)
F. Tirado. "Parallel wavelet transform for large scale image processing", Proceedings 16th International Parallel and Distributed Processing Symposium IPDPS-02, 2002

< 1% match (Rahul Rajendran, Shishir Paramathma Rao, Sos S Agaian, Karen Panetta. "A versatile edge preserving image enhancement approach for medical images using guided filter", 2016 IEEE International Conference on Systems, Man, and Cybernetics (SMC), 2016)
Rahul Rajendran, Shishir Paramathma Rao, Sos S Agaian, Karen Panetta. "A versatile edge preserving image enhancement approach for medical images using guided filter", 2016 IEEE International Conference on Systems, Man, and Cybernetics (SMC), 2016

< 1% match (student papers from 04-Aug-2022)
Submitted to University of Leeds on 2022-08-04

< 1% match (Internet from 11-Oct-2022)
https://acikbilim.yok.gov.tr/bitstream/handle/20.500.12812/615516/yokAcikBilim_10098885.pdf?isAllowed=y&sequence=-1

< 1% match (Internet from 13-Jun-2023)
https://ebin.pub/digital-multimedia-communications-the-9th-international-forum-iftc-2022-shanghai-china-december-89-2022-revised-selected-papers-9819908558-9789819908554.html

< 1% match (Internet from 20-Nov-2022)
http://ir.jkuat.ac.ke/bitstream/handle/123456789/3904/Isaac%20Warutumo.pdf?isAllowed=y&sequence=1

< 1% match (Internet from 08-Sep-2021)
https://mspace.lib.umanitoba.ca/xmlui/bitstream/handle/1993/4169/Jialin_Li.pdf

< 1% match (Internet from 06-Nov-2022)
https://pure.ulster.ac.uk/ws/files/98363410/Guo_et_al_Detailed_preserving_._Sensors_22_00085.pdf

< 1% match (Internet from 11-Jun-2021)
https://tamashanews.com/page/3/

< 1% match (Internet from 04-Nov-2021)
https://Www.businessinsider.com/best-gaming-laptops-under-1000-dollars

< 1% match (Internet from 13-Jul-2016)
https://www.scribd.com/doc/299633918/190397698-Dynamics-of-Structures-Volume-2-Applications-Chowdhury

< 1% match ("ICT and Critical Infrastructure: Proceedings of the 48th Annual Convention of Computer Society of India- Vol II", Springer Science and Business Media LLC, 2014)
"ICT and Critical Infrastructure: Proceedings of the 48th Annual Convention of Computer Society of India- Vol II", Springer Science and Business Media LLC, 2014

< 1% match (Katayoon Taherkhani, Gerd Cantzler, Christopher Eischer, Ehsan Toyserkani. "Development of control systems for laser powder bed fusion", Research Square Platform LLC, 2023)
Katayoon Taherkhani, Gerd Cantzler, Christopher Eischer, Ehsan Toyserkani. "Development of control systems for laser powder bed fusion", Research Square Platform LLC, 2023

< 1% match (Mahrooghy, Majid, Nicolas H. Younan, Valentine G. Anantharaj, and James V. Aanstoos. "Enhancement of Satellite Precipitation Estimation via Unsupervised Dimensionality Reduction", IEEE Transactions on Geoscience and Remote Sensing, 2012.)
Mahrooghy, Majid, Nicolas H. Younan, Valentine G. Anantharaj, and James V. Aanstoos. "Enhancement of Satellite Precipitation Estimation via Unsupervised Dimensionality Reduction", IEEE Transactions on Geoscience and Remote Sensing, 2012.

< 1% match (Song, Le, Yu-chi Lin, Yan-hua Chen, and Mei-rong Zhao. "", International Symposium on Photoelectronic Detection and Imaging 2011 Advances in Infrared Imaging and Applications, 2011.)
Song, Le, Yu-chi Lin, Yan-hua Chen, and Mei-rong Zhao. "", International Symposium on Photoelectronic Detection and Imaging 2011 Advances in Infrared Imaging and Applications, 2011.

< 1% match (student papers from 10-May-2010)
Submitted to University of Sheffield on 2010-05-10

< 1% match (Yafei Wang, Xueyan Ding, Ruoqian Wang, Jun Zhang, Xianping Fu. "Fusion-based underwater image enhancement by wavelet decomposition", 2017 IEEE International Conference on Industrial Technology (ICIT), 2017)
Yafei Wang, Xueyan Ding, Ruoqian Wang, Jun Zhang, Xianping Fu. "Fusion-based underwater image enhancement by wavelet decomposition", 2017 IEEE International Conference on Industrial Technology (ICIT), 2017

< 1% match (Internet from 18-Oct-2006)
http://ict.ewi.tudelft.nl/~frits/pabtot.pdf

< 1% match (Internet from 23-Mar-2023)
https://jntukmaterials249525680.files.wordpress.com/2018/10/digital-image-processing-notes1.pdf

< 1% match (Internet from 13-Nov-2022)
https://opus.lib.uts.edu.au/bitstream/10453/136030/2/02whole.pdf

< 1% match (Internet from 12-Aug-2021)
https://os.zhdk.cloud.switch.ch/tind-tmp-epfl/a84008bb-ea4a-46ae-85aa-66b137eb642c?AWSAccessKeyId=ded3589a13b4450889b2f728d54861a6&Expires=1628903755&Signature=v4ZJOp6lHK%2BIO1P62xKTR5ON6Rg%3content-disposition=attachment%3B+filename%2A%3DUTF-8%27%27GarciaPhD98.pdf&response-content-type=application%2Fpdf

< 1% match (Internet from 11-Jan-2023)
https://pdfcookie.com/documents/proteomics-analysis-and-agrobacterium-mediated-transformation-in-tomato-lycopersion-esculentum-mill-cultivars-0nvo3n4yndv8

< 1% match (Internet from 22-Feb-2023)
https://repository.nwu.ac.za/bitstream/handle/10394/10739/Jansen_van_Rensburg_SJ.pdf?isAllowed=y&sequence=1

< 1% match (Internet from 13-Oct-2022)
http://repository.smuc.edu.et/bitstream/123456789/6234/1/Final%20Thesis%20by%20%20Maereg%20Teferi%20.pdf

< 1% match (Internet from 22-Oct-2022)
https://spiral.imperial.ac.uk/bitstream/10044/1/6415/1/Gbenedio-EP-2011-PhD-Thesis.pdf

< 1% match (Internet from 13-Jun-2023)
https://technodocbox.com/3D_Graphics/76293089-On-image-denoising-methods.html

< 1% match (Internet from 18-Dec-2022)
https://the-eye.eu/public/Books/utolica.duckdns.org/Charles%20Petzold_PROGRAMMING%20WINDOWS%205th%20Edition%28calseu%20pejolde

UNIVERSITY OF NAIROBI FACULTY OF ENGINEERING DEPARTMENT OF ELECTRICAL AND INFORMATION ENGINEERING A Region-Based Histogram and Fusion Technique for Enhancing Backlit Images for Cell Phone Applications By Shaffa Korvawu Kokro Jr. F56/35720/2019 A thesis submitted in partial fulfilment of the degree of Master of Science in Electrical and Electronic Engineering in the Department of Electrical and Information Engineering in the University of Nairobi October 2022 i

ABSTRACT Many cell phone cameras perform poorly in backlighting situations due to low dynamic range, which then leads to the creation of low-quality pictures known as backlit images. Conventional image enhancement algorithms are not well suited to improve the quality of backlit images. Over-saturation or a loss of contrast are typical outcomes when these methods are applied. In this thesis, a novel image enhancement algorithm is presented for improving the visual perception of a single backlit image. The algorithm uses a region-based histogram specification scheme in combination with the discrete wavelet transform image fusion to correct exposure disparities between foreground and background scenes. Computer simulations in MATLAB R2018a and on a dataset of 162 backlit images revealed that the proposed algorithm significantly improves the backlit image's visual perception without distorting colours or adding artefacts. The Peak Signal-to-Noise Ratio, Structural Similarity Index Measure, and Naturalness Image Quality Evaluator metrics objectively validated these results. The algorithm produced PSNR values ranging from 19 dB to 30 dB for images with low backlit degradation while retaining more than (60-70) % structural similarity to the inputs. Lower PSNR and SSIM values were consistent with severely degraded images. These findings agreed with the outcomes of the subjective evaluations. However, multiple iterations of the proposed algorithm increased the PSNR quality by up to 12 dB after the first three iterations. By comparison, the proposed algorithm significantly outperformed existing image enhancement techniques such as Histogram Equalization, Multiscale Retinex, and Low-light Image Enhancement via Illumination Map Estimation. ii

CHAPTER 1 _____ INTRODUCTION 1.1. Background Backlit images are low-quality digital pictures produced due to backlighting, a poor lighting condition that causes significant degradation in image quality. As shown in Figure 1.1, foreground areas (F-region) in a backlit image are frequently under-exposed, whereas background sectors (B-region) are either well-lit or over-exposed. Traditional image enhancement algorithms are rendered ineffective by this type of illumination. Therefore, research in this domain focuses on alternative methods that improve backlit images while preserving their details and colours [1]. (a) (b) Figure 1.1. Examples of backlit images (a) Backlit portrait (b) Backlit cityscape [2] 1.2. Assessment of backlighting Backlighting is a poor illumination setting that occurs when an excessive reflection of light is incident to an image-capturing device or when the dominant light source in a picture scene lies behind the main object(s) [1]. As seen in Figure 1.1, it creates low contrast in an image's foreground and impairs its overall quality. Many digital cameras cannot perform well in backlighting due to their low dynamic range. An image sensor capable of detecting extremely low and high luminance simultaneously would be required to capture high-quality pictures in such a situation. A device of this type would have a dynamic range compared to the human visual system (HVS). Nonetheless, professional photographers have used digital cameras' low dynamic range to convey mystery, drama, emotion, and mood. This is known as silhouette photography, and it has grown in popularity over the last decade [3]. Figure 1.2 depicts a silhouette image. Figure 1.2. Example of silhouette photography [3] 1.3. Problem Statement Backlighting is a commonly encountered problem for cell phone users. It usually results in low-quality images known as backlit images. Conventional image enhancement methods such as the well-known histogram equalization algorithm [4] or Retinex-based algorithms [5]-[7] cannot achieve the desired enhanced effects of backlit images. Oversaturation and loss of contrast are typical outcomes when these methods are applied. Various research investigations have been conducted in recent years to address these challenges. The majority of these efforts have not however focused on the use of backlit image enhancement algorithms in cell phone applications. As a result, despite recent developments in smartphone technology, there is no commercially accepted technique for improving backlit pictures on cell phones. Alternative methods such as Auto-exposure (AE) [8] and High Dynamic Range (HDR) imaging [9] are being used by smartphone manufacturers to handle backlighting and other types of poor illumination situations. However, these methods have significant drawbacks that outweigh their benefits in poor lighting situations. For instance, under backlighting, AE cannot reveal items in the foreground while simultaneously exposing details in the background. As a result, a well-exposed foreground will cause a loss of information in the background scene and vice-versa. Likewise, HDR, developed primarily to handle low-light situations, is susceptible to motion blur since it relies on fusing two or more sequential images with varying exposures [9]. Furthermore, it cannot enhance low-quality photographs after they have been acquired. Therefore, this research investigation sought to develop a more optimal technique for enhancing backlit images, particularly on cell phones. 1.4. Objectives 1.4.1. Main objective This work aimed to develop a new image enhancement algorithm that can be employed in cell phone applications to improve the visual quality of backlit images. 1.4.2. Specific objectives The specific objectives were: (i) To investigate the use of histogram-based contrast-stretching techniques for backlit image enhancement, taking into consideration their applicability to cell phones. (ii) To develop an optimized backlit image enhancement algorithm with low-computational cost using a novel region-based histogram specification (RBHS) scheme in combination with the discrete wavelet transform (DWT) image fusion approach. (iii) To evaluate the performance of the work on standard backlit images captured in various backlit situations by commercially available cell phones, based on existing image quality assessment (IQA) techniques. 1.5. Justification for the study Smartphones have become the standard design for cell phones and other mobile devices, and they currently represent the fastest-growing market segment in the telecommunications industry [10]. According to Statista, global smartphone sales increased from 680 million in 2012 to about 1.54 billion in 2019, as shown in Figure 1.3 [11]. This significant increase is often due to the many capabilities offered within the device compared to regular mobile devices. Among these capabilities, the camera remains one of the most important. It is a principal factor influencing consumer choice of one mobile device over another. As the smartphone industry expands, consumers will continue to expect and demand high-quality cameras on their

A2. First Publication

Journal Name: Elsevier

Submission Date: November 15, 2022

A Region-based Histogram and Fusion Technique for Single Backlit Image Enhancement

Shaffa K. Kokro Jr. [1]*, Elijah Mwangi[2], George Kamucha[3]

Department of Electrical and Information Engineering, University of Nairobi, Kenya[1,2,3]

Abstract—Backlit images captured by commercial cell phones degrade due to different exposure settings for foreground and background illumination. This paper presents a novel exposure correction algorithm for single backlit image enhancement using a region-based histogram specification scheme with the discrete wavelet transform image fusion. The classical histogram matching algorithm is performed discriminately on two input masks generated with identical copies of the input image. A Two-stage DWT fusion is used to combine salient features of the enhanced input masks with the original backlit image. Experimental results demonstrate the superiority of the proposed method over existing techniques in improving perceptual quality without colour distortion or artefacts. The proposed method also achieved the highest PSNR, SSIM, and NIQE quality on average. Furthermore, multiple iterations of the algorithm increased the PSNR quality by up to 12 dB after the first three iterations.

Keywords—*Exposure correction, image fusion, discrete wavelet transform, histogram matching.*

I. INTRODUCTION

Backlit images are low-quality digital pictures generated due to backlighting, a poor illumination setting that occurs when an excessive reflection of light is incident to an image-capturing device or when the dominant light source in a picture scene radiates behind the main objects [1]. As shown in Fig. 1, backlit images are characterized by an under-exposed foreground and a well-lit and/or over-exposed background. The goal of backlit image enhancement is to remove or reduce the backlit degradation in the under-exposed foreground, referred to as "backlit scenes sectors", while preserving image details and colours [1],[2],[3]. Conventional image enhancement methods, such as Histogram equalization [4] and retinex-based algorithms [5-7], cannot achieve such desired enhanced effects. Over-saturation and loss of contrast are typical outcomes when these methods are applied.

Various techniques have been proposed in recent years. Trongtirakul *et al.* [1] proposed a full piece-wise nonlinear stretching function to improve contrast locally in dark, bright, and well-lit regions. However, the under-enhancement of some details in the dark sector is a shortcoming. Wang *et al.* [2] employ a multi-scale fusion based on the Laplacian pyramid decomposition. The high dependency on the choice of inputs and the weight maps acts as a constraint, such that if incorrect inputs and weight maps are used, the desired result cannot be achieved [2]. Li *et al.* [8] proposed a Learning-based algorithm for backlit improvement but with a high computation cost. Hence, not suitable for cell phone applications. Other methods,
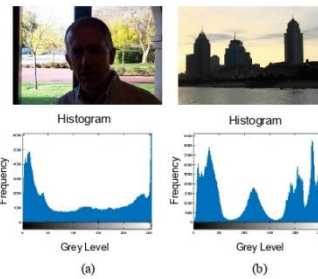
Figure 1. Example of backlit images (a) Backlit portrait (b) Backlit cityscape

such as Ueda *et al.* [9] and Guo *et al.* [10], can reveal details in under-exposed areas, but they fall short of preserving the natural hues of the backlit image.

In this paper, a novel backlit image enhancement algorithm based on histogram matching and image fusion is proposed. The main contributions include (i) an adaptive brightness control (ABC) mechanism to handle the low brightness problems caused by histogram matching; and (ii) the novelty of generating new ground truth images at low computational cost, with edges, textures, and colours preserved from the degraded backlit inputs.

The rest of the paper is organized as follows: Section II covers relevant literature used in developing the proposed technique. Section III describes the proposed method. Experimental results are presented and analyzed in Section IV. Finally, the conclusion and suggestions for future works are given in Section V.

II. THEORETICAL FRAMEWORK

In this section, theories related to the proposed method are discussed. The presentation starts with a brief discussion on histogram processing, histogram matching, and wavelet theory, then the Discrete Wavelet Transform (DWT) and image fusion.

A. Histogram processing

The histogram of a digital image with grey levels $[0, L-1]$ is a discrete function $h(r_k)$ that returns the relative frequency with which each grey level occurs, as given in (1) [11].

$$h(r_k) = n_k \qquad (1)$$

where r_k is the kth grey level for $k \in [0, L-1]$ and n_k is the number of pixels having a grey level r_k. A normalized histogram $p(r_k)$ is obtained by dividing n_k by the total number of pixels in the image (n), as shown in (2) [11].

$$p(r_k) = \frac{n_k}{n} \qquad (2)$$

Figs. 1(a) and 1(b) show the histogram of backlit images (a) and (b), respectively. Such histograms are typical of a bimodal distribution with peaks in the dark and bright regions [12].

B. Histogram Specification

Histogram specification, or histogram matching, is a process used to improve contrast in an image by mapping its grey levels to a specified histogram [9],[11]. Let $I(x, y)$ be an input intensity image with grey levels $[0, L-1]$ and $p_D(z_j)$ be a normalized target histogram. The grey-level probability $p_I(r_i)$ of $I(x, y)$ is calculated using (2). The cumulative distribution functions (CDFs) for $p_I(r_i)$ and $p_D(z_j)$ are given by (3) and (4), respectively.

$$T(r_k) = \sum_{i=0}^{k} p_I(r_i) \ ; \ k \in \{0, L-1\}/L-1 \qquad (3)$$

$$G(z_k) = \sum_{j=0}^{k} p_D(z_j) \ ; \ k \in \{0, L-1\}/L-1 \qquad (4)$$

Letting $U(\cdot)$ be a transformation function i.e., $U(r_k) = z_k$ the grey level r_k of the input is mapped to the desired value z_k such that the condition $T(r_k) = G(z_k)$ is satisfied. Applying $U(\cdot)$ to each pixel of $I(x, y)$ yields the histogram-specified image [11].

C. Discrete Wavelet Transform

In this section, a theory on the DWT is presented. First, the one-dimensional DWT is introduced, followed by the two-dimensional DWT.

1) One-Dimensional DWT

The DWT decomposes a signal $f(x)$ into various wavelet coefficients: approximation and detail coefficients. The one-dimensional (1-D) DWT of the signal $f(x)$ with length M is obtained using (5) and (6) [11],[13].

$$W_\varphi(m_0, k) = \frac{1}{\sqrt{M}} \sum_{k=0}^{M-1} f(x) \varphi_{m_0,k}(x) \qquad (5)$$

$$W_\psi(m, k) = \frac{1}{\sqrt{M}} \sum_{k=0}^{M-1} f(x) \psi_{m,k}(x) \qquad (6)$$

where $\varphi_{m_0,k}(x)$ and $\psi_{m,k}(x)$ are the scaled and translated versions of the scaling function $\varphi(x)$ and the wavelet $\psi(x)$, respectively; and $W_\varphi(m_0, k)$ and $W_\psi(m, k)$ are the approximation and detail coefficients, respectively. Taking the inverse DWT from the above coefficients yields the original signal $f(x)$. The 1-D inverse DWT is defined by (7) [11],[13].

$$f(x) = \frac{1}{\sqrt{M}} \sum_{k=0}^{M-1} W_\varphi(m_0, k) \, \varphi_{m_0,k}(x)$$

$$+ \frac{1}{\sqrt{M}} \sum_{m=0}^{M-1} \sum_{k=0}^{L-1} W_\psi(m, k, n) \, \psi_{m,k}(x) \qquad (7)$$

where m_0 is an arbitrary starting scale, $W_\varphi(m_0, k)$ is the approximation coefficient, and $W_\psi(m, k, n)$ is a detail coefficient.

2) Two-Dimensional DWT

The two-dimensional (2-D) DWT is an extension of the 1-D DWT. Given a 2-D signal $f(x, y)$ such as an image, the two-dimensional DWT is calculated as follows:

$$W_\varphi(j_0, m, n) = \frac{1}{\sqrt{MN}} \sum_{m=0}^{M-1} \sum_{n=0}^{N-1} f(x, y) \varphi_{j_0,m,n}(x, y) \qquad (8)$$

$$W_\psi^i(j, m, n) = \frac{1}{\sqrt{MN}} \sum_{m=0}^{M-1} \sum_{n=0}^{N-1} f(x, y) \psi_{j,m,n}^i(x, y) \qquad (9)$$

where $\varphi_{j_0,m,n}(x, y)$ is the scaled and translated version of the 2-D scaling function $\varphi(x, y)$; $\psi_{j,m,n}^i(x, y)$ for $i \in \{H, V, D\}$ are the scaled and translated versions of the 2-D wavelets $\psi^H(x, y)$, $\psi^V(x, y)$, and $\psi^D(x, y)$, which measure the signal variations in the horizontal (H), vertical (V), and diagonal (D) directions, respectively; while $W_\varphi(j_0, m, n)$ and $W_\psi^i(j, m, n)$ are the respective approximation and detail coefficients. The 2-D scaling and wavelet functions are obtained from the product of two 1-D basis functions as shown in (10) to (13) [11],[13].

$$\varphi(x, y) = \varphi(x)\varphi(y) \qquad (10)$$

$$\psi^H(x, y) = \psi(x)\varphi(y) \qquad (11)$$

$$\psi^V(x, y) = \varphi(x)\psi(y) \qquad (12)$$

$$\psi^D(x, y) = \psi(x)\psi(y) \qquad (13)$$

Equation (14) produces the original signal $f(x, y)$ by calculating the inverse DWT of the 2-D coefficients [11],[13].

$$f(x, y) = \frac{1}{\sqrt{MN}} \sum_{m=0}^{M-1} \sum_{n=0}^{N-1} W_\varphi(j_0, m, n) \varphi_{j_0,m,n}(x, y)$$

$$+ \frac{1}{\sqrt{MN}} \sum_{i=H,V,D} \sum_{j=j_0}^{J-1} \sum_{m=0}^{M-1} \sum_{n=0}^{N-1} W_\psi^i(j, m, n) \psi_{j,m,n}^i(x, y) \qquad (14)$$

D. Image Fusion

Image fusion is the process of combining features from two or more sources to produce a composite image [2],[14]. Various image fusion approaches have been investigated. The most basic methods are Maximum Selection (MaxS), Minimum Selection (MinS), and Averaging. Pixel intensities are compared at each spatial position in the MaxS or MinS procedure. The highest or lowest intensity value (in the case of MinS) at said position is then selected as the pixel value in the composite image. In the Averaging approach, the mean is determined and used as the resultant pixel [14]. Advanced image fusion techniques have been developed over the years. In the following sections, two of these techniques are presented.

1) Laplacian Pyramid-based image fusion

Image pyramids are data structures used for processing digital pictures at various spatial scales [15]. Two of the most often utilized pyramids are the Gaussian and Laplacian [2],[14].

The low memory requirement of the Laplacian pyramid is more beneficial in many image processing applications.

Fig. 2 shows the block diagram of an image fusion process based on the Laplacian pyramid. The procedure begins with a pyramid decomposition of each input image, then a selection or averaging process to blend multi-scale characteristics at each corresponding pyramid level, and finally, an inverse pyramid transformation to reconstruct the composite image from the fused pyramid. A similar principle is used in the discrete wavelet transform approach presented in the next section.
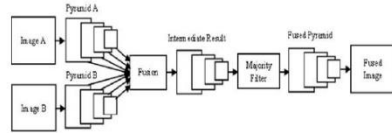

Figure 2. Image Fusion based on Laplacian Pyramid [14]

2) Discrete wavelet transform-based image fusion

The discrete wavelet transform has become an effective tool in the multiresolution analysis and processing of digital images [16]. The DWT, as described in Section II.C, decomposes an input signal into wavelet coefficients. Hence, image fusion using the DWT constitutes combining wavelet coefficients extracted from multiple sources to create a composite image [13],[16].

Fig. 3 shows a 2-D DWT image fusion process with one level. The process begins with the decomposition of each input image into four sub-bands: low-low (LL), high-low (HL), low-high (LH), and high-high (HH). The LL sub-band is an approximation image generated by (8). The HL, LH, and HH sub-bands represent salient features such as edges or lines obtained by (9) from the horizontal, vertical, and diagonal directions, respectively. The composite coefficients are then produced by applying a fusion rule to the wavelet coefficients at the same level and representation via selection or averaging. The final fused image is obtained by calculating the inverse DWT of the composite image, given by (14).
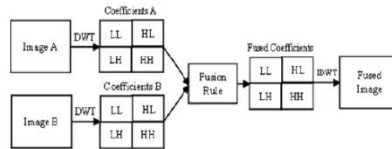

Figure 3. Single-level 2-D DWT Image Fusion [14]

III. PROPOSED METHOD

Backlit image enhancement can be limited to the problem of balancing exposure disparities between foreground (F-region) and background (B-region) scenes. This concept is established on the assertion that the F-region is darker than the B-region because of relatively shorter exposure times, defined as the amount of time a camera's sensor is exposed to light [17]. The
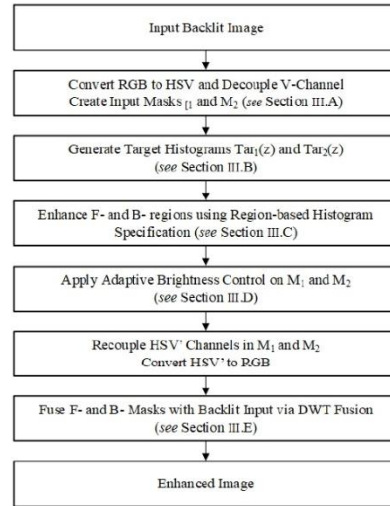

Figure 4. Block Diagram of Proposed Method

proposed method uses a region-based histogram specification scheme combined with the discrete wavelet transform (DWT) image fusion to resolve exposure disparities in a single backlit image and improve the overall perceptual quality. Fig. 4 describes the proposed procedure. The key steps are: (i) Pre-processing the input image; (ii) Generation of target histograms; (iii) Enhancement of F- and B- regions; (iv) Adaptive brightness control; and (v) Fusion of input masks with the backlit input image.

A. Pre-processing of input image

Various colour models have been developed for processing and storing digital pictures. In this paper, the HSV (Hue, Saturation, Value) colour model is employed since it allows the luminance component of an image to be processed without distorting the colour information. In Fig. 4, the proposed procedure begins with an *RGB* to *HSV* transformation [18] on the backlit input $I(r, g, b)$. Letting $I'(h, s, v)$ be the resultant image, two input masks, M_1 and M_2, are created with identical copies of the intensity image I'_v.

B. Generation of target histograms

Histogram specification, in its generic form, involves modifying input intensity values to match a target histogram derived from a mathematical model or a typical image [11]. By using a two-mask approach, the proposed procedure requires two unique target histograms, $Tar_1(z)$ and $Tar_2(z)$, to improve contrast in the under-exposed F-region and reduce over-exposure in the B-region, respectively. The choice of the target
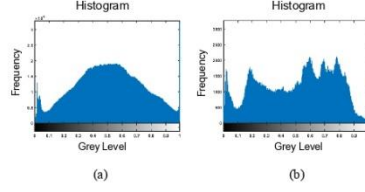
137

Figure 5. Target Histograms (a) Target 1 (b) Target 2

can affect the enhancement results after Histogram Specification is performed. Therefore, generating appropriate target histograms is a crucial step.

The target histograms in Fig. 5 are derived from the luminance component of two sample images. Target 1 is obtained from a well-lit, high-contrast image. Therefore, no peaks in the dark and light tones of the histogram. Target 2 is a high-contrast image captured in a relatively low-light situation, thus having peaks in the dark tones but none in the lightest tones. Such selection for Target 1 improves details in the under-exposed F-region at the expense of lowering contrast in well-lit areas, while Target 2 reduces high radiance in the over-exposed sectors of the B-region but exaggerates underexposure in the F-region.

C. Enhancement of F- and B- regions

Given the input masks, M_1 and M_2, and the target histograms, $Tar_1(z)$ and $Tar_2(z)$, the region-based histogram specification (RBHS) scheme in Fig. 6 is employed using (15).

$$G_k(x,y) = HS\{I'_v(x,y), Tar_k(z)\} \quad (15)$$

where $G_k(x,y)$ is the histogram-specified image of the input mask M_k, obtained by the target $Tar_k(z)$, for $k \in \{1,2\}$.
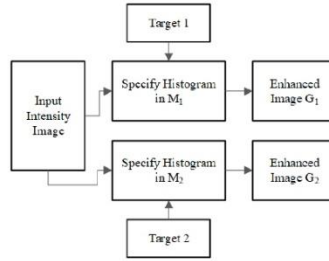

Figure 6. Region-based Histogram Specification scheme

Fig. 7 shows the effects of (15) on a sample backlit image. Fig. 7(a) is the intensity image of the backlit input. Fig. 7(b) and 7(c) are the enhanced output of M_1 and M_2, respectively. Details in the F-region of M_1 can be seen with more clarity, while high radiance is reduced in the B-region of M_2. The histograms of
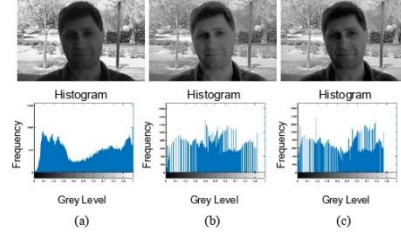

Figure 7. RBHS on sample backlit image (a) Intensity image (b) M_1 output (c) M_2 output

Figs. 7(b) and 7(c) show that the pixel intensities in the light tones of M_1 and M_2 are shifted to darker shades of grey. This property can create low brightness in the final enhancement stage. A brightness control mechanism is used to offset this effect.

D. Adaptive brightness control

Adaptive brightness control (ABC) is a term often associated with the automatic adjustment of a display panel's brightness level based on the ambient light environment [19]. This method is primarily employed in smartphones, tablets, and digital television systems as an energy-saving feature [19],[20]. By contrast, ABC is defined in this paper as a method of automatically compensating for low brightness in the input masks after RBHS is performed. Although the nomenclatures are the same, the difference rest within the methods and applications. Fig. 8 describes the proposed ABC procedure.

1) Brightness threshold

Brightness has been defined by Wyszecki *et al.* [21] as "an attribute of a visual sensation according to which a given visual stimulus appears to be more or less intense; or, according to which the area in which the visual stimulus is presented appears to emit more or less light". Therefore, the perception of brightness to a human viewer is subjective. Currently, there is no conventional method for measuring brightness despite the various methods proposed [22],[23],[24].

To compensate for low brightness in the input masks, first, a threshold value T is determined at a point of perceived brightness in the input. Given in (16), a pixel with an intensity value greater than T is considered a bright element, denoted as Φ^b. i.e., it contributes primarily to the lightness of the image.

$$\Phi^b = \begin{cases} 1, & if\ (L-1) \geq I'_v(x,y) > T \\ 0, & if\ I'_v(x,y) \leq T \end{cases} \quad (15)$$

where $I'_v(x,y)$ is an input intensity value and $L = 2^n$ is the maximum grey level of the input determined by its bit-depth (n). For an 8-bit image, $L = 256$. The threshold T is dependent on the bit-depth of the input. Therefore, the value of T must correlate with the range of grey levels in I'_v.

Various threshold values such as Otsu's [22] and Trongtirakul's [1], provide a basis for image segmentation but

Figure 8. Adaptive brightness control (ABC)

Figure 9. Some selected values for brightness threshold
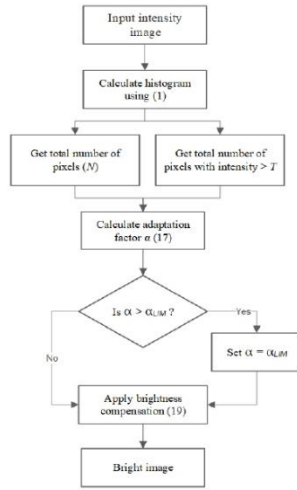
are not suitable for the nature of brightness compensation since they extend to a broader range of grey levels beyond the lightest tones. Therefore, a simple but intuitive approach is adopted in this paper.

In digital imagery, the luminous scale in a histogram estimates the amount of perceived brightness in each pixel as a percentage [25]. Hence, in a normalized histogram ranging from 0 (black) to 1 (white), 0% brightness is black, and 100% brightness is white. The shadow region constitutes about 25% and beyond 75% approximately is the highlight region in which high-intensity values localize [25]. The value of T can thus be obtained by experimenting with various brightness levels in the range [75%—100%]. Some examples are shown in Fig. 9.

After performing 20 experiments with different values, the threshold T was set at 94% brightness, i.e., $hsv(0°, 0\%, 94\%)$ in the HSV model and $rgb(240,240,240)$ in the RGB space. Pixels with grey levels greater than $T=240$ are considered bright elements.

2) Adaptation Factor

Equation (17) calculates the adaption factor α using the sum of bright elements n and the total number of pixels N in the input.

$$\alpha = \frac{N}{(N-n)} - 1 \qquad (17)$$

$$n = \sum_{k=0}^{L-1} H_v(r_k > T) \qquad (18)$$

where H_v is the histogram of l'_v; r_k is an input intensity in the range $[0, L-1]$; and T is a threshold. Table I shows the

values of α for some selected backlit images which are shown in Figs. 12 and 14. Images with many pixels in bins $H_v(r_k > T)$ are observed to have a high adaptation factor.

TABLE I. ADAPTATION FACTORS FOR VARIOUS INPUT

No.	Test Image	Description	Size	α
01	Backlit 1	Man window	448x296	0.3192
02	Backlit 6	Boy outdoor	480x316	0.0673
03	Backlit 17	Road signboard	694x460	0.0588
04	Backlit 40	Bi-cycle woods	640x480	0.0001
05	Backlit 77	Darkroom	1024x586	0.0043

3) Brightness Compensation

In an input mask, brightness compensation is performed by shifting pixel intensity values to the right (highlight region) of the histogram using the adaptation factor α, as given in (19).

$$G'_k(x,y) = \alpha + \sum_{i=1}^{x} \sum_{j=i}^{y} G_k(x,y), for\ k = 1,2 \quad (19)$$

where $G_k(x,y)$ is the histogram-specified image of an input mask M_k, and $G'_k(x,y)$ is the ABC output image that is coupled with the hue and saturation channels of the backlit input. The HSV to RGB transformation [18] is performed on $G'_k(h, s, v)$ to obtain the enhanced RGB colour image for M_k.

4) Alpha-clipping

Backlit images with high α values are frequently associated with excessive brightness compensation in the M_1 input mask. The ABC process incorporates the concept of alpha-clipping to address this problem. Letting α_{LIM} denote a limit parameter, all values of $\alpha > \alpha_{LIM}$ are clipped, as shown in Fig. 8. The parameter α_{LIM} is set to 0.23 based on the perceived quality of the output image. Moreover, excessive brightness compensation tends to occur for α values greater than 0.23, as shown in Fig. 9.

5) Fusion of F- and B- masks with input

Image fusion technology is based on the idea of combining the best features of two or more sources to produce one composite image [2],[14]. Various fusion methods have been explored [14]. In this paper, the DWT approach is employed. Its performance in minimizing colour distortion is a significant advantage [26].

139

a) Single-stage DWT fusion

Fig. 10 depicts a straightforward DWT fusion process that takes three inputs, I_1, I_2, and $\psi(x, y)$. The inputs I_1 and I_2 are the RGB images to be fused and $\psi(x, y)$ denote a wavelet type. To fuse two RGB inputs, first the 2-D wavelet decomposition of each input channel z^i is obtained using (8) and (9). Equation (20) further describes this procedure.

$$[cA_k, cH_k, cV_k, cD_k]^i = DWT\{I_k(z^i), \psi(x, y)\} \quad (20)$$

where cA_k is the approximation coefficient matrix; cH_k, cV_k, and cD_k, are the horizontal, vertical, and diagonal detail coefficient matrices, respectively. The variable $k \in \{1, 2\}$ and $i \in \{R, G, B\}$. After obtaining the coefficient matrices, the mean $\bar{X} = \frac{\sum X}{N}$ is calculated for each I_1 and I_2 channel pair as shown in Fig. 10. Next, the image reconstruction for channel i is done by calculating the inverse discrete wavelet transform using (21).

$$\theta^i = IDWT\{\bar{X}^i, \psi(x, y)\} \quad (21)$$

where $\bar{X}^i$ is the mean vector of the coefficient matrices $[cA, cH, cV, cD]^i$; $\psi(x, y)$ denotes the wavelet type; and the output θ^i is a greyscale image. Finally, the fused image θ is obtained by coupling the RGB channels $(\theta^R, \theta^G, \theta^B)$.

b) Optimization of DWT fusion

The algorithm in Fig. 10 uses a nested for loop to calculate the mean feature vector $\bar{X}^i$. As a result, the time complexity of the proposed method increases significantly by $O(n^2)$ for a given input. Equations (22) to (25) employ a vectorized approach to obtain the mean vector $\bar{X}^i \leftarrow [cA, cH, cV, cD]^i$.

$$cA^i = (cA_1 + cA_2)^i./2 \quad (22)$$

$$cH^i = (cH_1 + cH_2)^i./2 \quad (23)$$

$$cV^i = (cV_1 + cV_2)^i./2 \quad (24)$$

$$cD^i = (cD_1 + cD_2)^i./2 \quad (25)$$

where $[cA_k, cH_k, cV_k, cD_k]^i$ are the coefficient matrices obtained from (20) for $k \in \{1, 2\}$ and $i \in \{R, G, B\}$.

c) Two-stage RBHF fusion process

The proposed method uses a two-stage DWT fusion process as shown in Fig. 11. Salient features of the enhanced input masks, G'_1 and G'_2, are combined in the first stage, yielding the fused image $F_1(x, y)$. The final enhanced colour image $F_2(x, y)$ is created by combining $F_1(x, y)$ with the backlit input $I(x, y)$.

IV. EXPERIMENTAL RESULTS AND ANALYSIS

Various experiments were conducted on a dataset of 100 backlit images with an 8-bit resolution. Of these images, 24 samples were selected from Li's database [27], which contains 38 standard backlit photos used in similar research, and 76 were obtained from the Exclusively Dark (ExDark) database [28], which comprised 7,363 low-quality images captured in poor lighting settings. Due to space limitations, only a few selected

```
% Pseudo code for a single-stage DWT fusion

Input:I₁ = (x^R, x^G, x^B); I₂ = (y^R, y^G, y^B);
Wavelet-type: ψ(x, y);
Result: Θ(rgb);

for each Input k ∈ {I₁, I₂}:
    for each channel z^i of I_k:
        get the DWT{I_k(z^i), ψ(x, y)};
        output→ [cA_k, cH_k, cV_k, cD_k]^i;
    end;
end;

for each channel i ∈ {R, G, B} pair of I₁ · I₂:
    get the mean X̄^i ← [cA, cH, cV, cD]^i;
        cA^i = X̄(cA₁, cA₂);
        cH^i = X̄(cH₁, cH₂);
        cV^i = X̄(cV₁, cV₂);
        cD^i = X̄(cD₁, cD₂);
    calculate θ^i = IDWT{X̄^i, ψ(x, y)};
end;
Result: set Θ = (θ^R, θ^G, θ^B);
```

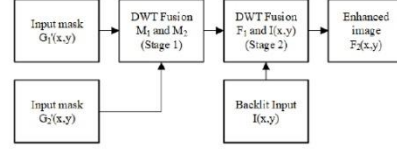Figure 10. Single-stage DWT fusion

Figure 11. Two-stage RBHF fusion process

images from the dataset are used to demonstrate the effectiveness of the proposed method. The full results are available at https://github.com/shaffakjr/backlit-research-rbhf for interested readers. All simulations were performed in MATLAB R2018a on a PC with 32GB RAM and a 2.60GHz Intel Core i7 processor. The parameters of the ABC fusion stages were set as follows: $T = 240$; $\alpha_{LIM} = 0.23$; and $\psi(x, y) = sym5$.

A. Performance evaluation of the proposed method

Fig. 12 displays the performance of the proposed method on five different backlit inputs: B1, B6, B17, B77, and B20. The original images are shown in Fig. 12(a), and the enhanced results are displayed in Fig. 12(b). Overall, the results show significant improvements in the visual quality of the backlit inputs without any noticeable distortion or artefacts. Furthermore, the outcomes of images B1, B6, and B20 demonstrate that the proposed algorithm can effectively expose the degraded backlit sectors.

B. Quality assessment

Three objective metrics are used to validate the performance of the proposed method. They include the PSNR, SSIM, and NIQE [32]. The PSNR and SSIM are well-known full-reference image quality metrics. The former is used to calculate the peak signal-to-noise ratio between the backlit input and enhanced output, while the latter measures structural similarity. The greater the PSNR value, or an SSIM score close to 1, the better

140

Figure 12. Enhancement results for some selected backlit images (a) Original (b) Enhanced

the image quality. The NIQE is a no-reference image quality metric that calculates the naturalness of an image using only observable deviations from statistical regularities identified in natural photographs. It requires no training or exposure to distorted images [29]. Given in (26), the NIQE is defined as a simple distance metric between the model statistics and the distorted image statistics [29].

$$D(V_1, V_2, \Sigma_1, \Sigma_2) = \sqrt{\left((V_1 - V_2)^T \left(\frac{(\Sigma_1 + \Sigma_2)^{-1}}{2}\right)(V_1 - V_2)\right)} \quad (26)$$

where V_1, V_2, and Σ_1, Σ_2 represent the mean vectors and covariance matrices of a natural Multivariate Gaussian (MVG) model and the MVG model of the distorted image, respectively. Several studies, including Wang *et al.* [2] and Ueda *et al.* [9], have adopted the NIQE quality metric, with low values indicating high picture quality.

Table II gives the objective quality scores for the simulations in Fig. 12. The PSNR and SSIM index are given in columns (5) and (6), respectively, followed by the NIQE score for the backlit input in column (7) and the enhanced output in column (8). The proposed method achieved high PSNR—19 to 25dB—for many images in the dataset. Some examples are seen in the outcomes of images B1, B6, and B17. However, low PSNR values were consistent with images of high backlit degradation like B77.

The SSIM results in Table II show that the proposed method achieves high structural similarity with the backlit inputs, ranging from 0.6 to 0.9. However, low SSIM scores below 0.5 were also frequent with highly degraded images. Nevertheless, since the nature of the problem is backlit enhancement, this is expected as more salient features are revealed in the enhanced images.

In terms of NIQE, the proposed method tends to improve or preserve the natural quality of the backlit inputs. Some examples can be seen in the outcomes of images B1, B6, B17, and B20. The lowest NIQE quality was realized by image B77.

C. Multiple RBHF process to improve enhancement quality

As seen in Table II, the proposed method can produce low PSNR values for some backlit inputs even when high perceptual quality is achieved. To improve such outcomes, establishing the proposed method as an iterative process can increase the enhancement quality of the backlit input, thereby improving the PSNR. In theory, this is a valid approach since the proposed

TABLE II.   OBJECTIVE ASSESSMENTS OF THE PROPOSED METHOD FOR SELECTED BACKLIT INPUTS

No.	Test Image	Description	Size	PSNR (dB)	SSIM	NIQE I/P	NIQE O/P
01	Backlit 1	Man window	448x296	20.7	0.81	3.38	3.20
02	Backlit 6	Boy outdoor	480x316	23.7	0.91	2.26	2.15
03	Backlit 17	Road signboard	694x460	20.5	0.69	2.95	2.41
04	Backlit 20	Office building	360x480	19.0	0.72	2.63	2.40
05	Backlit 77	Darkroom	1024x586	15.3	0.47	1.69	1.91
Average				19.8	0.72	2.58	2.42

141

method has shown properties of preserving details and colour in the enhanced output.

Fig. 13 depicts the proposed multiple region-based histogram and fusion (RBHF) process. The overall process is determined by the number of iterations given by the parameter $Iter$. A value of 1, i.e., $Iter = 1$, yields the outcomes of a single RBHF process. The outcomes of $2 \leq Iter < \infty$ are presented in the following sections.
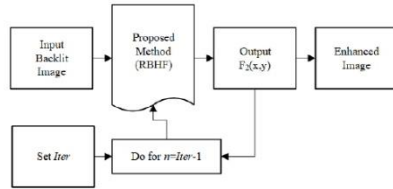

Figure 13. Proposed Multiple RBHF process

1) Performance of multiple RBHF process

Fig. 14 shows the results for multiple iterations of the proposed method on selected backlit inputs: B6, B77, B40, B20, and B21. The original images are shown in the first column. The enhanced image after each iteration is given in subsequent columns. Furthermore, the enhanced image $F_2^{[n]}(x,y)$ of the previous iteration $[n]$ is used as the input for the next $[n + 1]$ iteration to obtain the enhanced image $F_2^{[n+1]}(x,y)$. Except for the first iteration $n = 0$ where the input is the degraded backlit image. Finally, the experimental value of $iter$ was set to 5. After 5 iterations, there is no apparent difference between the input and the enhanced images as given by the SSIM index. The outcomes of each iteration are shown in Figs. 14(b)-(f), respectively.

The results in Fig. 14 show significant improvements in the perceptual quality of the backlit inputs. With each iteration, the proposed method increased exposure both in the F- and B-regions while details and colours were retained. However, intensity saturation is observed in the B-region of image B21, particularly after the third iteration. This effect uniquely occurs when the exposure levels become higher than what is required to properly reveal the entire picture scene.
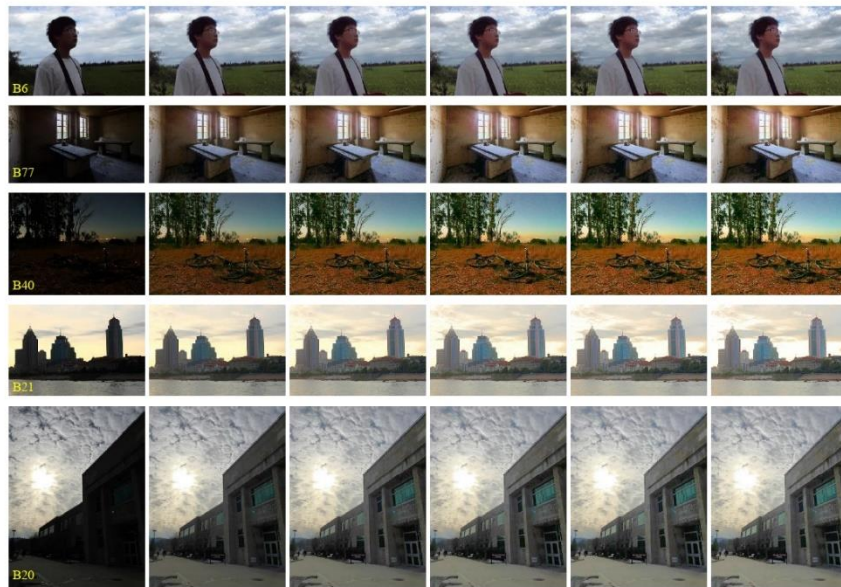

Figure 14. Performance of multiple RBHF on selected backlit images (a) Backlit input (b) iter =1 (c) iter =2 (d) iter =3 (e) iter =4 (f) iter =5
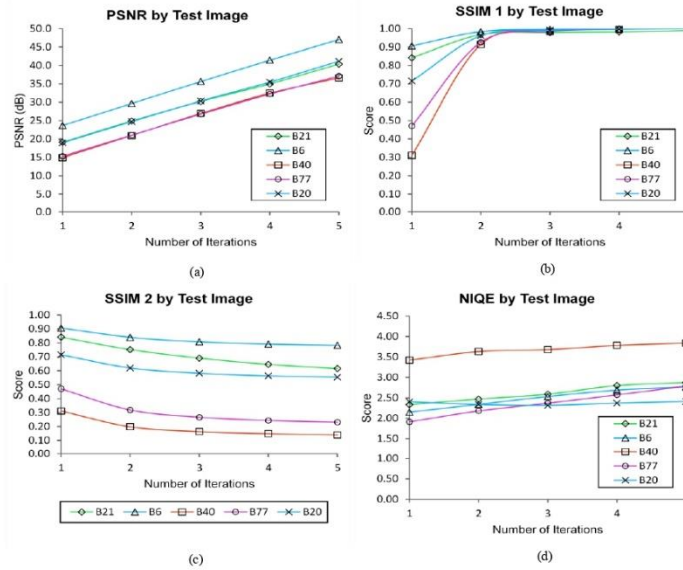
142

Figure 15. Quality assessments of multiple RBHF (a) PSNR (b) SSIM Evaluation 1 (c) SSIM Evaluation 2 (d) NIQE

2) Objective assessment

The PSNR, SSIM, and NIQE quality metrics are used to evaluate the performance of the multiple RBHF process in Fig. 14. The PSNR evaluation is given in Fig. 15(a). For each iteration, $F_2^{[n]}(x,y)$ is the new ground truth image compared to $F_2^{[n+1]}(x,y)$. In Fig. 15(a), the proposed method realized up to a 6dB increase in PSNR per iteration. Furthermore, the graph suggests that further improvements in the PSNR quality could be achieved after the 5th iteration.

Fig. 15(b) gives the SSIM assessment, and $F_2^{[n]}(x,y)$ is the new ground truth image compared to $F_2^{[n+1]}(x,y)$. Significant improvements in the SSIM quality can be seen in the first three iterations. However, after the third iteration, the SSIM values tend to converge at the absolute similarity.

Fig. 15(c) compares the structural similarity between the backlit input $I(x,y)$ and the enhanced image $F_2^{[n]}(x,y)$ for $n \in \{0,..,4\}$. The overall results show a decrease in the SSIM values with about a 10% reduction after the second iteration. Since the ground truth image is the degraded input and the problem domain is backlit enhancement, the SSIM values are expected to decrease as the enhancement quality increase. However, more than (60-80)% similarity is achieved by the proposed method for images B6, B21, and B20 whereas (20-40)% for B40 and B77, for the 5 iterations displayed.

Fig. 15(d) depicts varying changes in the NIQE values after each iteration. Within five iterations, the proposed method realized a slight decrease in the NIQE values for the backlit inputs. Some examples can be seen in the outcomes of images B21, B6, and B77. However, the method's overall performance yielded desirable results in terms of preserving the natural quality of the backlit inputs.

3) Subjective assessment

A subjective test was conducted to further evaluate the results in Fig. 14. Using the International Telecommunications Union's image quality assessment framework [33], 16 non-experts in digital image processing were asked to judge the enhancement results for each iteration and then choose the outcome with the best picture quality. The test subjects included twelve residents from the Plainsview community in South B and four students from the Railways Training Institute, Nairobi, Kenya. Table III gives the results of their assessments.

Table III shows that two iterations of the proposed method are often sufficient to produce a higher image quality. However, in some cases, as seen in the outcome of image B21, one iteration was deemed sufficient.

No.	Output Image by Iteration	Image Quality by Number of Test Subjects				
		B6	B77	B40	B21	B20
01	Iter 1	2	3	4	11	3
02	Iter 2	7	7	6	3	8
03	Iter 3	1	3	6	2	1
04	Iter 4	4	3	0	0	3
05	Iter 5	2	0	0	0	1

D. Computational time analysis for multiple RBHF

Table IV depicts the average execution time for each simulation of the multiple RBHF process based on the backlit inputs in Fig. 14. The time CTBO represents the computation time before the DWT fusion optimization, and CTAO is the time measurement after optimization. The computation time given by CTBO increased significantly with the input's size. For example, the average time for low-resolution images such as B6 and B20 was less than 2 seconds per iteration, whereas higher-resolution images like B77 yielded about 7 seconds. The DWT fusion optimization significantly improved the time complexity of the proposed algorithm when comparing the results of CTBO and CTAO in Table IV. As shown in column (5), the average time for all simulations was less than 0.65 seconds per iteration.

TABLE IV.   AVERAGE EXECUTION TIME PER ITERATION

No.	Test Image	Size	Time (s) CTBO	Time (s) CTAO
01	Backlit 6	480x316	1.78	0.12
02	Backlit 20	360x480	1.83	0.13
03	Backlit 21	600x400	2.64	0.17
04	Backlit 40	640x480	3.61	0.28
05	Backlit 77	1024x586	7.16	0.62

E. Comparative analysis with existing methods

In this section, the performance of the proposed method is compared to Histogram Equalization (HE) [4], Retinex [7], and LIME [10]. Various simulations were conducted on a dataset of 100 backlit images with an 8-bit resolution. Seven images are provided for comparative analysis due to space limitations.

1) Subjective comparison

Fig. 16 compares the results of the proposed method to existing image enhancement techniques. The backlit images are shown in Fig. 16(a) and the enhanced results of Histogram Equalization, Retinex, and LIME are shown in Figs 16(b)-(d), respectively. Figs 12(e) and 12(f) give the outcomes of two iterations of the proposed method.

Overall, the results of the proposed method show significant improvement in the backlit inputs without problems of under- or over-enhancement as with existing approaches. For instance, Histogram Equalization tends to improve visibility in the dark F-region of the backlit input but at the expense of distorting or washing-out colours, as seen in images B6, B3, and B23 of Fig. 16(b). Retinex, in Fig. 16(c), creates an unnatural effect in the enhanced image with distortion features similar to Histogram Equalization. In contrast, LIME tends to over-enhanced details in the backlit image while oversaturating colours, as shown in Fig. 16(d) images B6 and B21.

Compared to the existing methods, the proposed method has a superior performance in terms of visual quality. The main reason for this is that it increased contrast in the under-exposed F-region and adjusted exposure disparities in the overall image while suppressing colour artefacts, giving the enhanced image a more realistic appearance.

2) Objective comparison

Table V gives the average quality measurements for various methods on 100 backlit images. The PSNR results are shown in column (3) followed by the SSIM and NIQE scores in columns (4) and (5), respectively. On average, the proposed method outperformed existing methods in all quality metrics. As shown in Table V, the second iteration of the proposed method

Figure 16. Enhancement comparison of various methods (a) Backlit input (b) HE [4] (c) M-Retinex [7] (d) LIME [10] (e) Proposed method iter=1 (f) Proposed method iter=2
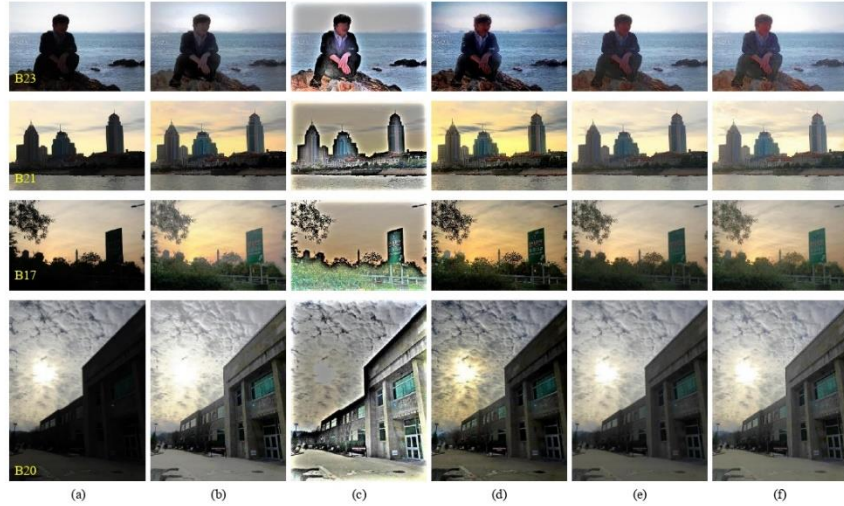
144

Figure 16 *(continued)*. Enhancement comparison of various methods (a) Backlit input (b) HE [4] (c) M-Retinex [7] (d) LIME [10] (e) Proposed method iter=1 (f) Proposed method iter=2

achieved the highest quality scores in both PSNR and SSIM while the first iteration attained the best NIQE quality.

TABLE V.   AVERAGE QUALITY SCORES FOR VARIOUS METHOD ON 100 BACKLIT IMAGES

No.	Method	PSNR (dB)	SSIM	NIQE O/P
01	Histogram Equalization [4]	11.6	0.44	3.86
02	M-Retinex [7]	9.2	0.42	3.86
03	LIME [10]	15.7	0.52	3.73
04	Proposed Method iter =1	18.2	0.61	3.19
05	Proposed Method Iter =2	24.1	0.94	3.52

V.   CONCLUSION

In this paper, a novel technique for single backlit image enhancement is presented. The proposed technique combined a global contrast stretching scheme based on histogram matching with the DWT image fusion to improve the visual perception of a single backlit image. The proposed algorithm was tested on standard backlit images from the Li's and ExDark databases. Both objective and subjective image quality metrics were used to validate the performance of the algorithm.

A multiple RBHF process was presented to improve the performance of the proposed algorithm. For five iterations, both qualitative and quantitative evaluations showed the absolute quality of the RBHF method. In most situations, one to two iterations were observed to be sufficient in achieving the desired enhanced effects.

A comparative investigation using standard backlit images from Li's and ExDark databases was conducted to compare the performance of the proposed technique to existing enhancement methods such as Histogram Equalization, Retinex, and Low-light image enhancement via Illumination Map Estimation. Experimental results demonstrated the superiority of the proposed method in improving contrast in the dark foreground while preserving details and colours in the overall image.

Future work shall focus on adopting an unsharp masking algorithm to improve the sharpness of the enhanced images as well as developing a mathematical model to generate optimal target histograms.

REFERENCES

[1] T. Trongtirakul, W. Chiracharit and S. S. Agaian, "Single Backlit Image Enhancement," in IEEE Access, vol. 8, pp. 71940-71950, 2020, doi: 10.1109/ACCESS.

[2] Q. Wang, X. Fu, X.-P. Zhang, and X. Ding, ''A fusion-based method for single backlit image enhancement,'' in Proceedings IEEE International Conference Image Processing (ICIP), Phoenix, Arizona, USA, Sep. 2016, pp. 4077–4081.

145

[3] C. Wei, W. Wang, W. Yang, and J. Liu, "Deep retinex decomposition for low-light enhancement," in Proceedings British Machine Vision Conference (BMVC). Newcastle, U.K., Aug. 2018

[4] S. M. Pizer, E. P. Amburn, J. D. Austin., "Adaptive histogram equalization and its variations," Computer vision, graphics, and image processing, vol. 39, no. 3, pp. 355–368, 1987

[5] D. J. Jobson, Z.U. Rahman and G.A. Woodell, "Properties and performance of a center/surround retinex," IEEE Transactions on Image Processing, vol. 6, no. 3,pp. 451–462, 1997

[6] D. J. Jobson, Z. U. Rahman and G. A. Woodell, "A multiscale retinex for bridging the gap between colour images and the human observation of scenes," IEEE Transactions on Image Processing, vol. 6, no. 7, pp. 965–976, 1997.

[7] A.-B. Petro, C. Sbert, and J.-M. Morel, "Multiscale Retinex," Image Processing On Line, vol. 4, pp. 71–88, April 2014, doi: 10.5201/ipol.2014.107.

[8] Z. Li and X. Wu, "Learning-based restoration of backlit images," IEEE Transactions on Image Processing, vol. 27, no. 2, pp. 976–986, February 2018

[9] Y. Ueda, D. Moriyama, T. Koga and N. Suetake, "Histogram Specification-Based Image Enhancement for Backlit Image," 2020 IEEE International Conference on Image Processing (ICIP), Abu dhabi, UAE, Oct. 2020, pp. 958-962, doi: 10.1109/ICIP40778.2020.9190929.

[10] X. Guo, Y. Li, and H. Ling, "LIME: Low-light image enhancement via illumination map estimation," IEEE Trans. Image Process., vol. 26, no. 2, pp. 982–993, Feb. 2017

[11] R. C. Gonzales and R. E. Woods, Digital Image Processing (4th Ed., Global Ed.). Pearson Publishing Co., Inc. New Jersey, USA, 2018.

[12] L. Seungwon, N. Kim, and J. Paik, "Adaptively partitioned block-based contrast enhancement and its application to low light-level video surveillance," SpringerPlus, vol. 4, p. 431, Aug. 2015, doi: 10.1186/s40064-015-1226-x.

[13] C. Chui, An Introduction to Wavelets. Academic Press, New York, USA, 1992

[14] V. Patil, D. Sale, and M. A. Joshi, "Image Fusion Methods and Quality Assessment Parameters," Asian Journal of Engineering and Applied Technology, vol. 2, no. 1, pp. 40–46, May 2013.

[15] R. J. Suthakar, J. M. Esther, D. Annapoorani, and F. R. S. Samuel, "Study of Image Fusion-Techniques, Method and Applications," 2014.

[16] K. Amolins, Y. Zhang, and P. Dare, "Wavelet based image fusion techniques -An introduction, review and comparison," Jul. 2007.

[17] "Exposure time," SmartRay. https://www.smartray.com/glossary/exposure-time/ (accessed May 06, 2022).

[18] A. R. Smith, "Colour Gamut Transform Pairs". SIGGRAPH 78 Conference Proceedings. Atlanta, GA, USA, Aug. 1978, pp. 12–19.

[19] T. Ma, C. Lin, S. Hsu, C. Hu and T. Hou, "Automatic brightness control of the handheld device display with low illumination," 2012 IEEE International Conference on Computer Science and Automation Engineering (CSAE), Zhangjiajie, China, May 2012, pp. 382-385, doi: 10.1109/CSAE.2012.6272797.

[20] M. Schuchhardt, S. Jha, R. Ayoub, M. Kishinevsky and G. Memik, "Optimizing mobile display brightness by leveraging human visual perception," 2015 International Conference on Compilers, Architecture and Synthesis for Embedded Systems (CASES), Amsterdam, Netherlands, Oct. 2015, pp. 11-20, doi: 10.1109/CASES.2015.7324538.

[21] G. Wyszecki, W. S. Stiles, "Colour Science. Concepts and Methods, Quantitative Data and Formulae", Second Edition, John Wiley & Sons, USA, (2000)

[22] N. Otsu, "A threshold selection method from graylevel histograms," IEEE Trans. Syst., Man, Cybern., vol. SMC-9, pp. 62–66, (1979)

[23] S. Bezryadin, P. Bourov, and D. Ilinih, "Brightness Calculation in Digital Image Processing," International Symposium on Technologies for Digital Photo Fulfilment, vol. 2007, pp. 10–15, Nevada, USA, January 2007, doi: 10.2352/ISSN.2169-4672.2007.1.0.10.

[24] S. Bezryadin and P. Bourov, "Colour coordinate system for accurate colour image editing software," in The International Conference Printing Technology SPb, San Francisco, USA, June 2006, vol. 6, pp. 145–148.

[25] "Understanding Histograms in Photography," Photography Life, Feb. 22, 2013. https://photographylife.com/understanding-histograms-in-photography (accessed March 08, 2022).

[26] K. Amolins, Y. Zhang, and P. Dare, "Wavelet based image fusion techniques -An introduction, review and comparison," 2007.

[27] Li's Database. Accessed: October 18, 2021. [Online]. Available: https://github.com/7thChord/backlit

[28] Exclusively Dark (ExDark) Database. Accessed: May 27, 2022. [Online].Available: https://github.com/cs-chan/Exclusively-Dark-Image-Dataset

[29] A. Mittal, R. Soundararajan, and A. Bovik, "Making a 'Completely Blind' Image Quality Analyzer," Signal Processing Letters, IEEE, vol. 20, pp. 209–212, Mar. 2013, doi: 10.1109/LSP.2012.2227726.

[30] RECOMMENDATION ITU-R BT.500-14, "Methodologies for the subjective assessment of the quality of television images," p. 102., October 2019

146

A3. Second Publication

Conference Name: IEEE Imaging Systems & Techniques

Conference Dates: October 17 – 19, 2023

Venue: Copenhagen, Denmark

Submission Date: July 7, 2023

A Low-Light Image Enhancement Technique Based on Histogram Matching and Fusion

Shaffa K. Kokro Jr.
Dept. of Electrical and Information Engineering
University of Nairobi
Nairobi, Kenya
shaffakokro@students.uonbi.ac.ke

Elijah Mwangi
Faculty of Engineering
University of Nairobi
Nairobi, Kenya
elijah.mwangi@uonbi.ac.ke

George Kamucha
Faculty of Engineering
University of Nairobi
Nairobi, Kenya
gkamucha@uonbi.ac.ke

Abstract— **The enhancement of low-light images is a critical area of research in computer vision and image processing. It is essential for many applications, including surveillance, medical imaging, and astronomy. Existing image enhancement methods, however, often exhibit colour distortions, over-saturation, and other abnormalities that lead to a drastic reduction in the low-light image fidelity. In this paper, we propose a novel image enhancement algorithm that effectively addresses these challenges. Our approach leverages histogram matching and image fusion techniques to improve the perceptual quality of the low-light image. We employ a region-based histogram matching scheme to enhance contrast in the foreground and background scenes distinctly. An adaptive brightness control mechanism adjusts the overall brightness to ensure that details enhanced in dark areas are perceptible. We combined salient features from the foreground and background scenes with the original low-light image via a two-stage discrete wavelet transform fusion. Finally, we employ the classical unsharp masking algorithm to sharpen details in the resulting image. Computer simulations on a benchmark dataset show the efficacy of our method in both objective quality and subjective visual inspection. Compared to existing approaches, our method achieved high PSNR and SSIM quality, demonstrating the potential of our algorithm for low-light image enhancement applications.**

Keywords— *Histogram matching, image fusion, discrete wavelet transform, low light image enhancement*

I. INTRODUCTION

Low-light images are digital pictures captured in low-lighting conditions such as at night, dusk, dawn, indoor settings with dim light, etc. These images often have higher noise levels and poor visibility in the foreground and background scenes which can reduce the effectiveness of computer vision algorithms like object detection [1] and recognition [2]. Over the years, various techniques have been proposed to improve the visual quality of low-light images. Some of these methods are based on conventional image processing techniques, including histogram equalization [3], contrast stretching [4][5], and Retinex theory [6]-[8]. Histogram-based techniques improve the perceptual quality of low-light images by redistributing pixel intensity values in bright and dark regions to create a more balanced histogram, while contrast stretching alters the image contrast range to differentiate its features. Retinex algorithms, on the other hand, operate on the notion that an image can be split into reflection and illumination components and seek to separate them to improve its visual quality [7]. Despite the effectiveness of these algorithms in enhancing the visibility of low-light images, they often result in over-saturation, colour distortion, or loss of contrast in well-lit areas [4][9].

To address these limitations, researchers have investigated several deep learning techniques with convolutional neural networks (CNNs) to conduct intrinsic mappings between the low-light input and the enhanced image [10]-[11]. Deep learning techniques have demonstrated remarkable performance in reducing noise and improving the perceptual quality of low-light pictures. However, they may not be appropriate for real-time applications due to their high computational cost. Additionally, deep neural networks require large training datasets and may not generalize well to images with different characteristics or from other domains [12].

The guided image filtering (GIF) and the dark channel prior (DCP) approaches are alternative methods to traditional image processing and deep learning techniques. The GIF and DCP techniques can be effective in many low-light situations. However, GIF methods can lead to colour distortions and they perform poorly in very dark scenes [13][14]. On the other hand, DCP methods heavily focus on outdoor settings where the light distribution is impacted by atmospheric scattering which creates a prominent dark channel in the low-light input [15][16]. Frequently, this limits the performance of DCP techniques in situations where the lighting conditions are controlled, such as in indoor settings [16].

In this paper, we proposed a novel and flexible low-light image enhancement algorithm that focuses on correcting the exposure disparities between well-lit and under- or over-exposed parts in the image. To achieve this, we employ a region-based histogram specification scheme for stretching contrast globally in foreground and background scenes, a two-stage discrete wavelet transform (DWT) fusion to combine salient features of the contrast-stretched images with the low-light input, and the classical unsharp masking algorithm to further improve contrast.

The rest of the paper is organized as follows: Section II covers relevant literature utilised in the development of the proposed method. In Section III, the proposed algorithm is presented. Section IV then discusses the experimental results and Section V highlights the conclusion and future study.

II. THEORETICAL FRAMEWORK

A. Histogram Matching

Histogram is a powerful tool for analysing the visual characteristics of images, such as contrast, brightness, and dynamic range. As given in (1), it is a discrete function that counts the number of pixels having a particular grey value in the range $[0, L-1]$ [17].

$$h(r_k) = n_k \ , \ for \ k \in [0, L-1] \qquad (1)$$

where r_k is the kth grey level, n_k is the number of pixels having a grey level r_k, and $L = 2^n$ is the maximum grey level
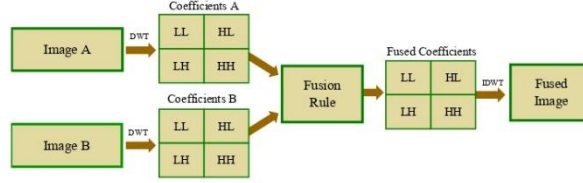
Fig. 1. *Single-level 2-D Discrete Wavelet Transform Image Fusion*

determined by the image bit depth (n). Described in (2), is a normalized histogram $p(r_k)$ obtained by dividing n_k by the total number of pixels in the image (N) [17].

$$p(r_k) = \frac{n_k}{N} \quad (2)$$

The histogram matching technique is used to modify the pixel distribution of an input image $I(x,y)$ to match a desired histogram $p_D(z_j)$, usually obtained from a mathematical model or a sample image [17][18]. To perform the classical histogram matching, first, we compute the cumulative distribution function (CDF) of the input, $T(r_k)$, and the CDF of the target histogram, $G(z_k)$, as given in (3) and (4), respectively.

$$T(r_k) = \sum_{i=0}^{k} p_I(r_i) \; ; \; k \in \{0, L-1\}/L-1 \quad (3)$$

$$G(z_k) = \sum_{j=0}^{k} p_D(z_j) \; ; \; k \in \{0, L-1\}/L-1 \quad (4)$$

where $p_I(r_i)$ and $p_D(z_j)$ are the normalized input and target histograms. Next, letting $U(\cdot)$ be a transformation function such that $U(r_k) = z_k$, we can map the grey level r_k to the desired value z_k to satisfy the condition $T(r_k) = G(z_k)$. Finally, applying $U(\cdot)$ to every pixel in $I(x,y)$ will yield the histogram-specified image [17].

B. Discrete Wavelet Transform

The DWT is a mathematical technique widely used in image processing applications for compression, feature extraction, or denoising. Using a set of wavelet functions, the DWT decomposes an image signal at the first level into four frequency sub-bands, namely the Low-Low (LL), Low-High (LH), High-Low (HL), and High-High (HH). Each of these sub-bands contains different frequency components of the input [19].

The LL or approximation sub-band is the low-frequency component obtained by applying a low-pass filter across the input. The LH and HL sub-bands represent the high-frequency details extracted from filtering the signal in the horizontal and vertical directions, respectively. The difference between the LH and HL sub-bands is their method of filtering. For example, features within the LH sub-band are obtained by applying a low-pass filter to the rows of the signal and then a high-pass filter across the columns. The opposite is true for the HL sub-band. Lastly, the HH or diagonal detail sub-band contains high-frequency information in both the horizontal and vertical directions of the image. It uses a high-pass filter across both the rows and columns of the signal [19].

C. DWT Image Fusion

Image fusion is a technique used to form a composite image by combining several image sources using a fusion rule such as averaging, maximum selection, or minimum selection. The goal of image fusion in any application is to produce a final image with a higher perceptual quality than each source [20].

The DWT approach to image fusion involves combining DWT coefficients at corresponding levels and sub-bands to form a composite image. This method has widely been employed in medical imaging, surveillance, and remote sensing applications [20]. Illustrated in Fig. 1 is a single-level 2-D DWT fusion used to blend two grey-image sources denoted 'A' and 'B'. The procedure begins with a 2-D decomposition of the inputs. Next, a fusion rule such as averaging, is applied to each coefficient pair at the same level to obtain the fused coefficients. The final fused image is obtained by computing the inverse DWT of the fused coefficients.

D. Unsharp Mask Filtering

Unsharp mask filtering is a widely used technique in image processing for sharpening details and edges. The procedure involves subtracting a blurred version of an image from itself, as described in (5) [17].

$$f_s(x,y) = f(x,y) - f_b(x,y) \quad (5)$$

where $f(x,y)$ is the original image, $f_b(x,y)$ and $f_s(x,y)$ are blurred and sharpened versions, respectively.

III. PROPOSED METHOD

In this section, we present our proposed method for enhancing low-light images. The proposed algorithm can be summarized in three steps:

(i)   Contrast enhancement
(ii)   Feature extraction and reconstruction
(iii)   Unsharp masking

The first step is to make the low-light image more perceptible by improving contrast in the under- and over-exposed scenes while balancing the overall exposure levels in the image. To do this, we create two identical copies of the input and enhance them using a region-based histogram specification scheme (RBHS) based on the classical histogram matching algorithm discussed in section II.A. The second step involves extracting relevant features from the enhanced images and using them to reconstruct a high-quality representation of the scene. In the final step, we apply an

148

Fig. 2. *Pseudo code of the Proposed Method*

Fig. 3. *RBHS Target Histograms generated from sample images (a) Target 1 (b) Target 2*

unsharp mask filter to improve the details and edges in the reconstructed image.

A. Region-Based Histogram Specification

Given an input $I(R,G,B)$, we first perform an RGB-to-HSV transformation [21] to separate the intensity component $I(V)$ from the hue and saturation channels $I(H)$ and $I(S)$, respectively. This allows us to modify the intensity component of the input without affecting its colour profile. Next, we generate two input masks, M_1 and M_2, with identical copies of the intensity image $I(V)$ and enhance them using (6).

$$G_k(x,y) = HS\{I_v(x,y), Tar_k(z)\} \tag{6}$$

where $G_k(x,y)$ is the histogram-specified image of M_k obtained by the target histogram $Tar_k(z)$ for $k \in \{1,2\}$. The function $HS\{*\}$ denotes a histogram-matching process.

The target histograms, $Tar_1(z)$ and $Tar_2(z)$, play an important role in the RBHS scheme, as they dictate the desired distribution of grey level in each input mask. Our objective is for Target 1 to improve contrast in the under-exposed regions of M_1, while Target 2 aims at reducing high radiance in the over-exposed sectors of M_2. For such purpose, the shape of these histograms must be carefully selected to reflect the desired changes in the contrast and brightness of the image.

To guide the selection of $Tar_1(z)$ and $Tar_2(z)$, we propose the following framework: The contour of $Tar_1(z)$ should represent a well-lit high-contrast image with no peak in the shadow and highlight tonal ranges. In contrast, the shape of $Tar_2(z)$ should be the histogram of a high-contrast image captured in a relatively low-light situation, thus having peaks in the dark tones but none in the brightest tones. Such selection of $Tar_1(z)$ and $Tar_2(z)$ are displayed in Fig. 3.

B. Intensity Mappings

We note that the mappings of intensity values between the input $I_v(x,y)$ and the histogram-specified images $G_{k=1,2}(x,y)$ in (6) are based on generalization. This means that $G_k(x,y)$ will always approximate $Tar_k(z)$ rather than achieving an exact match as proposed in [22]. Such flexibility enables our method to handle a wider range of low-lighting scenarios without requiring significant structural changes.
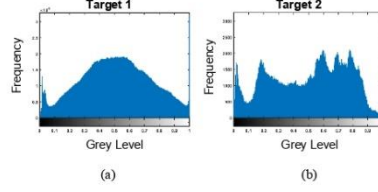
C. Brightness Control and Localization

Low brightness in $G_k(x,y)$ is a commonly encountered problem when $I_v(x,y)$ contains a bimodal intensity distribution. To address this, we propose an adaptive brightness control mechanism which shifts pixel values in $G_k(x,y)$ to the right of the histogram based on the local brightness profile in $I_v(x,y)$. By doing so, we can ensure that the brightness of $G_k(x,y)$ is better aligned with that of the input.

Fig. 4 illustrates the proposed Adaptive Brightness Control procedure. To begin, we first obtain the histogram of $I_v(x,y)$ using (1), then compute the total number of pixels (N) and the total number of pixels greater than a certain threshold, (n). Together, these parameters determine the adaptation factor α used to control the amount of brightness compensation, as given in (7).

$$I'_{v_k}(x,y) = \alpha + \sum_{i=1}^{x}\sum_{j=i}^{y} G_k(x,y), \; for \; k = 1,2 \tag{7}$$

where $G_k(x,y)$ is the histogram-specified image of M_k and $I'_{v_k}(x,y)$ is the Adaptive Brightness Control output that is coupled with the low-light input's $I(H)$ and $I(S)$ channels. The parameter α adapts to the input subjective brightness, as defined in (8).

$$\alpha = \frac{N}{(N-n)} - 1 \tag{8}$$

$$n = \sum_{k=0}^{L-1} H_v(r_k > T) \tag{9}$$

where H_v is the histogram of $I_v(x,y)$; r_k is an input intensity in the range $[0, L-1]$; and T is a "subjective" brightness threshold. This threshold is localized within the highlight region of the histogram which is mostly affected

Fig. 4. *Pseudo code for the proposed Adaptive Brightness Control*

when grey levels in $G_k(x, y)$ are stretched. We defined the value of T based on the objective and subjective criteria discussed in section IV.A.

D. Feature extraction and reconstruction

The proposed method relies on enhancing contrast globally in M_1 and M_2 to improve exposure in specific parts of the image. This technique improves visibility discretely in dark and bright regions of the low-light image, however, it can also lead to over- or under-enhancement in well-lit areas. To address this, we employed a two-stage DWT fusion process to combine salient features of M_1 and M_2 with the original low-light image $I(x, y)$.

In the first stage, the RGB images $I'_{v_1}(x, y)$ and $I'_{v_2}(x, y)$ are fused to produce $F'_1(x, y)$, then $F'_1(x, y)$ and $I(x, y)$ are combined in the second stage to obtain $F'_2(x, y)$. Averaging is the fusion rule employed in each stage and the average DWT coefficients are taken at corresponding sub-bands.

Mathematically, we can model a single-stage DWT fusion using (10).

$$[cA_k, cH_k, cV_k, cD_k]^i = DWT\{I'_{v_k}(z^i), \psi(x, y)\} \quad (10)$$

where $I'_{v_{k=1,2}}$ is an RGB image of the input mask M_k; z^i, for $i \in \{R, G, B\}$, represents a colour channel; $\psi(x, y)$ is a 2-D wavelet; cA_k is the approximated feature matrix; and cH_k, cV_k, and cD_k, are the detail matrices in the horizontal, vertical, and diagonal directions, respectively.

From (10), the average feature $\bar{X} = \frac{\sum X}{N}$ for each input-channel pair, I'_{v_1} and I'_{v_2}, is computed as follows:

$$\begin{aligned} cA^i &= \bar{X}(cA_1, cA_2)^i; \\ cH^i &= \bar{X}(cH_1, cH_2)^i; \\ cV^i &= \bar{X}(cV_1, cV_2)^i; \\ cD^i &= \bar{X}(cD_1, cD_2)^i; \end{aligned} \quad (11)$$

Letting $\bar{X}^i = [cA, cH, cV, cD]^i$ represent the mean feature vector, we reconstruct the fused image by computing the inverse DWT, as given in (12).

$$\Upsilon^i = IDWT\{\bar{X}^i, \psi(x, y)\} \quad (12)$$

where $\psi(x, y)$ is the 2-D wavelet employed in (17) and Υ^i is a greyscale image. Coupling the RGB channels $(\Upsilon^R, \Upsilon^G, \Upsilon^B)$, yield the final fused image $\Upsilon(x, y)$.

E. DWT-F Optimization

The computational complexity of the DWT fusion can be improved programmatically by adopting a vectorized approach in computing the mean feature vector $\bar{X}^i$. Rather than using a nested *for loop*, we perform matrix operations on each input-channel pair, as shown in (13)-(16). This reduced the total number of multiplications and additions required for computation.

$$cA^i = (cA_1 + cA_2)^i/2 \quad (13)$$
$$cH^i = (cH_1 + cH_2)^i/2 \quad (14)$$
$$cV^i = (cV_1 + cV_2)^i/2 \quad (15)$$
$$cD^i = (cD_1 + cD_2)^i/2 \quad (16)$$

F. Unsharp Masking

The output image $\Upsilon(x, y)$ is often blurry as a result of the DWT fusion. To address this, we employed the classical unsharp masking algorithm introduced in section 2.4. We let η be a sharpening factor that determines the degree of sharpness in $\Upsilon(x, y)$ and obtained the final enhanced image using (17).

$$\Upsilon'(x, y) = USM\{\Upsilon(x, y), \eta\} \quad (17)$$

IV. EXPERIMENTAL RESULTS AND ANALYSIS

We conducted various experiments to assess the performance of our proposed method using standard low-light images from the Night-time Photo Enhancement (NPE) dataset [23]. The NPE dataset consists of 74 low-quality photos captured in different low-light settings. We utilized three metrics, Peak-Signal-to-Noise Ratio (PSNR), Structural Similarity Index (SSIM) [24], and Natural Image Quality Evaluator (NIQE) [24], to objectively evaluate our results. The PSNR measures the noise level in an image by comparing it to its original representation, while SSIM computes the structural similarity between the original and enhanced images. The NIQE metric estimates naturalness quality by analysing statistical properties observed in natural images. A lower NIQE score indicates better image quality, while higher PSNR or SSIM scores represent better image quality [24][25].

Computer simulations were performed in MATLAB R2018a on a PC with 32GB RAM and a 2.60GHz Intel Core i7 processor. In all simulations, we used the Target histograms given in Fig. 3 and set the parameters η and $\psi(x, y)$ to 0.5 and $'sym5'$, respectively, to ensure consistency.

A. Brightness Thresholding and α-clipping

The threshold T in the Adaptive Brightness Control procedure plays a crucial role in computing α. In this section, we investigated various techniques to obtain a desirable value of T. First, we explored popular thresholding methods such as the methods proposed by Otsu [26] and Trongtirakul [4]. These methods are widely used for image segmentation, but they proved inadequate for addressing the specific problem of brightness compensation, as they extend to a broader range of grey levels beyond the highlight region of the histogram. Therefore, we performed a simple procedure to obtain a suitable threshold.

We considered the intensity level of each pixel to be between 0% (dark) and 100% (highly radiant) and set the initial threshold T_{init} to 76%, a minimum point of perceived brightness, which is located within the histogram highlight region. Next, we enhance the image using our proposed method and evaluated the results using the PSNR, SSIM, and NIQE metrics. We then vary the threshold value up to 100%, with a step size of 3, and repeated the enhancement procedure for each value. It is important to note that the grey value of T is dependent on the bit-depth (n) of the input and can be computed by multiplying the maximum grey level $L = 2^n$ in the image by the desired threshold T_{des}, as given in (18).

$$T = floor[(L)(T_{des}/100)] \quad (18)$$

Fig. 5 compares the performance of various threshold values on a sample low-light image. In Fig. 5, colour distortion and loss of details can be seen for values of $T < 88\%$. Furthermore, under-exposure tends to persist in the
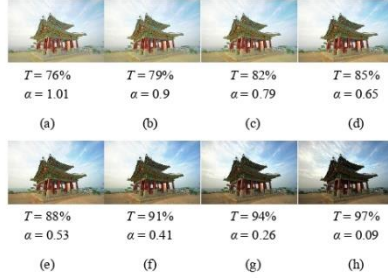
$T = 76\%$	$T = 79\%$	$T = 82\%$	$T = 85\%$
$\alpha = 1.01$	$\alpha = 0.9$	$\alpha = 0.79$	$\alpha = 0.65$
(a)	(b)	(c)	(d)
$T = 88\%$	$T = 91\%$	$T = 94\%$	$T = 97\%$
$\alpha = 0.53$	$\alpha = 0.41$	$\alpha = 0.26$	$\alpha = 0.09$
(e)	(f)	(g)	(h)

Fig. 5. *Performance of the proposed method at different values of T*

foreground of the enhanced image for values beyond 94%, as seen in Fig. 5(h).

The outcomes of the PSNR, SSIM, and NIQE assessments of Fig. 5 are provided in Table I. Table I shows that increasing the value of T from 76% to 98% improved the PSNR from 15dB to 25dB, which also led to a gradual increase in the SSIM index from 0.69 to 0.9. Significant changes, however, were not observed in the NIQE assessment as the threshold varied. This could imply that the NIQE metric is not as sensitive to changes in the Adaptive Brightness Control procedure as the PSNR and SSIM.

Given the results in Table I, we observed that a high brightness compensation, which is associated with a lower value of T, can result in an increased amount of noise in the enhanced image, affecting the structural similarity between the input and enhanced image. Therefore, to obtain the optimal brightness compensation threshold, we compared the outcomes of T and α. We found that values of $\alpha (< 0.5)$ yield better PSNR and SSIM quality, with less artefact generation as seen in Fig. 5. On the other hand, values of $T > 94\%$ do not improve the image perceptual quality, leaving parts of the image under-exposed. Based on these findings, we desired T at 94% brightness and applied a ceiling for α, denoted $\alpha_{LIM} = 0.23$.

TABLE I. PERFORMANCE EVALUATION FOR VARIOUS THRESHOLDS

T	α	PSNR (dB)	SSIM	NIQE
76%	1.01	12.1	0.69	2.29
82%	0.79	13.0	0.70	2.00
88%	0.53	15.6	0.75	2.02
94%	0.26	21.7	0.85	2.15
98%	0.09	25.0	0.90	2.22

B. Evaluation of Night-time Photo Enhancement Dataset

In this section, we evaluated and compared the performance of the proposed method against existing image enhancement methods such as Histogram Equalization [3], Retinex [7], and Low-light Image Enhancement via Illumination Map Estimation (LIME) [8]. Our simulations were based on the NPE dataset. Due to space limitations, only selected results are presented here for analysis. Interested

readers can obtain the full data at https://github.com/shaffakjr/low-light-enhancement.

Fig. 6 shows the result of the various method on selected images from the NPE dataset. In each column, the topmost image is the original low-light image, followed by the enhanced results from Histogram Equalization, Retinex, and LIME. The outcomes from our proposed method are displayed at the bottom. Visually, our proposed technique presents several advantages over the existing methods. Our method performs superior to Histogram Equalization and Retinex in persevering the original hues of the low-light image, as demonstrated in Fig. 6(b) to 6(e), and 6(h). Furthermore, our approach outperforms LIME for images degraded by haze, such as Fig. 6(b). In some instances, LIME tend to over-enhance details and saturate colours. This is evident in the results of Fig. 6(d) and 6(h).

The proposed technique, however, has some limitations. For example, in Figs. 6(a) and 6(g), our technique yields slightly darker images. Also, in some cases, our method does not remove image noise as effectively as LIME. This can be observed in the results of Fig. 6(g). Another limitation is the occurrence of highlight and shadow clipping. They often lead to overexposed or underexposed regions with no discernible information. When shadows or highlights in the source image are clipped, the effects seen in Fig. 6(f) tend to occur.

In Table II, the average PSNR, SSIM, and NIQE scores for various techniques on the NPE dataset are compared. According to the results in Table II, our method achieved the second-best quality in the NIQE metric but outperform existing methods in terms of the average PSNR and SSIM indices. This implies that our method can produce enhanced images with higher structural similarity and less noise compared to other methods.

TABLE II. AVERAGE IQA SCORES FOR VARIOUS METHOD ON NPE

Method	PSNR (dB)	SSIM	NIQE
HE [3]	13.6	0.57	3.37
Retinex [7]	10.6	0.52	3.65
LIME [8]	16.7	0.65	3.73
Proposed Method	19.9	0.74	3.55

V. CONCLUSION

In this paper, we have proposed a novel technique for low-light image enhancement using histogram matching and image fusion. Experimental results on the NPE dataset demonstrate the superiority of our method over existing techniques in improving perceptual quality while preserving image details and colours. The results also prove the effectiveness of our method in producing images with high PSNR quality.

Future work will focus on developing a mathematical model to generate optimal target histograms and a denoising algorithm for noise reduction in extremely low-light situations.

REFERENCES

[1] S. Nadimi and B. Bhanu, "Physical models for moving shadow and object detection in video," IEEE Trans. Pattern Anal. Mach. Intell., vol. 26, no. 8, pp. 1079–1087, Aug. 2004.
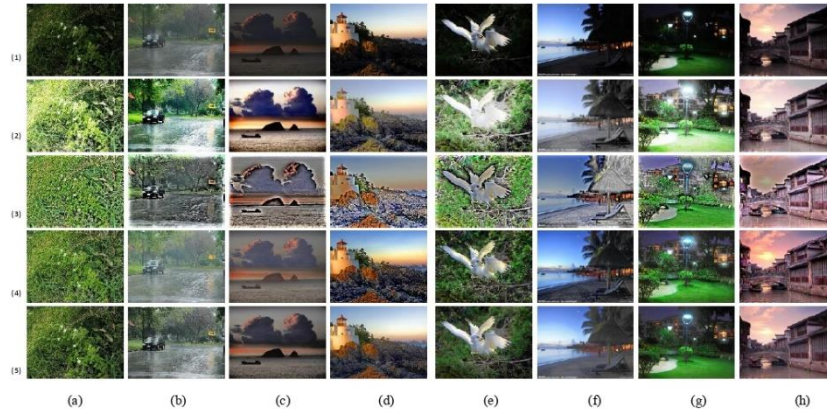
Fig. 6. *Enhanced Results by Various Methods on Selected low-light images (a) Bush (b) Hazy Day (c) Ocean Ride (d) House on Hill (e) Bird (f) Shore (g) Night (h) Dusk: (1) Original Image; (2) Histogram Equalization [3]; (3) Retinex [7]; (4) Low-light Image Enhancement via Illumination Map Estimation [8]; (5) Proposed Method*

[2] W. Kim, S. Suh, W. Hwang, and J.-J. Han, "SVD Face: Illumination invariant face representation," IEEE Signal Process. Lett., vol. 21, no. 11, pp. 1336–1340, Nov. 2014.

[3] S. M. Pizer, E. P. Amburn, J. D. Austin, "Adaptive histogram equalization and its variations," Computer vision, graphics, and image processing, vol. 39, no. 3, pp. 355–368, 1987

[4] T. Trongtirakul, W. Chiracharit and S. S. Agaian, "Single Backlit Image Enhancement," in IEEE Access, vol. 8, pp. 71940-71950, 2020, doi: 10.1109/ACCESS.2020.2987256.

[5] Y. Zeng, Q. Zhao, and J. Chen, "Low-light image enhancement based on adaptive contrast stretching and multi-scale fusion," Signal Processing: Image Communication, vol. 85, p. 115894, 2020. doi: 10.1016/j.image.2020.115894.

[6] D. J. Jobson, Z. U. Rahman and G. A. Woodell, "A multiscale retinex for bridging the gap between color images and the human observation of scenes," IEEE Transactions on Image Processing, vol. 6, no. 7, pp. 965–976, 1997.

[7] A. B. Petro, C. Sbert, and J.-M. Morel, "Multiscale Retinex," Image Processing On Line, vol. 4, pp. 71–88, April 2014, doi: 10.5201/ipol.2014.107.

[8] X. Guo, Y. Li, and H. Ling, "LIME: Low-light image enhancement via illumination map estimation," IEEE Trans. Image Process., vol. 26, no. 2, pp. 982–993, Feb. 2017

[9] Y. Gao, C. Su and Z. Xu, "Color image enhancement algorithm based on improved Retinex algorithm," 2022 Asia Conference on Algorithms, Computing and Machine Learning (CACML), Hangzhou, China, 2022, pp. 234-238, doi: 10.1109/CACML55074.2022.00046.

[10] M. Wang, J. Li, and C. Zhang, "Low-light image enhancement by deep learning network for improved illumination map," Computer Vision and Image Understanding, vol. 232, p. 103681, 2023, doi: https://doi.org/10.1016/j.cviu.2023.103681.

[11] C. Li, J. Guo, Z. Li, Y. Hou, W. Hu, and M. Cheng, "Lighting the Darkness in the Deep Learning Era," CoRR, vol. abs/2104.10729, 2021, [Online]. Available: https://arxiv.org/abs/2104.10729

[12] J. Deng, W. Dong, R. Socher, L.-J. Li, K. Li, and L. Fei-Fei, "ImageNet: A large-scale hierarchical image database," in Proceedings of the IEEE Conference on computer vision and pattern recognition, 2009, pp. 248-255.

[13] C. Zhang, W. Liu, and W. Xing, "Color image enhancement based on local spatial homomorphic filtering and gradient domain variance guided image filtering," Journal of Electronic Imaging, vol. 27, no. 6, p. 063026, 2018, doi: 10.1117/1.JEI.27.6.063026.

[14] Q. Mu, X. Wang, Y. Wei, and Z. Li, "Low and non-uniform illumination color image enhancement using weighted guided image filtering," Computational Visual Media, vol. 7, no. 4, pp. 529–546, Dec. 2021, doi: 10.1007/s41095-021-0232-x.

[15] Z. Shi, M. mei Zhu, B. Guo, M. Zhao, and C. Zhang, "Night-time low illumination image enhancement with single image using bright/dark channel prior," EURASIP Journal on Image and Video Processing, vol. 2018, no. 1, p. 13, Feb. 2018, doi: 10.1186/s13640-018-0251-4.

[16] K. Kim, S.-H. Kim, and K.-S. Kim, "Effective Image Enhancement Techniques for Fog-Affected Indoor and Outdoor Images," IET Image Processing, vol. 12, Nov. 2017, doi: 10.1049/iet-ipr.2016.0819.

[17] R. C. Gonzales and R. E. Woods, Digital Image Processing (4th Ed., Global Ed.). Pearson Publishing Co., Inc. New Jersey, USA, 2018.

[18] Y. Ueda, D. Moriyama, T. Koga and N. Suetake, "Histogram Specification-Based Image Enhancement for Backlit Image," 2020 IEEE International Conference on Image Processing (ICIP), United Arab Emirates, 2020, pp. 958-962, doi: 10.1109/ICIP40778.2020.9190929.

[19] C. Chui, An Introduction to Wavelets. Academic Press, New York, USA, 1992

[20] H. Kaur, D. Koundal, and V. Kadyan, "Image Fusion Techniques: A Survey," Archives of Computational Methods in Engineering, vol. 28, no. 7, pp. 4425–4447, Dec. 2021, doi: 10.1007/s11831-021-09540-7.

[21] A. R. Smith, "Color Gamut Transform Pairs". SIGGRAPH 78 Conference Proceedings. 1978, pp. 12–19.

[22] D. Coltuc, P. Bolon, and J.-M. Chassery, "Exact histogram specification," IEEE Transactions on Image Processing, vol. 15, no. 5, pp. 1143–1152, 2006, doi: 10.1109/TIP.2005.864170.

[23] M. Gharbi, J. Chen, J. Barron, S. W. Hasinoff, and F. Durand, "Deep bilateral learning for real-time image enhancement," ACM Transactions on Graphics, vol. 36, no. 4, pp. 118:1-118:12, 2017. DOI: 10.1145/3072959.3073617.

[24] Z. Wang, A. C. Bovik, H. R. Sheikh, and E. P. Simoncelli, "Image Quality Assessment: From Error Visibility to Structural Similarity," IEEE Transactions on Image Processing, vol. 13, no. 4, pp. 600-612, April 2004.

[25] M. N. Saad, A. C. Bovik, and C. Charrier, "Blind Image Quality Assessment: A Natural Scene Statistics Approach in the DCT Domain," IEEE Transactions on Image Processing, vol. 21, no. 8, pp. 3339-3352, August 2012.

[26] N. Otsu, "A threshold selection method from gray-level histograms," IEEE Transactions on Systems, Man, and Cybernetics, vol. 9, no. 1, pp. 62-66, Jan. 1979. doi: 10.1109/TSMC.1979.4310076

A4. Patent Application

Disclosure Submission

Date: November 11, 2022

Form F.2

UNIVERSITY OF NAIROBI
INTELLECTUAL PROPERTY MANAGEMENT OFFICE

INVENTION/INNOVATION DISCLOSURE FORM: Article: 14

1. **NOTES**

Explain your invention/innovation in such a way as to be clear to one who is not familiar with it. Be careful to describe what, specifically, makes your invention *different from what has gone before?* Why is it better, or what makes it better? If you use any unusual terms, or ordinary terms in an unusual way, explain them. In addition to describing all the parts, describe *how the parts work together*. Has the design, or part of the design, been used before, even if for a different purpose? How else have people accomplished the same function as your invention in the past? What are the possible problems? *Drawings are always helpful,*

2. **INVENTION DISCLOSURE FORM**

Name of Inventor(s):

Shaffa Korvawu Kokro Jr.
Department of Electrical and Information Engineering
University of Nairobi, Kenya
Cell: +254758955207 / +231776477527
E-mail: shaffakokro@gmail.com

Professor Elijah Mwangi
Department of Electrical and Information Engineering
University of Nairobi, Kenya
Cell: +254725949898
E-mail: elijah.mwangi@uonbi.ac.ke

Dr. George Kamucha
Department of Electrical and Information Engineering
University of Nairobi, Kenya
Cell: +254720729161
E-mail: gkamucha@uonbi.ac.ke

Name of invention:

Region-based Histogram and Fusion Technique for Enhancing Backlit Images for Cell phone Applications

1

Describe the invention in general terms: What does it do? How does it do it?

Backlit images are low-quality digital pictures generated due to backlighting, a poor illumination setting that occurs when an excessive reflection of light is incident to an image capturing device or when the dominant light source in a picture scene radiates behind the main objects. The region-based histogram and fusion (RBHF) algorithm improve the perceptual quality of a single backlit image captured on a cell phone using a region-based histogram specification scheme with the discrete wavelet transform (DWT) image fusion. The region-based histogram specification scheme employs two unique target histograms, denoted Target 1 and Target 2, to correct exposure disparities between the foreground and background picture scenes. Following this process, the DWT fusion combines salient features of the histogram-specified images with the original input to produce the final enhanced image.

Details of the invention/Innovation:

What parts (steps, if a process) make up the invention, in its best (preferred) form? What does each contribute to the invention?

Displayed in Figure 1 is the system architecture for the novel region-based histogram and fusion (RBHF) algorithm. The procedure begins with an RGB to HSV transformation of the input image. Such colour space conversion is done to separate the input's luminance component (V) from the Hue (H) and Saturation (S) channels. Next, two input masks, M1 and M2, are created with identical copies of the luminance component. The input masks M1 and M2 are the foreground (F) and background (B) masks, respectively. i.e., M1 contains the backlit foreground information to be processed, whereas M2, the well-lit and/or over-exposed background details. Histogram specification is performed discriminately on each input mask using the target histograms Target 1 and Target 2. This scheme is referred to as region-based histogram specification. A centric part of the region-based histogram specification process is the selection method for the target histograms.
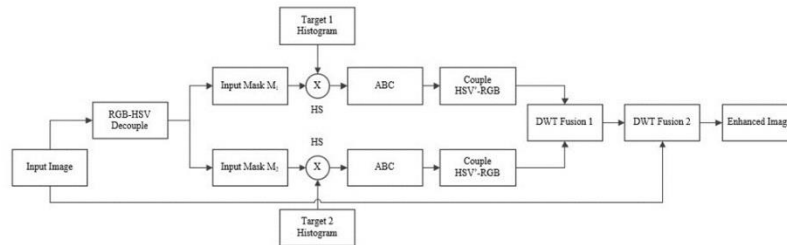

Figure 1. System architecture of the RBHF algorithm

Following the region-based histogram specification scheme, an adaptive brightness control (ABC) procedure is applied to the histogram-specified images of M1 and M2. The ABC procedure ensures a desired brightness level in the final output image. The enhanced luminance components (V') from the two ABC processes are coupled with the input's original hue and saturation channels. An HSV' to RGB transformation is performed to generate the new colour images. Next, a two-stage DWT image fusion is employed to combine the best features of the input masks with the original backlit image to yield the final enhanced image. Figure 2 displays the results of the RBHF algorithm on some selected images from Li (2021) database and the Exclusively dark dataset.
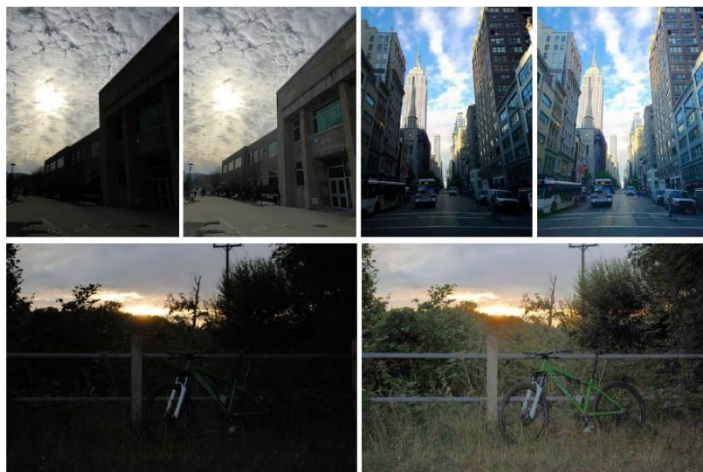
2

Figure 2. Enhancement results for some selected backlit images

The details of some major processes and their configurations are provided below:

1. Generation of target histograms

The selection of Targets 1 and 2 play an important role in the RBHF algorithm. Target 1 is used to improve details in the under-exposed foreground of the backlit image while Target 2 suppress high radiance in the over-exposed background sectors. Therefore, Target 1 must represent a well-lit, high-contrast image with no peaks in the dark and light tones of the histogram, whereas Target 2 be a relatively low-light and high-contrast image with peaks in the dark tones but none in the lightest tones, i.e., grey levels beyond 240 for 8-bit images. Examples of such target histograms are provided in Figure 3.
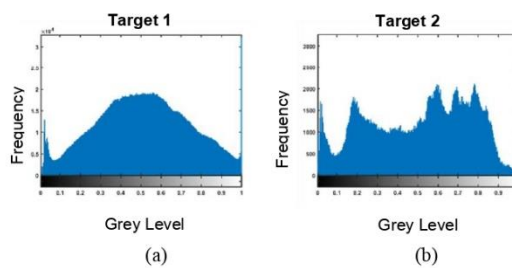

Figure 3. Sample Target histograms (a) Target 1 (b) Target 2

3

155

2. Region-based Histogram Specification

Given the selection of target histograms, the enhancement of each input mask is performed as illustrated in Figure 4.
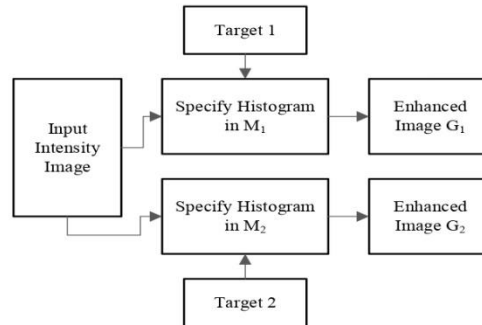

Figure 4. Region-based histogram specification (RBHS)

3. Adaptive brightness control

The term "adaptive brightness control" or "automatic brightness control" is often associated with the automatic adjustment of a display panel's brightness level based on the ambient light environment. This method is used mostly as an energy-saving feature in smartphones, tablets, and digital television systems. On the contrary, adaptive brightness control (ABC) is defined in this work as a method of automatically compensating for low brightness in the input masks after RBHS is performed. Though the nomenclatures are the same, the differences rest within the methods and applications. Figure 5 describes the ABC procedure.

Step (i):   Given an input intensity image, compute the histogram properties.
Step (ii):   Get (N), the total number of pixels in the image.
Step (iii):   Get (n), the total number of pixels greater than the threshold T=240, for 8-bit images.
Step (iv):   Calculate the coefficient α = [N / (N − n)] − 1, referred to as the adaptation factor.
Step (v):   For α > 0.23, set α to 0.23.
Step (vi):   Compensate brightness in the input by increasing each pixel value by α.

4. Discrete wavelet transform Fusion

Each DWT fusion stage uses a 2-D wavelet function for decomposing the input image and reconstructing the final fused image. The choice of wavelet function has limited impact on the enhancement quality of the algorithm. However, wavelets from the Symlets family, precisely 'sym5', are recommended as they tend to produce desired outcomes. Furthermore, an averaging method is used to combined salient features at each stage.

Which parts <u>are new</u> to this invention (in form or usage), which are old (conventional, used in the expected way)?

New to this invention / innovation:

1. The framework for generating optimal target histograms for backlit image enhancements.

4

2. An adaptive brightness control mechanism to handle the low-brightness problems caused by histogram specification.
3. The combination of a region-based histogram specification scheme and the discrete wavelet transforms image fusion for digital image enhancement.

Conventional and used in the expected way:

1. The two histogram specification processes used by the RBHF algorithm to match the input histogram with the target histograms are conventional and are based on generalization.
2. The discrete wavelet transforms used in the DWT-Fusion for decomposing the input image and reconstructing the final fused image are conventional.

In order to be patentable, an invention must be <u>NEW</u>, <u>HAVE AN INVENTIVE STEP</u> (NOT OBVIOUS to one skilled in the art, based upon everything that was available at the time of the invention), <u>USEFUL</u> OR IS A <u>NEW USE</u>.

<u>Alternatives:</u>
You have described the best way to build (perform) your invention. Now consider the alternatives under.
- **Structural Alternatives:**

1. **Multiple RBHF process**

Multiple iterations of the RBHF algorithm can be performed on a single backlit image to improve the enhancement quality. This entails establishing the RBHF procedure as an iterative process described in Figure 5. The value of *Iter* determines the number of iterations. An *Iter* of 1 will yield the outcomes of a single RBHF process. Note that for *Iter* > 1, the value of *n* decreases after each iteration.
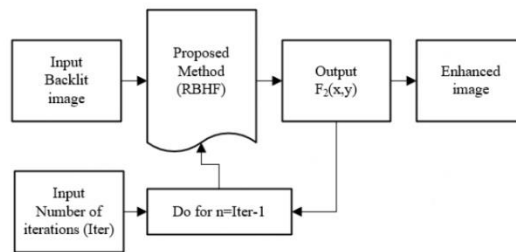

Figure 5. Multiple RBHF process to improve enhancement quality

2. **Vectorized computing**

The use of nested for loops in the 'mean' computation of the DWT fusion process significantly increases the algorithm's computation time for high-resolution images. A vectorized computational approach is recommended for averaging salient features in the DWT Fusion stages. This implies that, each corresponding pair of feature-coefficient matrices will be added then divided by 2. This procedure significantly reduces the algorithm's time complexity by 95%, approximately.

5

157

3. Unsharp Masking

The primary objective of the RBHF algorithm is to correct exposure disparities between an under-exposed foreground and a well-lit or over-exposed background. To improve sharpness in the enhanced output images, the classical unsharp masking algorithm can be applied to the output stage of the RBHF process, as shown in Figure 6. Note that for *Iter* > 1, the value of *n* decreases after each iteration.
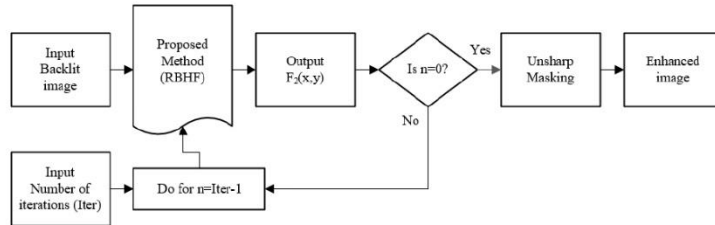

Figure 6. RBHF algorithm with unsharp masking

Figure 7 shows some selected results of the RBHF algorithm with the classical unsharp masking.
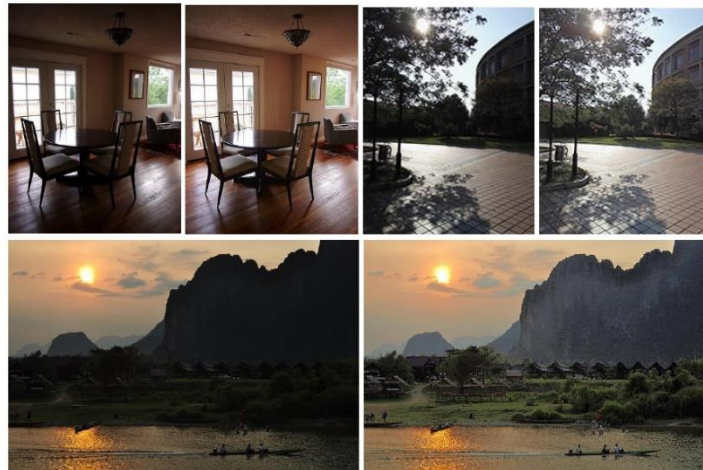

Figure 7. Enhancement results using unsharp masking

6

- **Alternate Use:** Can your invention be used for anything other than its preferred use?

The RBHF algorithm can be used to enhance images degraded by low lighting conditions. These images are generally referred to as low-light images. Figure 8 shows the performance of the algorithm on some selected low-light images.
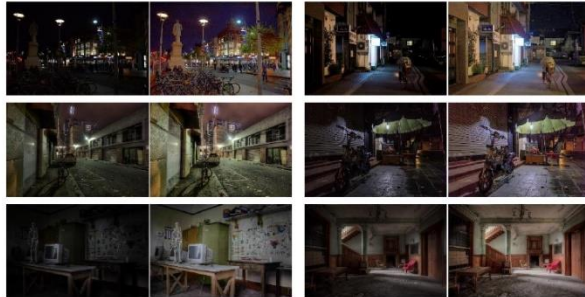

Figure 8. Enhancement results for some selected low-light images

<u>**Limitations:**</u>   When will the invention *not* work?

The RBHF algorithm performs poorly on images affected by shadow clipping or highlight clipping. Shadow and highlight clippings occur in an image when the information being recorded exceeds the dynamic range of the image capturing device. They frequently result in a loss of detail in the captured image. The RBHF algorithm cannot recover lost information. Figure 9 shows some examples of this phenomena.
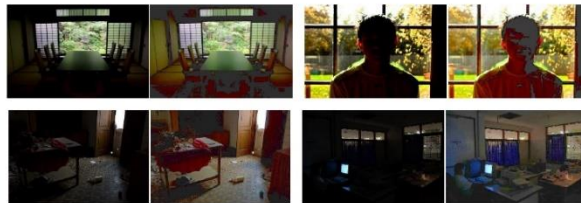

Figure 9. Performance of the algorithm on shadow-clipped images

State of the Art:

- What was already in existence (whether patented or not) before the invention? How is the function of the invention being done today?

7

159

Histogram equalization and Retinex-based algorithms are conventional image enhancement methods. They however perform poorly on backlit images. Over-saturation or a loss of contrast are typical outcomes when these methods are applied. Various techniques have been proposed in recent years. They include:

(i) Single backlit image enhancement proposed by T. Trongtirakul, W. Chiracharit and S. Agaian (2020)
(ii) A fusion-based method for single backlit image enhancement by Q. Wang, X. Fu, X.-P. Zhang, and X. Ding (2016)
(iii) Learning-based restoration of backlit images by Z. Li and X. Wu (2018)
(iv) Histogram specification-based image enhancement for backlit image Y. Ueda, D. Moriyama, T. Koga and N. Suetake (2020)
(v) Low-light image enhancement via illumination map estimation X. Guo, Y. Li, and H. Ling (2017)
(vi) Backlit images enhancement using global tone mappings and image fusion A. Buades, J.-L. Lisani, A. B. Petro, and C. Sbert (2020)
(vii) Low-light image enhancement via pair of complementary gamma functions by fusion C. Li, S. Tang, J. Yan and T. Zhou (2020)
(viii) Adaptively partitioned block-based contrast enhancement and its application to low light-level video surveillance by S. Lee, N. Kim, and J. Paik (2015)

Due to enhancement flaws and expensive computation, many of these methods cannot be applied directly in cell phone applications. As a result, there is no conventional method for enhancing backlit images on cell phones. Alternative methods have been adopted by smartphone manufacturers. They include Auto-exposure (AE) and High Dynamic Range (HDR) imaging. These methods are being used by smartphone manufacturers such as Apple, Samsung, and Google to handle backlighting and other types of poor illumination situations. However, these methods have significant drawbacks that outweigh their benefits in poor lighting situations. For instance, under backlighting, AE cannot reveal items in the foreground while simultaneously exposing details in the background. As a result, a well-exposed foreground will cause a loss of information in the background scene and vice-versa. Likewise, HDR, developed primarily to handle low-light situations, is susceptible to motion blur since it relies on fusing two or more sequential images with varying exposures. Furthermore, it cannot enhance low-quality photographs after they have been acquired.

- What is the closest device (or process or use) you are aware of to your invention?

Y. Ueda, D. Moriyama, T. Koga and N. Suetake (2020) proposed a "straightforward" histogram specification-based technique to enhance backlit images [9]. In this approach, foreground-background segmentation is first performed using a linear discriminant analysis (LDA) threshold, which is then used to obtain the triangular target histogram. The goal was to convert the intensity of the backlit image via histogram specification. However, the conversion between the foreground and background scenes was observed to be unbalanced. Therefore, they employed two modified target histograms, Target 1 and Target 2. Target 1 was obtained by equalizing the ratio of background and foreground regions with the area ratio of the input image, while Target 2 was obtained by making the foreground region the same shape as the input image histogram. To produce an enhanced backlit image with hue and saturation preserved, the algorithm looks for a point on a constant-hue plane in an RGB colour space.

The method proposed by Ueda et al. (2020) has several limitations. The use of thresholding for segmentation is one of the drawbacks. Thresholding techniques have proven effective in a variety of applications, but they do not account for spatial interactions between pixels and are vulnerable to unintended and uncontrolled changes in the light field in general. Furthermore, the target histograms used produce washed-out and unnatural hues. To minimize noise and prevent colour artefacts in the enhanced image, more processing is required. Lastly, the method increases details in both the foreground and the background without distinction. As a result, the well-exposed regions of the image are further exaggerated.

- Is there something that performs the same function in a different way?
- Is there any combination of existing devices (or processes) which would be similar to your invention?

8

160

The combination of histogram processing and image fusion would be similar to the RBHF procedure.

- How does your invention perform its function different from, or better than, these prior devices (or processes)? How are they similar?

The RBHF technique combined a global contrast stretching scheme with the DWT image fusion to improve the visual perception of a single backlit image. The algorithm results in no colour distortion or artefacts as seen in prior devices. Multiple iterations of the RBHF algorithm can be employed to further improve the enhancement quality of the backlit inputs. This is not common with prior methods. In most situations, two to three iterations are sufficient to produce a significantly higher image quality. The mapping functions for foreground and background contrast enhancement automatically adapt to changes in the luminance profile of the backlit input. The mappings are based on generalization. This flexibility permits the proposed method to be employed in other types of poor illumination situations, such as low lighting.

Date of invention:

"Invention" means a combination of conception (coming up with the idea of the invention) and reduction it to practice (building it, or applying for a patent).

- When did you first begin to work on the invention?

February 2021: Research proposal for the degree of Master of Science in Electrical and Electronic Engineering in the department of Electrical and Information Engineering in the University of Nairobi.

August 2021: Final Research proposal for the degree of Master of Science in Electrical and Electronic Engineering in the department of Electrical and Information Engineering in the University of Nairobi.

- Reduction to Practice: Has the invention been built? If so, when?

Yes. The invention has been built.

Software prototype version 1 completed on August 23, 2022. Figure 10 shows a screenshot of the GUI.

Software prototype version 2 (final) completed on September 10, 2022. Figure 11 shows a screenshot of the GUI.
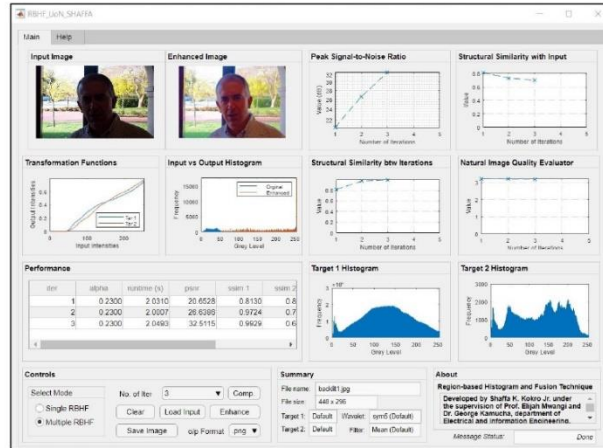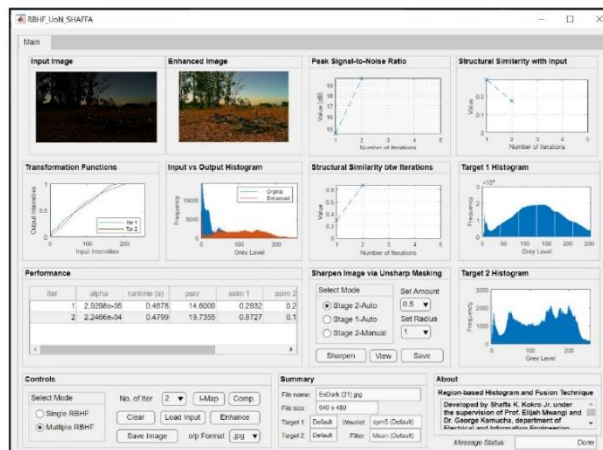
9

Figure 10. GUI of the RBHF prototype version 1

Figure 11. GUI of the RBHF prototype version 2 (*FINAL)

10

162

Prior Filings: Have you filed a Disclosure Document or Provisional Patent Application on this invention, or has there been an application for patent in the Kenya or elsewhere? No.

    Type of Filing: N/A
    Date of Filing: N/A
    Serial Number: N/A
    Where filed: N/A

Third Party Rights

- **Other Inventors:** Is there anyone else who contributed to the conception or reduction to practice of the invention, in more than a **purely mechanical** way? No
- **Rights in Others:** Are you under any obligation to **assign** any rights in the invention to others? No
  Was the invention developed in the course of your study or employment, or using any facilities belonging to the **University of Nairobi?** Yes

Any additional notes or comments?

*Be sure to sign and date the form, and have it witnessed by someone who is **not an inventor**.*

Signed: _____

Dated: 09/23/2022

Read, witnessed and understood: _____

Date: 09/23/2022

11

163

A5. Patent Publication

Journal Name: Kenya Industrial Property Institute, Journal of Patents,
Industrial Designs, Utility Models and Trademarks
Date Published: May 31, 2023

KENYA INDUSTRIAL PROPERTY INSTITUTE

INDUSTRIAL PROPERTY JOURNAL
(Journal of Patents, Industrial Designs, Utility Models and Trade marks)

No. 2023/05

31st May, 2023

Published Monthly

4.0 Utility Model Applications Published under Section 42 and Regulation 35

4.1 National Application

(21) Application no.: KE/U/2022/1975 (22) Filing Date: 11/11/2022

(30) Priority:

(51) Int.Cl.

(54) Title: REGION BASED HISTOGRAM AND FUSION TECHNIQUE FOR ENHANCING BACKLIT IMAGES FOR CELL PHONE APPLICATIONS

(72) Inventors: SHAFFA KORVAWU

(73) Applicant(s): UNIVERSITY OF NAIROBI, Kenya, c/o INTELLECTUAL PROPERTY MANAGEMENT OFFICE, P. O. BOX 30197-00100, NAIROBI, Kenya

(74) Agent:

(57) The invention discloses a region-based histogram and fusion algorithm which improves the perceptual

quality of a backlit image captured on a cell phone using a region-based histogram specification scheme with the discrete wavelet transform image fusion. The region- based histogram specification scheme employs two unique target histograms to correct exposure disparities between the foreground and background picture scenes. The discrete wavelet transform fusion combines salient features of the histogram-specified images with the original input to produce the final enhanced image.

14

A6. Patent Certificate

KIPI
Kenya Industrial Property Institute.

The Industrial Property Act, 2001

CERTIFICATE

OF REGISTRATION OF UTILITY MODEL

It is hereby certified that a utility model with utility model number **436** has been registered in the name **UNIVERSITY OF NAIROBI of** c/o **INTELLECTUAL PROPERTY MANAGEMENT OFFICE, P. O. BOX 30197-00100, NAIROBI, Kenya in** respect of an invention disclosed in an application number **KE/U/2022/1975** having a date of filing of **11/11/2022** and priority date of being an invention titled **REGION BASED HISTOGRAM AND FUSION TECHNIQUE FOR ENHANCING BACKLIT IMAGES FOR CELL PHONE APPLICATIONS.**

Dated at **Nairobi** this **13th day of June, 2023.**

John Onyango
Ag. Managing Director

(19)

K I P I
Kenya Industrial Property Institute

(12) UTILITY MODEL

(21)	**Application Number:** 2022/1975	**(73) Owner:** UNIVERSITY OF NAIROBI of c/o INTELLECTUAL PROPERTY MANAGEMENT
(22)	**Filing Date:** 11/11/2022	OFFICE, P. O. BOX 30197-00100, NAIROBI, Kenya

(72) Inventor:
SHAFFA KORVAWU KORKO JR.; ELIJAH
MWANGI and GEORGE KAMUCHA

(74) Agent/address for correspondence:
UNIVERSITY OF NAIROBI, c/o INTELLECTUAL
PROPERTY MANAGEMENT OFFICE, P. O. BOX
30197-00100, NAIROBI, KENYA

(51) Int.Cl.2018.01: G 09G 3/34

(54) Title: REGION BASED HISTOGRAM AND FUSION TECHNIQUE FOR ENHANCING
BACKLIT IMAGES FOR CELL PHONE APPLICATIONS

(57) Abstract: The invention discloses a region-based histogram and fusion
algorithm which improves the perceptual quality of a backlit image captured
on a cell phone using a region-based histogram specification scheme with
the discrete wavelet transform image fusion. The region-based histogram
specification scheme employs two unique
target histograms to correct exposure disparities between the foreground
and background picture scenes. The discrete wavelet transform fusion
combines salient features of the histogram-specified images with the original
input to produce the final enhanced image.

167

A7. Enhancement of low-light images

The proposed algorithm is flexible and robust. It can be used to enhance images affected by low lighting. Figure A.1 depicts the results of one iteration of the proposed method on some selected low-light images from the ExDark dataset [59].
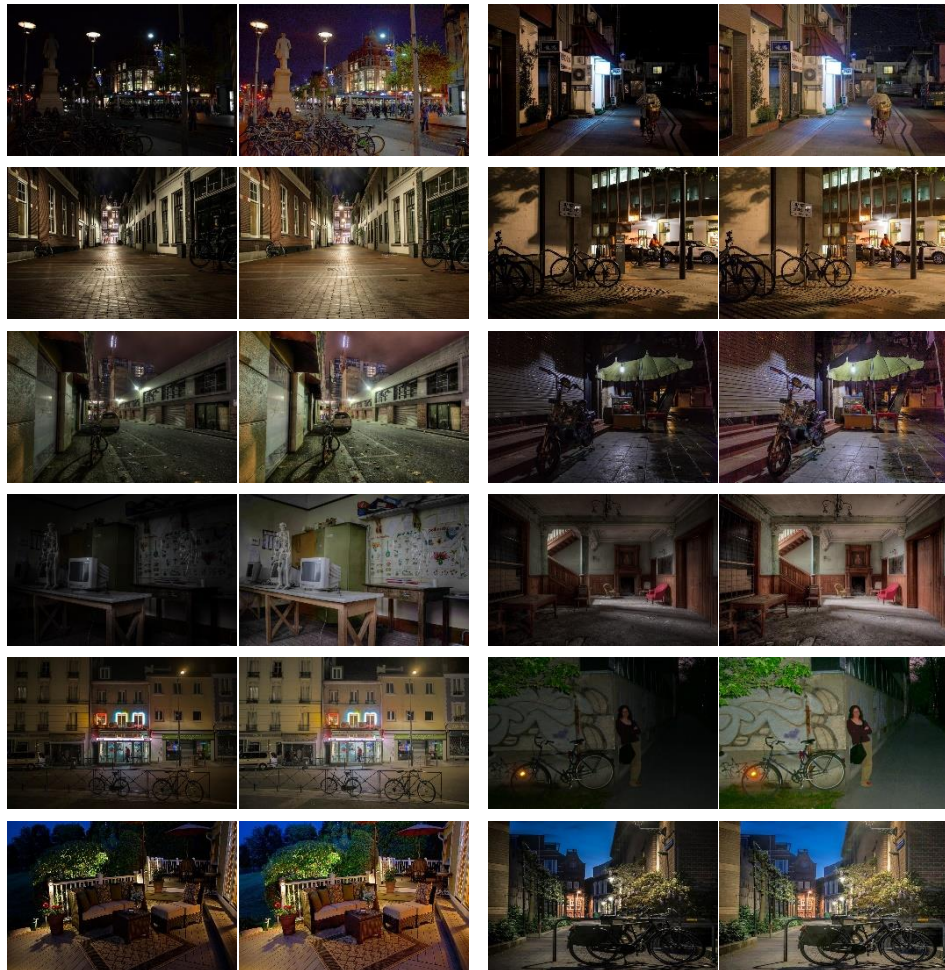

Figure A.1. Enhancement results for some selected low-light images

A8. RBHF with unsharp masking

The classical unsharp masking algorithm can be used to sharpen the enhanced images produced by the proposed technique. Figure A.2 provides the results for some selected backlit images.
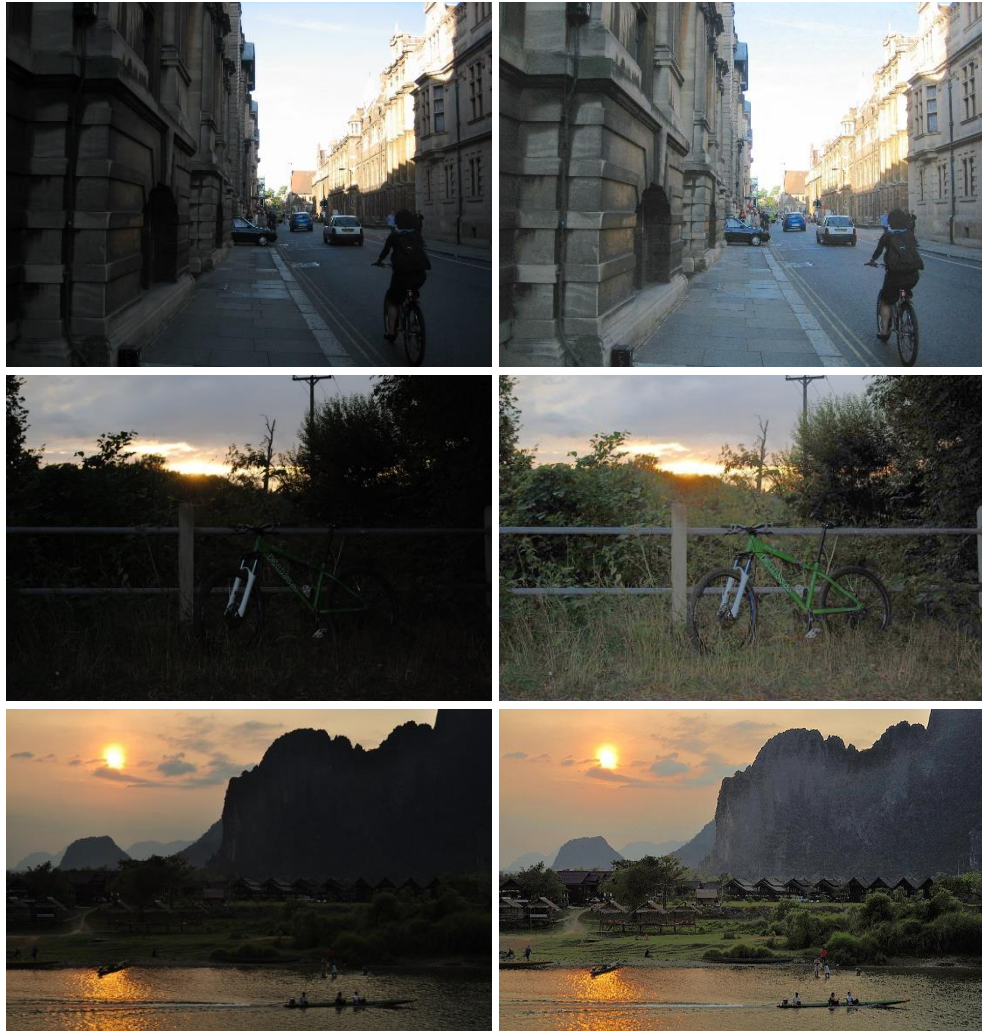

Figure A.2. Result of the proposed method with unsharp masking

A9. MATLAB codes

```matlab
function
% rbhf enhances a single backlit or low-light image
% Using region-based histogram specification & fusion
% Developed By Shaffa K. Kokro Jr., 16th October 2021
% MSc. research supervised by Prof. Elijah Mwangi
% And Dr. George Kamucha
% Department of Electrical & Information Engineering
% University of Nairobi
% RBHF corrects exposure disparities in an input
% Results in no colour distortion or artefacts

[outputImage,alpha_]=rbhf(inputImage,Tar1Hist,...
Tar2Hist,wType)

I=inputImage;
wavelet_type=wType; % data type 'char'
Tar1_v_hist=Tar1Hist; % Target 1 histogram
Tar2_v_hist=Tar2Hist; % Target 2 histogram

%% Pre-processing
I_hsv = rgb2hsv(I); % RGB to HSV conversion
[I_h,I_s,I_v]=decouple_hsv(I_hsv); % Decouple channels
[alpha_,beta_]=adapt_coeff(I_v); % Adaptation factors
% beta_ is for experimental purposes.

%% Enhance Foreground Mask
I_fmask_v = I_v; % Input intensity image
% Match histogram
F_mask_en = histeq(I_fmask_v,Tar1_v_hist);
% Brighten F-mask
bright_F_mask_en=brighten_img(F_mask_en,alpha_);
% New HSV image
new_F_hsv = cat(3,I_h,I_s,bright_F_mask_en);
new_Fmask = im2uint8(hsv2rgb(new_F_hsv)); % HSV to RGB
% Note: I_v can also be passed directly to histeq()
% I_fmask_v is only used for convenience

%% Enhance Background Mask
I_bmask_v = I_v; % Input intensity image
% Match histogram
B_mask_en = histeq(I_bmask_v,Tar2_v_hist);
% Brighten B-mask
bright_B_mask_en=brighten_img(B_mask_en,alpha_);
% New HSV image
new_B_hsv = cat(3,I_h,I_s,bright_B_mask_en);
new_Bmask = im2uint8(hsv2rgb(new_B_hsv)); % HSV to RGB
% Note: I_v can also be passed directly to histeq()
% I_bmask_v is only used for convenience
```

```matlab
%% Fuse Enhanced F & B Masks with input image, RGB
fusedimage1=fusemasks(new_Fmask,new_Bmask,...
wavelet_type); % stage 1
fusedimage2=fusemasks(fusedimage1,I,...
wavelet_type); % stage 2
outputImage=fusedimage2; % Enhanced Image
end

function [a,b]=adapt_coeff(I_v)
% Generate coefficients for ABC
% I_v is an intensity image
% a = alpha; b = beta
% beta is experimental
I_v_hist=imhist(I_v); % Calculate histogram
N=sum(I_v_hist); % Total number of pixels in I_v
n=sum(I_v_hist(240:256)); % sum of bright elements
val=(N/(N-n))-1; % adaptation factor
if val > 0.23
    a=0.23; % alpha clipping
    b=0.23; % beta clipping
else
    a=val; % set alpha value
    b=val; % set beta value
end
end

function out=brighten_img(image,val)
% Apply brightness compensation
% image = input image
% val = adaptation factor
out=image; % output image
[x,y]=size(image); % get input size
for i=1:1:x
    for j=1:1:y
        out(i,j)=image(i,j)+val; % increase brightness
    end
end
end

function fusedimage=fusemasks(Fmask,Bmask,wtype)
% Fuse two inputs given a wavelet function wtype
% Developed with support from Dr. A. K. Verma
% Check if F & B have similar resolution
[row,col]=size(Fmask(:,:,1));
if ~isequal(size(Fmask),size(Bmask))
    Bmask=imresize(Bmask,[row,col]); % resize B
End
```

```matlab
% Decompose RGB channels
% fuse each colour channel pair
fusedR=imgfusion(Fmask(:,:,1),Bmask(:,:,1),wtype);%Red
fusedG=imgfusion(Fmask(:,:,2),Bmask(:,:,2),wtype);%Blue
fusedB=imgfusion(Fmask(:,:,3),Bmask(:,:,3),wtype);%Green

% Couple Fused RGB channels
fusedimage=uint8(cat(3,fusedR,fusedG,fusedB)); %fused
end

function outimage=imgfusion(Im1,Im2,wtype)
% Function compute the 2-D scaling and
% wavelet coefficients
% Im1, Im2, and outimage are greyscale images
[cA1,cH1,cV1,cD1]=dwt2(double(Im1),wtype,'per'); % DWT
[cA2,cH2,cV2,cD2]=dwt2(double(Im2),wtype,'per'); % DWT
% Calculate the mean of each coefficient pairs
% This step uses vectorized computation
cA=(cA1+cA2)./2; % approximation coefficient
cH=(cH1+cH2)./2; % horizontal coefficient
cV=(cV1+cV2)./2; % vertical coefficient
cD=(cD1+cD2)./2; % diagonal coefficient
outimage=idwt2(cA,cH,cV,cD,wtype,'per'); % inverse DWT
end

% Multiple RBHF configuration
% Perform multiple iterations of the RBHF Function
% This improves enhancement quality
% iter defines number of iterations
%% Program Parameters
Tar1 = imread('image_3.jpg'); % Target 1 Image
Tar1_hsv = rgb2hsv(Tar1); % RGB to HSV
[Tar1_h,Tar1_s,Tar1_v]=decouple_hsv(Tar1_hsv);
Tar1_v_hist = imhist(Tar1_v); % Tar 1 histogram
Tar2 = imread('image 3.jpg'); % Target 2 Image
Tar2_hsv = rgb2hsv(Tar2); % RGB to HSV
[Tar2_h,Tar2_s,Tar2_v]=decouple_hsv(Tar2_hsv);
Tar2_v_hist = imhist(Tar2_v); % Tar 2 histogram
wavetype='sym5'; % default wavelet function
images=cell(1,1); % output container
v=1; % counter

%% Read input
I_original = imread('filename.jpg'); % Input
I= I_original; % value in I is dynamic
iter; % The user defines iteration value
images(1,1)={I}; % store input image
```

```matlab
%% Enhance input image with RBHF
if iter == 1
  [outputImage]=rbhf(I,Tar1_v_hist,...
  Tar2_v_hist,wavelet_type);
else
  for r=1:iter
    % perform multiple RBHF
    [outputImage]=rbhf(I,Tar1_v_hist,...
    Tar2_v_hist,wavelet_type);
    % store output image
    images(v+1,1)={outputImage};
    iter=iter+1; % update iter
    v=v+1; % update counter
    I=outputImage; % Update input image
  end
end
```

A10. Software prototype

This section presents a windows-based prototype for the proposed method. The prototype was developed using the MATLAB R2018a framework. Therefore, to operate, it must be installed with the MATLAB R2018a Runtime which is included in the software package. Alternatively, the user can download and install the Windows Runtime version from the MathWorks website using the link: http://www.mathworks.com/products/compiler/mcr/index.html

Figure A.3. displays a snapshot of the graphical user interface (GUI).
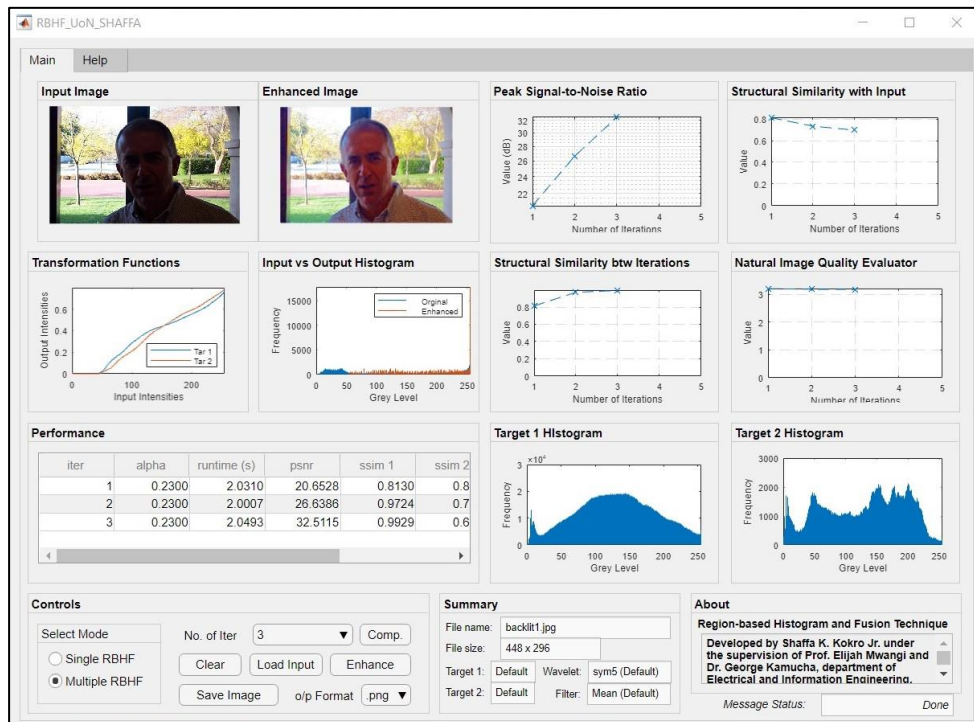

Figure A.3. GUI of the proposed RBHF prototype

The basic controls are discussed as follows:

1. Selection for the mode of operation

The 'select mode' defines the mode of operation for the proposed algorithm. If set to "single RBHF", the algorithm performs one iteration of the RBHF

process. Otherwise, multiple RBHF processes are performed on the input image based on the number of iterations given by 'No. of iter'.

2. Set number of iterations

The number of RBHF iterations is set by the 'No. of Iter' dropdown button. For simplicity, the maximum value is set at five. In the multiple RBHF modes, the number of iterations is set to 2 by default.

3. Load input

The 'Load Input' button is used to load an image into the software. When click, it opens a window that allows users to select an image file from their local directory. All input images must be RGB. There is no method employed to process input images of different colour spaces.

4. Enhance input

Given an input image, the 'Enhance' button initiates an instance of the RBHF algorithm based on the configurations provided. After the enhancement is completed, results are automatically displayed in the table and figures.

5. Save output image

The 'save' control button allows the user to save the enhanced image on their local directory. Users can choose which directory to save the output file as well as define its name and format.

6. Set output format

The 'o/p Format' dropdown allows users to choose between two types of image formats: JPEG and PNG. The JPEG format will lead to a smaller file size as compared to PNG, however at the expense of lowering quality due to lossy compression.

175

7. Clear enhancement data

To clear tables and figures, the 'Clear' button is used. This allows users to begin a new instance of the algorithm without the clustering of data, particularly in the performance table. Figures do not need to be clear after every instance. This process is handled by the algorithm during the next instance. Lastly, 'Clear' does not affect the input data and the default parameters.

8. Compare output images

The comparing of output images is a control feature initiated by 'Comp.'. This feature allows users to view the output image for each iteration. This is particularly useful in cases where a user wants to identify the best picture quality for a higher number of iterations.

Finally, a snapshot of the installation process is given in Figure A.4.

Figure A.4. Snapshot of prototype installation in Windows